Design and Analysis of a Metallic Erosion Protective Solution for Wind Turbine Blades

Petri Suurnäkki

School of Engineering

Thesis submitted for examination for the degree of Master of Science in Technology.

Espoo 28.01.2020

Thesis supervisor:

Prof. Luc St-Pierre

Thesis advisor:

M.Sc. (Tech.) Raul Prieto

Aalto University
School of Engineering

AALTO UNIVERSITY
SCHOOL OF ENGINEERING

ABSTRACT OF THE
MASTER'S THESIS

Author: Petri Suurnäkki

Title: Design and Analysis of a Metallic Erosion Protective Solution for Wind Turbine Blades

Date: 28.01.2020 Language: English Number of pages: 83+1

Master programme: Master's Programme in Mechanical Engineering

Code: ENG25

Supervisor: Prof. Luc St-Pierre

Advisor: M.Sc. (Tech.) Raul Prieto

Erosion on wind turbine blades is an ever increasing problem, as more wind power is built and the average size of turbines is growing. Especially when most of the unused capacity is in offshore, where rain erosion is a large issue. Currently issued erosion protective solutions are at their limits and offering only a limited time of protection. Metallic solutions have grown interest in the field, but still no commercial solution has been developed. Objective of this thesis is a preliminary design of such solution and analyses for it are done.

For the structural analyses a wind turbine blade FEA model was recreated and validated. This was done to provide a realistic attachment for the designed shield to do the structural analyses. The blade was put under loading resembling operational conditions and the results of the shield was then observed. An ultimate load and fatigue life cases were defined for the structural analyses. For the aerodynamic analysis, a 2D CFD case for representative airfoil with added shield was defined. Both the linear-elastic 3D FEA and the 2D CFD analyses were done using the commercial software package ANSYS. In more detail ANSYS Mechanical and Composite PrepPost were used for the structural analyses and ANSYS Fluent for the CFD.

The analyses yielded that the designed solution would structurally be a lifetime solution, handling the worst cases of ultimate and fatigue loads. All the stresses for respective cases were under the yield and endurance limits of the selected material. Additionally, the solution only had a minor effect on the structural response of the wind turbine blade. For the aerodynamic analysis the shield has a small, but noticeable effect on the lift coefficient of the airfoil. No changes in the drag coefficient was observed.

Keywords: Wind turbine, blade, leading edge, rain, metallic erosion protection, FEA, CFD, composites, wind power

AALTO-YLIOPISTO
INSINÖÖRITIETEIDEN KORKEAKOULU

DIPLOMITYÖN
TIIVISTELMÄ

Tekijä: Petri Suurnäkki

Työn nimi: Tuuliturbiinin Metallisen Eroosiosuojuksen Suunnittelu ja Analysointi

Päivämäärä: 28.01.2020 Kieli: Englanti Sivumäärä: 83+1

Maisteriohjelma: Master's Programme in Mechanical Engineering

Koodi: ENG25

Työn valvoja: Prof. Luc St-Pierre

Työn ohjaaja: DI Raul Prieto

Eroosio on kasvava ongelma tuulivoimaloiden lavoissa, kun lisää tuulivoimakapasiteettia rakennetaan ja voimaloiden keskimääräinen koko kasvaa. Etenkin kun valtaosa käyttämättömästä kapasiteetista on merellä, jossa vesisade on iso ongelma. Nykyisin käytetyt ratkaisut eroosiolta suojautumiseen ovat kohdanneet rajoitteensa ja tarjoavat vain väliaikaisen suojan. Metalliset ratkaisut ovat kasvattaneet kiinnostusta alalla, mutta yhtään kaupallista ratkaisua ei silti ole vielä kehitetty. Työn tavoite on luoda alustava malli tällaisesta ratkaisusta ja analysoida se.

Rakenneanalyysejä varten olemassa oleva tuulivoimalan lavan elementtimalli uudelleenmallinnetaan ja validoidaan. Tätä mallia käytetään realistisena kiinnityspisteenä suunitellulle kilpimallille rakenneanalyysejä varten. Lapaan kohdistetaan voimia, jotka kuvastat oikeita olosuhteita tuotannon aikana ja kilpeen aiheutuneita muodonmuutoksia ja jännityksiä havainnoidaan. Kuormitustapaukset maksimikuormalle ja väsymiselle määritellään erikseen analyysejä varten. Aerodynaamista analyysiä varten tehdään 2D virtaussimulaatio sopivalle siipirpofiilille lisätyllä kilvellä. Kaikki analyysit suoritetaan kaupallisella ANSYS-ohjelmistolla. Tarkemmin, rakenneanalyyiseissä käytetään ANSYS Mechanical- ja Composite PrepPost-ohjelmia, ja virtaussimulaatio suoritetaan ANSYS Fluentilla.

Analyysien tulokset näyttävät, että suunniteltu kilpi olisi rakenteellisesti elinikäinen ratkaisu selviytyen määritellyistä maksimi- ja väsymiskuormista. Kaikki jännitykset kullekin tapauksille olivat alle käytetyn materiaalin myötö- ja väsymisrajojen. Lisäksi, metallisella kilvellä oli vain pieni vaikutus lavan mekaanisiin ominaisuuksiin. Aerodynaamisesti kilvellä on pieni, mutta havaittava laskeva vaikutus nostovoimakertoimeen. Mitään muutosta vastuskertoimeen ei havaittu.

Avainsanat: Tuuliturbiini, lapa, johtoreuna, sade, metallinen eroosio suojaus, FEA, CFD, komposiitit, tuulivoima

Preface

"Part of the journey is the end."

- Tony Stark

As the Tony Stark quote goes, part of the journey is the end, and this thesis is the end of my first journey in engineering, but hopefully not the last one. This means that I'll finally achieve one of my dreams about getting the master's degree in engineering and fulfilling the childhood dream of being an "inventor". Getting to this point, means a journey of 5.5 years studying mechanical engineering in Aalto , and an intensive exchange year of aerospace engineering studies at Technische Universteit Delft. While combining studies, work and personal life has sometimes been harsh, finally seeing the end feels amazing.

First of all I'd want to thank VTT and the Wind Power Technologies group for providing me this chance to do my thesis, especially my thesis advisor M.Sc. (Tech) Raul Prieto and our former research team leader M.Sc. (Tech) Geert-Jan Bluemink. I'm especially grateful for the chance to finally work in the field of aerospace engineering. Additionally, I want to give my thanks to my supervisor Prof. Luc St-Pierre for his time and support during the process. I'm also grateful to my academic advisors Prof. Jani Romanoff and D.Sc. (Tech) Tommi Mikkola for their guidance and support during my studies and also for throwing more fuel to the fire in the right occasions. I acknowledge that I may not have been the easiest to be advised, but thanks to both of them I've achieved what I started studying for, and been able to feed my constant hunger for new knowledge. Our programme director Prof. Sven Bossuyt also deserves my thanks for his approval of creating a degree that looks my own, and support during the exchange process. From TU Delft I have to thank Prof. Bertus Beaumont for teaching the beauty of biology, and how an engineer like me can find inspiration from the world of nature. He also provided an amazing chance to take part in the BioDesign Challenge even as an exchange student. Here I'd also want to thank all the other inspirational and amazing professors, whose courses I've attended during the past years, and learnt a lot more than I thought I could.

During my studies I have also been working and starting my career in engineering. For this I have to express my gratitude to Space Systems Finland for hiring me to my first engineering job, providing interesting projects and experience for the few years I worked there. Especially I want to thank my project managers and colleagues in the space and defense projects I worked on. There were many good lunch conversations about various topics between heaven and earth, and everyone I worked with were also constantly supporting me in my studies. Related to my career, Prof. Jani Romanoff requires additional thanks for hiring me for half a year in his maritime engineering research team and getting a first touch of working in academia. I want to thank the whole team for their help and interesting conversations.

Studying wouldn't have been nothing without my fellow students, from which I found a lot of new friends. Getting this far wouldn't have happened without all the great people from The Guild of Mechanical Engineers, Aalto Formula Team and all the people I've done courses together with, both in Aalto and in TU Delft. Getting help and providing help during courses has helped enormously and taught a lot more than I could have done alone. Also, the many projects done together has taught a lot and provided experiences that I may not have gotten otherwise.

Finally, I want to thank my friends and family for the constant support throughout this journey. Especially my parents and older siblings who have done their best on feeding my curious mind throughout my life and given their full support during my studies. I'm grateful that also my grandfather Sakari gets to see me graduating. Thanks for my friends, old and new, who have provided chances to take a nice time off from studies and work, especially the evenings playing board games. Last but not at all the least, I want to thank my girlfriend of soon 10 years and fiancée Kirsi for her love and encouragement to reach for my dreams, and especially enduring me this long.

Thanks for everyone else not specifically mentioned, but who have been part of this journey and contributed in the completion of this thesis. Journey for completing this degree is ending and new journeys as an engineer will begin.

Otaniemi, 28.01.2020

Petri Suurnäkki

Contents

Symbols and abbreviations

Symbols

a		Axial flow induction factor
C	[kg/s]	Damping matrix
c	[m]	Local chord
c_0	[m/s]	Speed of sound in fluid
C_D		Drag coefficient
C_L		Lift coefficient
c_L		Local lift coefficient
c_l	[m/s]	Speed of sound in fluid
c_{opt}	[m]	Optimum chord distribution
c_R	[m/s]	Rayleigh wave velocity
c_s	[m/s]	Speed of sound in solid
c_w	[m/s]	Compressional wave speed in water
D	[N]	Drag force
d	[m]	Droplet diameter
d_w	[m]	Droplet diameter
E	[GPa]	Young's Modulus
$\mathbf{F}$	[N]	External force vector
F	[N]	Instantaneous impact force
G	[GPa]	Shear modulus
I_{15}		Turbulent intensity at mean wind speed of 15 m/s
I_u		Longitudinal turbulent intensity
K	[N/m]	Stiffness matrix
K_{IC}	[MPa $\cdot$ $m^{1/2}$]	Material fracture toughness
L	[N]	Lift force
M	[kg]	Mass matrix
m	[kg]	Droplet mass
N		Number of rotor blades
P	[Pa]	Waterhammer pressure
p	[Pa]	Pressure
p_w	[W/m^2]	Wind power density
$p_{w,a}$	[W/m^2]	Average annual wind power density
R	[m]	Blade radius
r	[m]	Local rotor radius
U	[m/s]	Wind speed
$\bar{U}$	[m/s]	Mean component of wind speed
$\mathbf{u}$	[m/s]	Flow velocity vector
$\mathbf{u}_n$	[m]	Nodal displacement vector
V	[m/s]	Impact velocity
V_0	[m/s]	Impact velocity
v_{res}	[m/s]	Local effective flow velocity
v_{WD}	[m/s]	Design wind speed

W	[m/s]	Resultant wind velocity
λ		Tip speed ratio
μ		Non-dimensional radial position
ν		Poisson's ratio
ρ	$[kg/m^3]$	Density
ρ_0	[kg/m^3]	Undisturbed density field
ρ_l	[kg/m^3]	Liquid density
ρ_s	[kg/m^3]	Solid density
ρ_w	[kg/m^3]	Water density
σ_r		Rotor solidity
ϕ	[$^\circ$]	Resultant velocity W flow angle
ϕ_j^e		Shape function
ψ		Shape function matrix

Abbreviations

ACP	Ansys Composite PrePost
BEM	Blade Element – Momentum Theory
CAD	Computer-Aided Design
CFD	Computational Fluid Dynamics
CFRP	Carbon-fiber Reinforced Plastic
DLC	Design Load Case
DTU	Technical University of Denmark
DTV	Damage Threshold Velocity
EC	European Comission
EU	European Union
FEA	Finite Element Analysis
FEM	Finite Element Method
FSI	Fluid-Structure Interaction
FVM	Finite Volume Method
GFRP	Glass-fiber Reinforced Plastic
GL	Germanischer Lloyd
GPa	Gigapascal
GW	Gigawatt
GWEC	Global Wind Energy Council
HAWT	Horizontal Axis Wind Turbine
Hz	Hertz
IEC	International Electrotechnical Comission
kW	Kilowatt
kWh	kilowatt Hour
L/D	Lift-to-drag
LCoE	Levelized Cost of Energy
Ma	Mach Number
MPa	Megapascal
MW	Megawatt
MWh	Megawatt Hour
N-S	Navier-Stokes
NiCo	Nickel-Cobalt
OWT	Offshore Wind Turbine
RANS	Reynolds-Averaged Navier-Stokes
Re	Reynolds Number
RWT	Reference Wind Turbine
SE	Endurance Limit
SET	Strategic Energy Technology
TI	Turbulent Intensity
TSR	Tip Speed Ratio
UN	United Nations
VAWT	Vertical Axis Wind Turbine
VTT	VTT Technical Research Centre of Finland
WWEA	World Wind Energy Association

1 Introduction

The history of wind power is long, dating back to the ancient times and to areas like India, Tibet, Afghanistan and Persia [1]. Windmills have been used for at least 3000 years, initially used for grinding grain or pumping water. These have through time evolved to large onshore and offshore turbines used for energy generation today [2]. Power generation with wind turbines began as prototypes of 100 kW with rotor diameters of around 38 meters during the 70s oil crisis, from which they have grown to the current large offshore turbines generating up to 12 MW of power and blades being up to 107 meters in length [2, 3]. Example of modern offshore wind turbines can be seen in Figure 1.

Figure 1: Offshore HAWTs at the Scroby Sands Wind Farm, off Great Yarmouth [4].

The growth in size has not been only thing that has grown with wind turbines, but also the overall installed capacity and interest towards it has grown now with the overall interest towards renewable energy sources. World currently living in the era of climate change brings increased political, social and economic pressure for the sustainable energy sources. One key point can be seen to be the Paris Agreement under the United Nations Framework Convention on Climate Change [5] with the objective to stop Earth's temperature rise to 1.5 degrees. Actual actions towards this objective are for example European Union's (EU) decisions [6] to cut CO2-emissions by 40% by 2030 and increase the amount of renewable energy sources to 32% from the 17.5% in 2017 [7]. So EU has the target of decarbonization of energy production and for this wind energy has played a prominent role. EU's Strategic Energy Technology

Plan (SET plan) [8] has the objective to accelerate the development and deployment of low carbon technologies in order to improve new technologies and bring down their costs. This is a plan in order to achieve the EU objectives for the Paris Agreement. Alongside the other renewable sources the SET Plan raises actions for Offshore Wind Energy. By 2030 the forecasts suggest the wind power generation to increase to 240-445 GW, which would add up to 30% of power demand and 80% of European wind resource potential is located in waters. Figure 2 shows the wind power density potential globally and this also shows that the most prominent areas in Europe and also globally are located along coastal regions. The implementation plan addresses also the operation and maintenance, since costs of both are higher in the case of offshore compared to onshore and represent a significant part of the levelised cost of energy (LCoE). With this plan the aim is also to reduce the LCoE to less than 12 CT€/kWh by 2025 and to less than 9 CT€/kWh by 2030. [8]

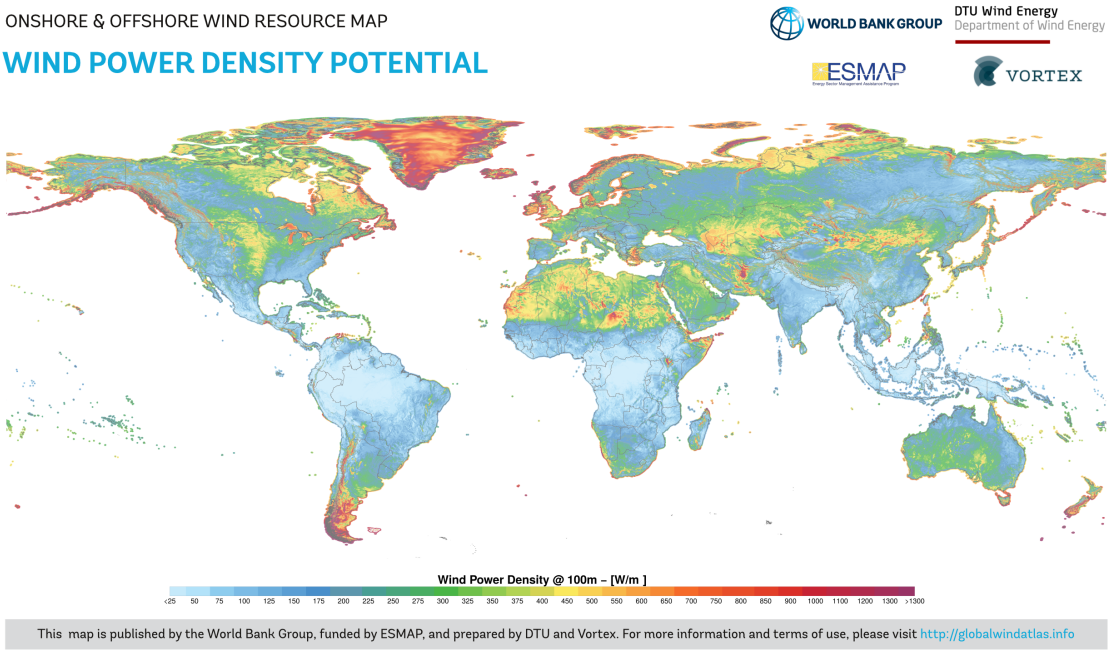

Figure 2: Wind power density potential globally [9].

Based on WindEurope's [10] statistics, Europe has by 2018 189 GW of wind power installed from which 65% was installed in just four countries: Germany, UK, France and Sweden. Based on GWEC's report [11], in 2018 globally there was 51.3 GW of new wind power installations raising the total cumulative installations up to 591 GW. In offshore new installations were 4.5 GW during the same time totalling to 23 GW and making around 4% of total cumulative installations. Also looking into figure 3, it can be seen that there is a rising trend both in new and cumulative installations of wind power in Europe but also a rising trend in how much from those is offshore wind. Especially looking the cumulative installations in figure 3b the rising trend of offshore can be clearly seen. Similar trend could be observed globally. From the Figure 3c the actions set in SET plan [8], set by the EU's decarbonization

targets [6] in order to respond to the Paris Agreement [5] objectives, can be seen by the increasing amount of new wind power installations. Additionally as stated in the SET plan, most of Europe's wind power potential is in offshore and this is seen as increased amounts of offshore installations in comparison to earlier years seen in Figure 3a.

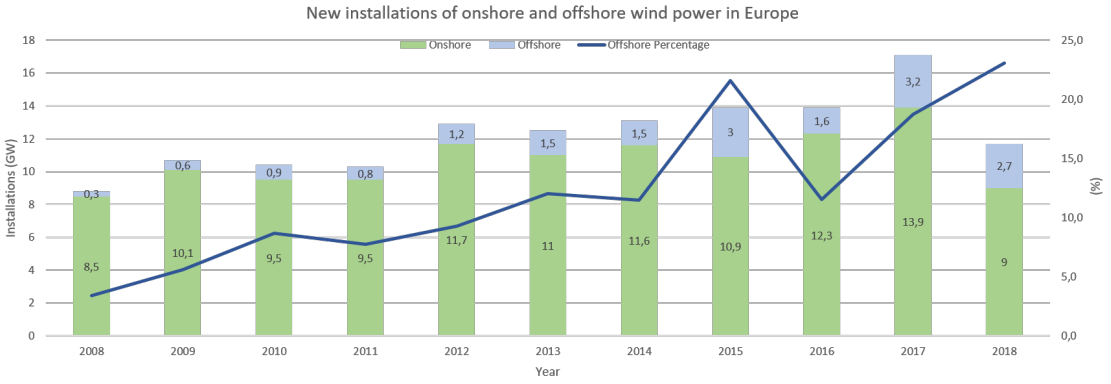

(a) New installations in Europe between 2008-2018.

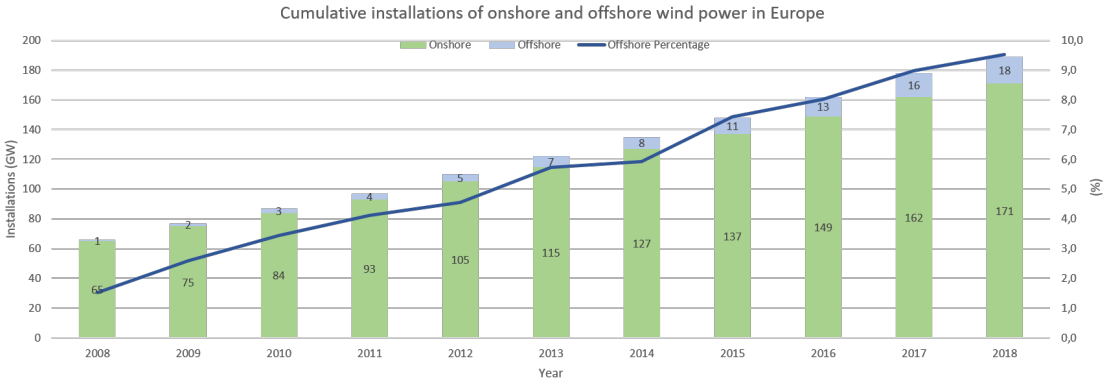

(b) Cumulative installations in Europe between 2008-2018.

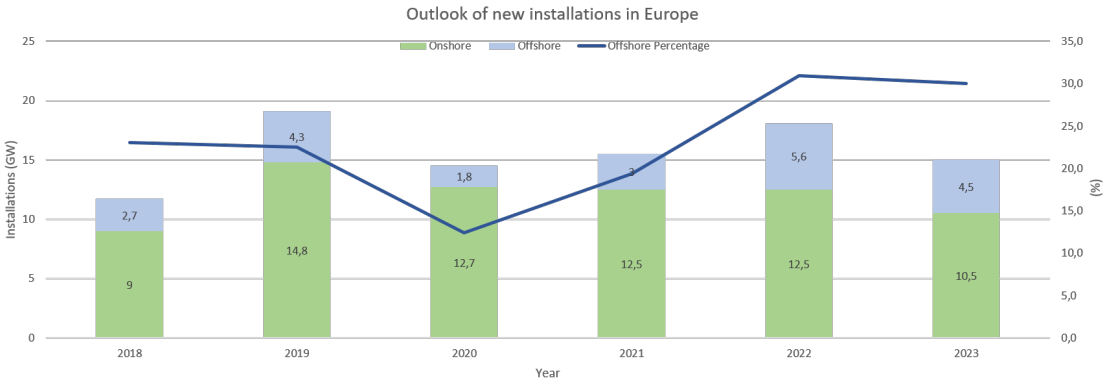

(c) Outlook of future installations in Europe.

Figure 3: Wind power installations development in Europe between 2008-2018 and outlook of future installations [10, 11].

As stated earlier the trend globally is similar to Europe. The trend of new installations has been growing as has been the cumulative installations. Also, apart from the first few years of the GWEC [11] statistics, the percentage of offshore has also been growing globally, as the future new installations are staying around the same, the amount of what is offshore would be almost doubling in comparison to the earlier years.

Figure 4 shows the growth of turbine size and power during last years and the prospects, and Figure 5 represents that the average and largest diameter of installed onshore wind turbines has been growing. As the installed capacity of wind power has grown so has grown the power of individual turbines and also the size of them. This growth of rotor diameter has also increased the rotor tip speeds which generally means higher erosion rate. Figure 6 shows how the rotor diameters and tip speeds vary with different manufacturers for utility scale wind turbines. It is notable to see that tip speeds over 80 m/s and even 90 m/s are now relatively common. [12].

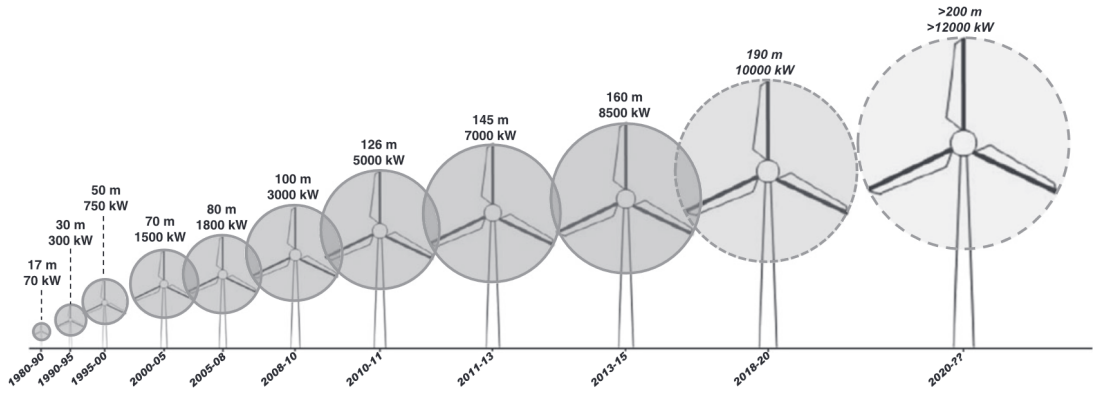

Figure 4: Power and size growth of wind turbines [13].

As pointed out by Keegan [12], numerous service and repair companies raise erosion as a concern of wind turbine operation. Some operators have found out that leading edge erosion becomes a problem only after two years of operation, which is much sooner than usually expected. An example of leading edge erosion can be seen in Figure 7. There are variety of temporary solutions of coatings [15] available to combat erosion and with careful manufacturing, transportation and installation the chances of small tears or scratches can be decreased. These structural flaws can act as initiation sites for erosion [12].

But still leading edge erosion is an issue in wind turbine operation dropping the power generation and requiring frequent maintenance. With the growing amount of installations and larger turbines with larger tendency of erosion, this is an ever growing problem which needs new innovations and solutions. If new protection methods can be found, they allow to lower the operation costs with less frequent maintenance and enable the blades to last for the whole lifetime of their operation.

Objective of this thesis is to design and analyse a metallic erosion protective solution for wind turbine blades. This includes the whole design process from defining

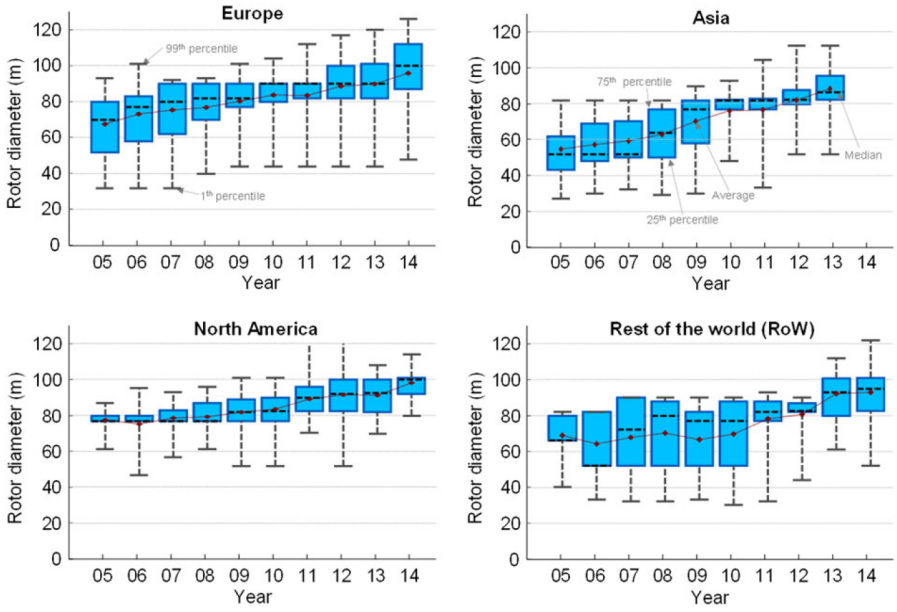

Figure 5: Box plots of rotor diameter growth of onshore wind turbines installed annually [14].

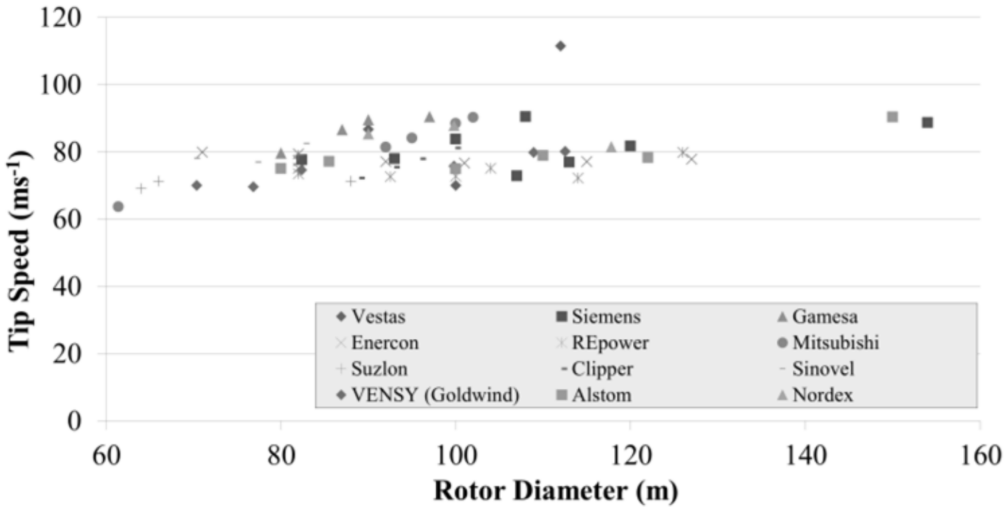

Figure 6: Collection of blade tip speed vs. diameter values for different manufacturer wind turbines [12].

requirements into creation of a suggested design. Structural and aerodynamic analyses are done for the solution to ensure that it can handle the fatigue and ultimate loads during operation and that it doesn't degrade the aerodynamic performance of the blade. Scope of this thesis is limited to the design phase, so physical testing and manufacturing is not covered.

Thesis is structured into three main parts in addition to the introduction and conclusions. The introduction chapter is followed by chapter describing the the current knowledge related to wind turbine operational environment, blade design,

Figure 7: Example of leading edge erosion [16].

industry standards, analysis methods and erosion. These are crucial background to design an additional solution to be attached to a wind turbine.

Chapter 3 following the background knowledge. represents the methods to design and model the erosion protective solution. The chapter describes the reference wind turbine used as the baseline for the process, used design methodology and numerical analysis setups. This is then followed by Chapter 4 showing the results of done analyses.

End of the chapter 4 combines the results to the background literature as a conclusion how successful the design of the new erosion protective solution is. Pros and cons about the new design are discussed and compared into existing solutions. Possible arising changes or upgrades are also discussed. Finally Chapter 5 explains what are the next steps to continue this work.

2 Current knowledge

This chapter includes the relevant background knowledge of the operational environment, wind turbine blade structure and manufacturing methods, how the environmental erosion affects the blades and what kind of erosion protective solutions currently exist. The structural and aerodynamic analysis methods of wind turbine blades are discussed as part of this chapter. These represent the same analysis which are used to validate the protective solution to be fitted on a wind turbine blade. These all are crucial knowledge for designing and analysing the metallic erosion protective solution and ensuring its performance when attached to an actual wind turbine blade and fulfil the required standards in the field.

2.1 Wind turbine operational environment

In order to choose a production site, design a turbine and understand the environment they operate in, it is crucial to understand wind as a resource and how the offshore environment differs from onshore. These both affect directly the design process of blades and what kind of environment they need to sustain. These are also applicable on understanding in what kind of environment the protective solution needs to perform.

2.1.1 Wind as a resource

Like all natural processes wind is stochastic by its nature and from the point of view of wind energy the most striking characteristic is the variability. There are variations in the wind speed and direction, but also sudden gusts. The wind also varies both geographically and temporally, and the variability persists over a very wide range of scales, both in space and time. [17, 2]

According to Burton [2] the wind energy available in the wind varies as the cube of the wind speed as following:

$$p_w = 0.5\rho U^3 \tag{1}$$

Here the p_w is the available wind power density, ρ is the air density and U is the wind speed. Because of this, understanding of the wind resource characteristics is essential in wind energy exploitation. This is to identificate suitable production sites, predict the economic viability of wind farms and also to design wind turbines themselves. [2]

As is known, the primary cause of air motion in the atmosphere is uneven heating of the earth by solar radiation. Amount of energy that gets absorbed varies both in space and time due to the earth not being homogeneous, which then creates differences in the temperature, density and pressure. These difference create forces that move the air. [1]

Additionally to uneven heating of Earth, another factor in the large scale air movement is the rotation of Earth. This brings two effects into play; the Coriolis forces and conservation angular momentum which increases the component of velocities

in the west-to-east direction. The Coriolis forces accelerate air particles to different direction on different sides of the globe, and when air movements reach a steady state geostrophic wind is formed. This is when Coriolis forces balance the pressure gradient forces, leaving resultant motion along isobars. The increasing velocity in the west-to-east direction due to Earth's rotation is small near the equator, but at the temperate zones it forms the Westerlies, which are in direction opposite to the general flow. As can be seen from Figure 8, some semi-permanent wind patterns are formed due to the effects of heating and rotation. Out of these, the Trade winds and Westerlies are well-suited for wind energy. [1, 18]

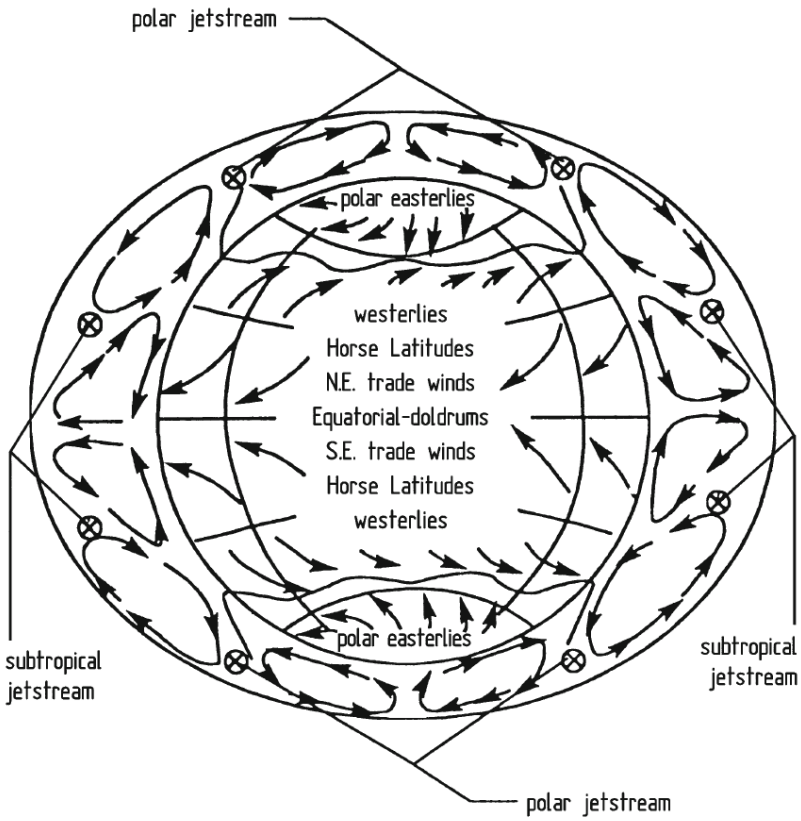

Figure 8: Global wind patterns as presented by Spera [1].

As stated earlier, the variation of wind in the atmosphere happens on many scales of time and space, going from seconds and fractions of a meter all the way to years and thousands of kilometers. In the large climatic scale, seasonal and annual fluctuations in wind are included and are used for resource assessment. In large scale, which is comparable to weather maps, large-scale synoptic fluctuations are identified by the patterns of moving isobars across countries. These on the other hand affect wind power stations' outputs. Local anemometer records observe the small-scale fluctuations, which then are locally sized and higher in frequency. These provide data for wind turbine design and siting of individual turbines. [1]

On top of the variation of wind with the global wind patterns, other spatial variation is apparent. Earth has many different climatic regions of which some are

much windier than others. These climatic regions are dictated by the latitude, but there is also variation within a climatic region due to physical geography. The amounts of land mass and sea, presence of mountains or plains, even the type of vegetation has an influence to the wind through effects on absorption, reflection, temperature or humidity. [2]

Topography also affects the wind in a more local scale. For example, higher locations are in general windier than lower areas like sheltered valleys. Also, wind speeds are reduced by physical obstacles such as trees or buildings. [2]

As the wind is changing spatially, there are also major temporal changes. On a large scale, the amount of wind varies from year to year and even larger scale variations going over decades. These variations are not well understood and are difficult to make accurate predictions for wind-farm projects. [2]

Figure 9 represents the wind energy spectrum, developed by van der Hoven, showing that the majority of fluctuating energy is contained at the macro- and micro-meterological scales represented by the synoptic, diurnal and turbulent peaks [1]. So, on shorter time-scales than a year variations during seasons are more predictable, even though are not easily predictable for longer periods than few days. As stated by Burton [2], these synoptic variations are associated with the passage of weather systems and depending on the location considerable and fairly predictable diurnal variations may occur.

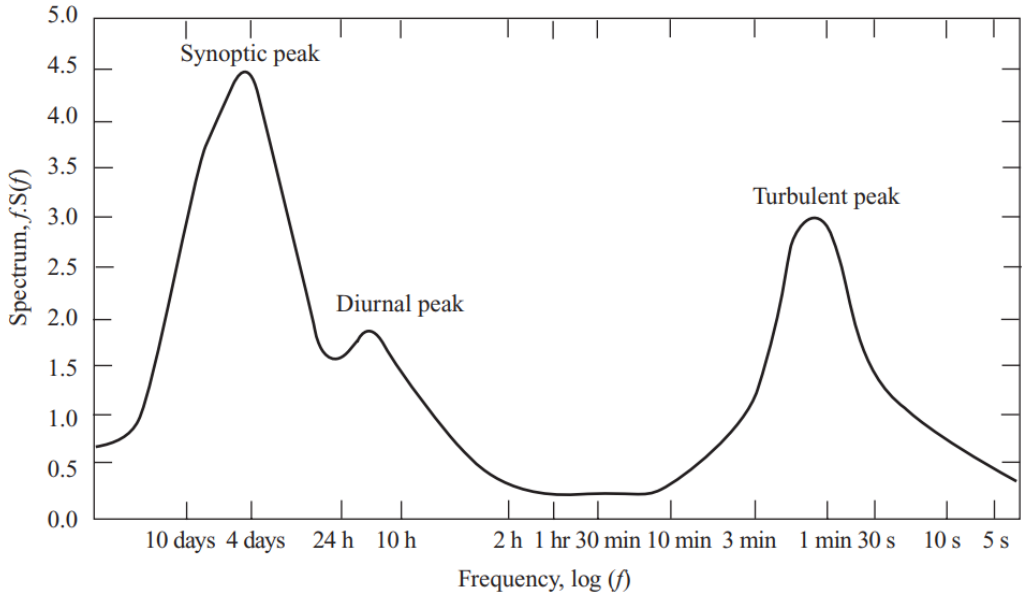

Figure 9: Wind Spectrum by van der Hoven [2].

On the right side of the Figure 9 is the turbulent peak, which shows that one-minute average wind constains high level of fluctuation energy and wind turbines might be sensitive to it. Here the performance and design of individual turbines might be largely affected by turbulence and thus affects the quality of power generated. The spectral gap between diurnal and turbulent peak means that fluctuations of turbulence can be treated distinctly from the synoptic and diurnal variations as there

is very little energy in that parts of the spectrum. [1, 2]

A modification of Equation 1 can be done to describe annual average wind power density:

$$p_{w,a} = \frac{0.5\rho}{8760} \int_{year} \rho U^3 dt \tag{2}$$

In this equation the wind speeds are averaged across a year and can be used to generate wind resource maps. Table 2 by Spera [1] represents wind power classes used for wind resource maps. In this table each class represents a range of annual average wind power densities and equivalent mean wind speeds for those. Areas suitable for most wind power generation are those of wind power class 3 or higher. [1]

Table 2: Wind Classification as presented by Spera [1].

Wind power class	Annual average wind power density [W/m^2]		Equivalent mean wind speed [m/s]		
	10 m elevation	50 m elevation	10 m elevation	50 m elevation	80 m elevation
1	0 - 100	0 - 200	0.0 - 4.4	0.0 - 5.6	< 5.9
2	100 - 150	200 - 300	4.4 - 5.1	5.6 - 6.4	5.9 - 6.9
3	150 - 200	300 - 400	5.1 - 5.6	6.4 - 7.0	6.9 - 7.5
4	200 - 250	400 - 500	5.6 - 6.0	7.0 - 7.5	7.5 - 8.1
5	250 - 300	500 - 600	6.0 - 6.4	7.5 - 8.0	8.1 - 8.6
6	300 - 400	600 - 800	6.4 - 7.0	8.0 - 8.8	8.6 - 9.4
7	400 - 1000	800 - 2000	7.0 - 9.4	8.8 - 11.9	> 9.4

2.1.2 Offshore environment

While wind is present both in onshore and offshore installations, offshore has some additional aspects to consider due to the marine environment. In addition to wind for offshore the presence of ocean waves create additional loading for the wind turbines. As described by Vorpahl [19], constant wind over sufficient time and length in theory leads to unidirectional waves with height correlated to the respective wind speed in fully developed sea states. In reality, the sea surface is short-crested and irregular due to the wind's directional changes, wave systems intersecting each other, variation in water depth, natures of the bed and the influence from the coastlines. [19]

Key difference for wind turbine behaviour comes from the support structures used in offshore. Commonly used ones are monopiles and gravity-based structures, but some floating structures have been installed as prototypes. Generally the support structure for an offshore wind turbine (OWT) is slender and the top is heavily loaded. The support structures on the other hand are relatively light weight and compliant and thus prone to vibrations and exposed to significant ocean loads. [19]

This leads to that OWT experience static loads per Vorpahl [19] from mean wind and current and from gravity, but additionally periodic loads due to gravity on the rotating components, regular waves, wind shear, tower disturbances and yaw errors. Also stochastic loads are present from irregular waves and turbulent wind. So OWTs are highly dynamic systems and in design fatigue loads are the main driver for several components. [19]

In addition to these, there are various other effects on wind turbines arising from the marine environment, but related more closely to erosion. These are presented in more detail in the end of Chapter 2.5.1.

2.2 Blade design & manufacturing

Typical configurations for the modern wind power generation are the horizontal-axis and vertical-axis wind turbines (HAWTs and VAWTS). From these the HAWTs being the dominating configuration for larger turbines. For HAWTs there has been a large variety of materials been used for the blades, which include glass-fiber reinforced plastics (GFRP), laminated wood composites and various steel based structures. How these materials are chosen is based on considerations of size, strength, stiffness, weight design, manufacturing, maintenance and cost. [1] For blades a successful design satisfies a wide range of objectives which some may conflict with each other and according to Burton [2], the summary of the objectives is as follows:

1. Maximize annual energy yield for the specified wind speed distribution
2. Limit maximum power output (in the case of stall regulated machines)
3. Resits extreme and fatigue loads
4. Restrict tip deflections to avoid blade/tower collisions (in the case of upwind machines)
5. Avoid resonance
6. Minimize weight and cost

Process of designing a wind turbine blade for the whole 20 to 25-year lifetime of the wind turbine can be divided into two stages; the aerodynamic design and the structural design [2, 1]. The first one addresses the design of the optimum blade geometry which is defined by the airfoil family, together with the chord, twist and thickness distributions. On the other hand, structural design includes the blade material selection and design of the spar within the external envelope. There is also interaction between the two stages in order to have sufficient blade thickness to accommodate the blade spars. [2]

2.2.1 Blade aerodynamic design

Starting with the aerodynamic design, the process encompasses to choice of airfoil family and optimizing the chord and twist distributions. The thickness variation is usually set to be the minimum value allowed by the structural requirements in order to minimize the drag losses [2]. The mechanical power captured by the rotor from the wind is influenced directly by the shape of the designed rotor blades. Calculating these optimum shapes can be done by applying Betz's momentum theory and the strip theory. For these calculations crucial criterion is the demand that at each blade radius, the wind speed in the rotor plane be delayed to two thirds of the undisturbed wind speed [18]. The lift coefficient will be selected so that at the design tip-speed ratio (TSR) of the rotor, the blade itself will be operated with the best possible lift-to-drag (L/D) ratio. By simplifying and mainly by neglecting airfoil drag and tip vortex losses an analytical formula for aerodynamically optimum chord distribution over the blade length can be resolved [18]:

$$c_{opt} = \frac{2\pi r}{N} \frac{8}{9 \cdot c_L} \frac{v_{WD}^2}{\lambda \cdot v_{res}} \tag{3}$$

In this equation c_{opt} is the optimum chord distribution, N is the amount of rotor blades, c_L is the local lift coefficient, v_{WD} is the design wind speed, λ is the TSR and v_{res} is the local effective flow velocity.

Similarly, based on Burton [2], optimizing the blade design is done based on the machine operating at a fixed TSR, which leads to a following analytical expression for the blade geometry parameter:

$$\sigma_r \lambda c_L = \frac{Nc(\mu)}{2\pi r} \lambda c_L \tag{4}$$

Additionally to the earlier equation, in this equation σ_r is the rotor solidity, c is the blade chord, μ is a non-dimensional radial position and r is the local rotor radius.

Equation 3 presented by Hau [18], gives useful results for an approximate of the blade's contour and respectively the optimum chord length distribution is a hyperbolic function of the blade length. But in the case of a turbine operating at constant rotational speed, meaning varying TSR, there is no parallel analytical solution for the optimum blade geometry. In this case the design must be made with numerical methods based on the blade element - momentum theory (BEM). [2]

These kinds of theoretical shapes can be seen in Figure 10 for different TSRs and blade amount. It can be observed, that for high TSR and large number of blades the geometry becomes more and more slender. This is obviously a problem regarding the strength and stiffness of the blade. This leads that for high-speed rotors they must have small number of blades, since large TSRs with more blades leads into really slender geometries. So, the hyperbolic contours present challenges in manufacturing, for which it is beneficial to have straight-bladed planforms. [18]

Figure 11 represents basic blade shape based on straight-bladed planforms. For these blades the Figure 12 shows the power losses due to deviations from the

aerodynamically optimum shape. As an approximation the trapezoidal planform with the straight leading and trailing edges is good. From the figure it can be seen that the maximum power coefficient is only slightly smaller than the optimum hyperbolically delimited shape. [18]

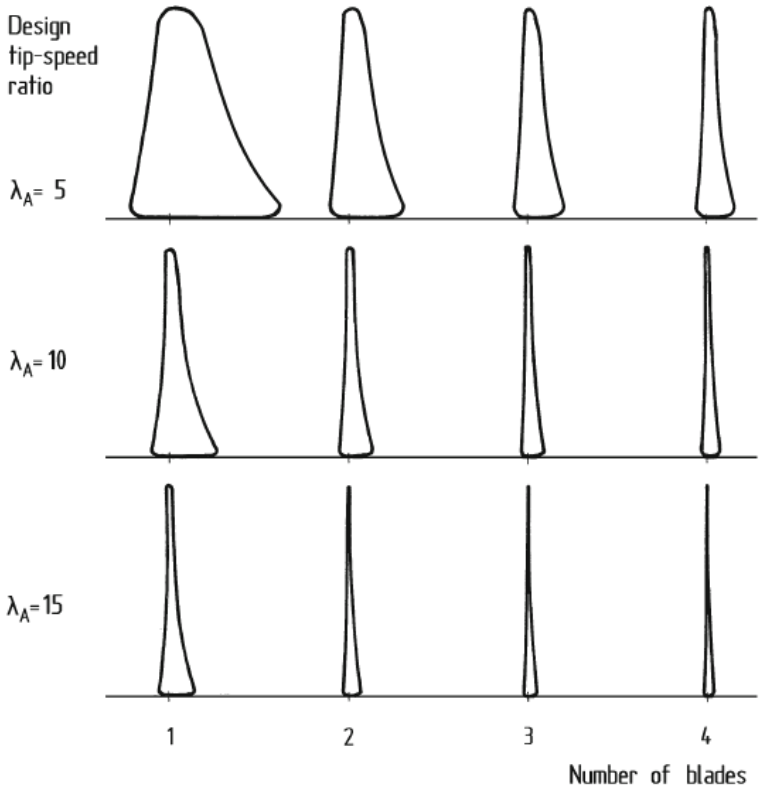

Figure 10: Optimum blade shapes based on aerodynamics with different TSRs and amount of rotor blades [18].

The blade design done thus leads typically to blade geometry, where both blade chord and blade twist vary approximately inversely with radius. Due to the inboard section of the blade is only a small fraction of the total power output based on blade element theory, the airfoil section isn't generally continued inboard to about 15 percent radius and the chord at this location is substantially reduced. Blade root is normally circular to match with the pitch bearing, if pitchable blades are used, or to allow pitch angle adjustment with bolted flange with stall-regulated blades. Transition between the root and airfoil sections should be smooth for structural reasons. [2, 18]

Since the outer blade area is much higher importance for the rotor performance aerodynamically, the choice of the blade shape and surface quality must be given close attention. So the chord length distribution should remain as close as possible to the optimum shape, which also applies to the shaping of the outer blade tip. This has an analogy to the airplane wings where the tip shape influences the formation of wingtip vortices and affects the induced drag. [18] The wingtip vortices can be controlled with the use of different winglets and wingtip shapes to decrease the

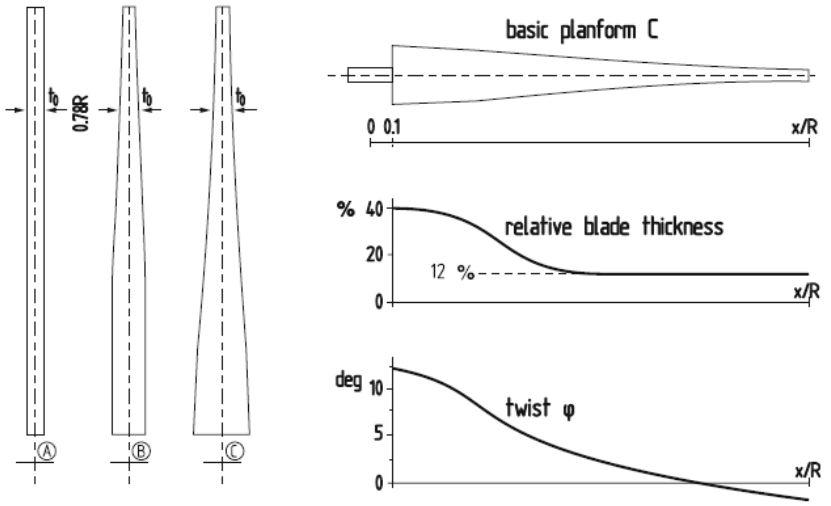

Figure 11: Basic blade shape calculated for a two-bladed rotor [18].

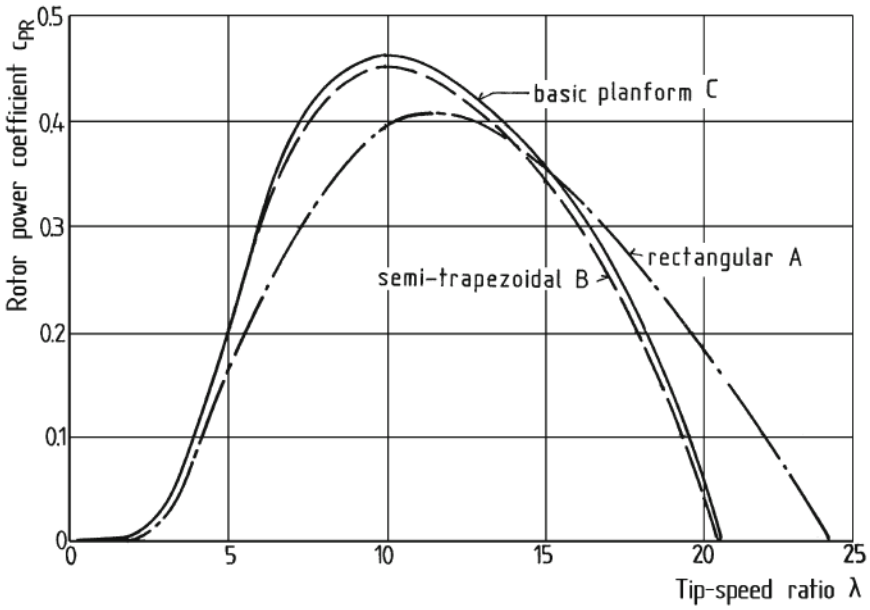

Figure 12: Blade planform influence to the rotor power coefficient [18].

induced drag due to the vortices [20]. Attachment of tip vanes have been proposed occasionally with the same aim, but apparently the effectiveness is greatly reduced due to the unsteady and turbulent winds in the atmosphere [18].

2.2.2 Blade structural design

While the aerodynamic design comes up with the optimum blade shape, this is still done in cooperation with the structural design to accommodate required structural solutions. With modern composite materials the structural design follows closely the models of aircraft construction. The predefined blade envelope is a hollow shell that

provides a simple and efficient structure to resist flapwise, edgewise and torsional loads. Some manufacturers use this hollow shell construction, but in the case of small and medium sized turbines a great benefit comes from concentrating skin material to the forward half of the blade. This is where the blade thickness is at maximum and it acts more efficiently in resisting out-of-plane bending moments. On the other hand, these hollow shell structures defined only by the airfoil sections are not very good with out-of-plane shear loads. To combat these, one or more shearwebs are included which are oriented perpendicular to the blade chord. Depending on dimensions and manufacturing process, the shearwebs can also form a wound spar as seen in Figure 13a or a boxspar design found from Figure 13b can be used. [2, 18, 21]

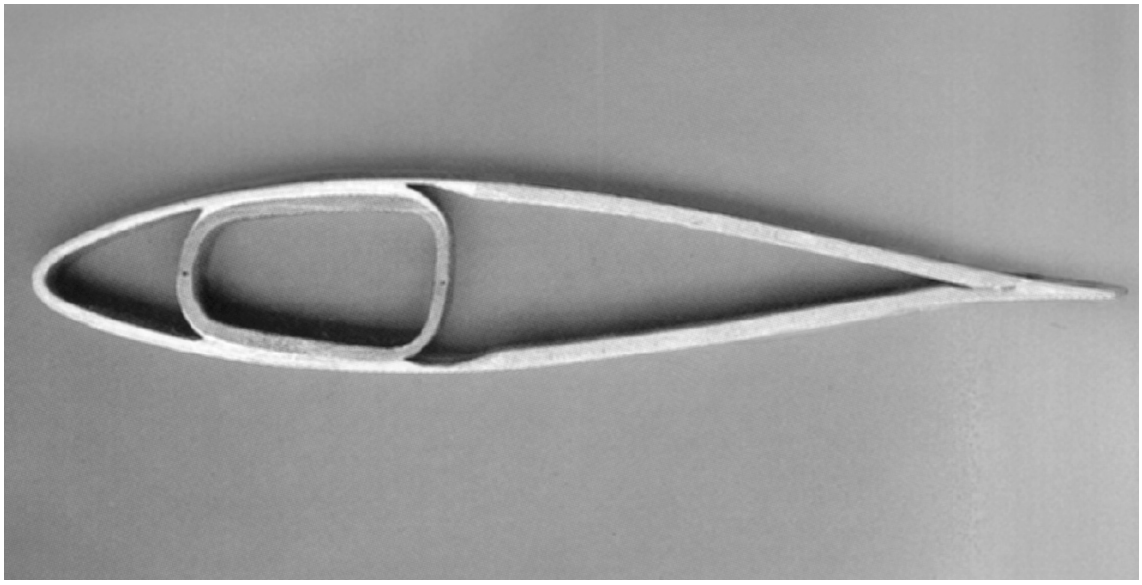

(a) A wound spar with a laminated shell.

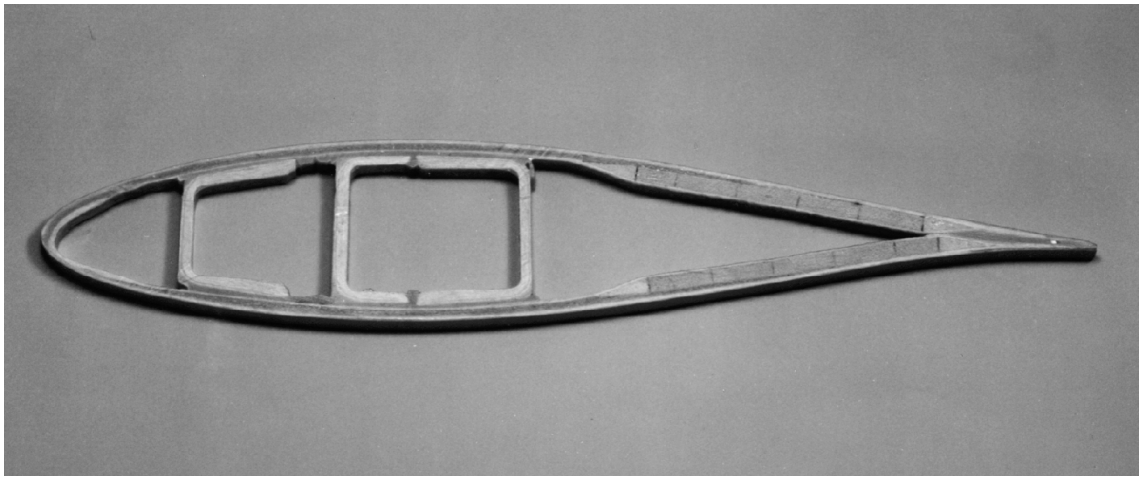

(b) A lightewight spar box and spar webs with a laminated shell.

Figure 13: Examples of a wound spar and sparbox designs [18].

While the webs are made of laminated composite materials, the shells are produced as a sandwich construction. Here only the outer layers have hard fiber composites

and softer support materials - such as balsa wood or foams - are used on the inside. Figure 14 shows on example of the different layups across the blade section. This is to achieve lower weight construction. In the outer and thinner blade sections these core materials are also used in the place of the webs. Largest portion of the load, and especially the bending moment, is absorbed by the webs and sparboxes. [18]

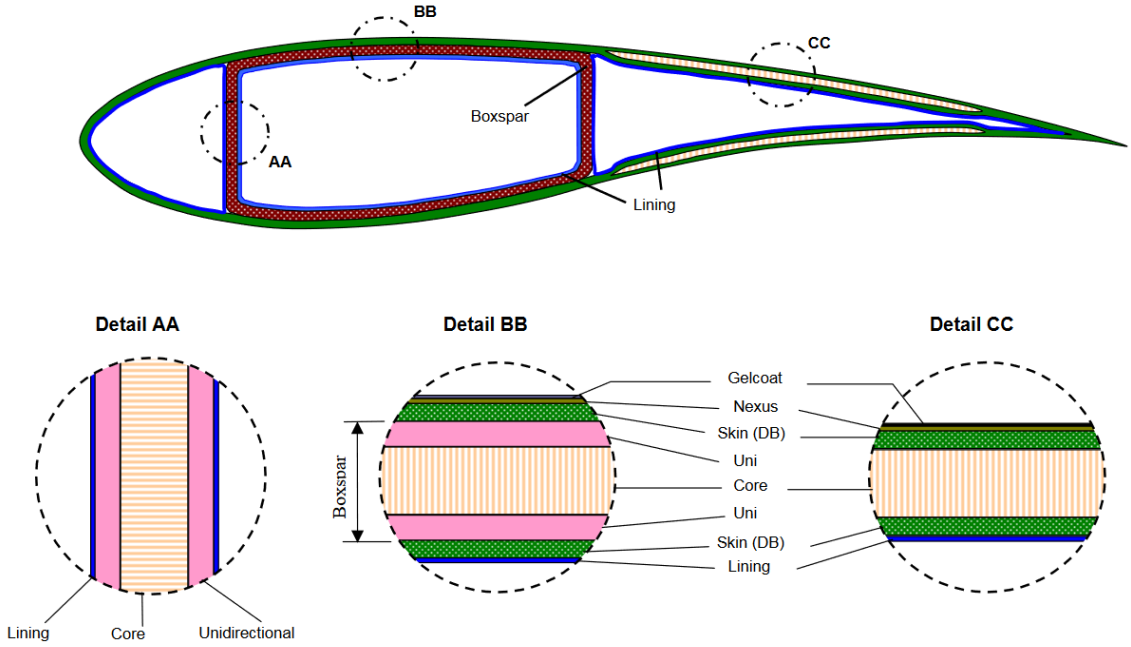

Figure 14: A typical blade cross-section and structural layup [21].

Typically all wind turbine blades are manufactured from glass-fiber composites, and in many cases carbon fiber is used as reinforcement for large blades. According to Burton [2], the ideal material would combine necessary structural properties; high strength to weight ratio, fatigue life and stiffness, together with low cost and ability to be formed to desired shape. Manufacturing blades only from carbon fiber is too expensive for commercial turbines. Example of carbon fiber usage is reinforcement of spar flanges in the main stress direction. For large turbines that have over 120 meters of rotor diameter carbon fiber has to be used. Construction consisting of only glass fiber composites would make the rotor too heavy with required stiffness. To protect the materials from the environment, they are protected with some form of gel coats. [18, 2]

One crucial part of the structural design is how the blade is connected to the rotor hub, and this is also closely related with the selected materials. This design of connection also affects the quality and weight of the blades. A challenge of the connection is transferring forces from the composite structures to the metallic hub due to the difference of material properties. Additionally, the rotor forces are concentrated around the blade root and the hub, while also being subjected to extremely high dynamic loads. [18]

There are few concepts of the connection design currently used. Heavy dual steel flanges are a common design particularly in older rotor blades. Here, the blade root

is clamped between an inner and outer flange, which are then bolted together. This was connected to the rotor hub with an external flange ring with tension bolts. This design frequently constitute up to one third of the total rotor blade weight. Another design, which is a step to reduce rotor blade weight, is a cross-bolt connection. The principle is familiar from helicopter rotors and has since found its way to commercial rotor blade production. In this joint, the epoxy resin composite materials should be used, since polyester is prone to plastic deformation with point load concentration. Alternative to the cross-bolt connection is bonded-in lightweight flanges or sleeves. Here flanges are lightweight, made from example high-strength aluminium, and bonded into the blade root structure. The bonded-in sleeves make it possible to screw in the fastening bolts directly. Lastly the simplest solution for design, and a way to save weight, is to directly bond connecting bolts to the root structure. This is however seemed risky and is not yet in mass production. A general example of the blade root connection can be seen in Figure 15 with bonded-in sleeves. [18]

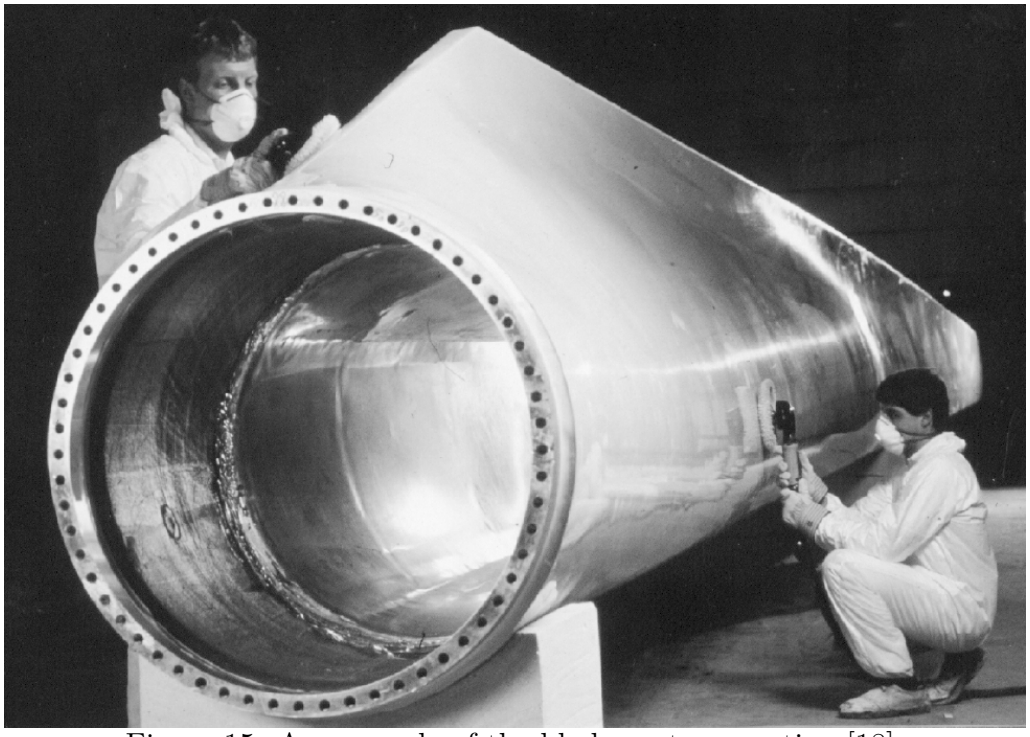

Figure 15: An example of the blade root connection [18].

2.2.3 Blade manufacturing

The selected materials dictate what manufacturing methods are available for them, and with composites the most common one is lamination. This means that various layers of fiber material are laid into a mould of the component and impregnated with a resin. These are then cured at either ambient or higher (80–90 °C) temperatures depending on the used resins. With the layering, the fibers can be oriented in various directions depending on the desired strength properties. This capability to customize the laminates is a major advantage of laminated composite structures. In production

laminating permits to manufacture almost any complicated shape with high surface quality, but the major disadvantage is that most of the work is manual labour. [18]

Based on Hau [18], important part of the laminating technique is the requirement of the mould of the outer rotor blade contour. Depending on the technique and resins used, the mould has to withstand heat to dry the composite material.

There are four major techniques for laminating which are hand-wrapping, prepregs, vacuum infusion and filament winding. Out of these hand-wrapping is the oldest and simplest method suitable only to relatively small components made in small numbers. Here the fiber mats are impregnated normally in the resin and layered into the mould. Quality is directly affected by the skill and reliability of the person. [18]

Alternative to wet-layups is using prepregs, short for pre-impregnated fiber mats. The prepregs are provided as semi-finished products, laid then into the mould and cured at relatively high temperatures (100–150 °C). While this still is labour intensive method and quite expensive, it provides good conditions for high quality products. [18]

Alternative to prepregs is using vacuum infusion, that is frequently used today. Here the dry fiber mats are placed into the mould, then sealed with plastic foil and evacuated. Resin is then pumped into the mould and sucked by the vacuum. This prevents the formation of air inclusions and reduces the formation of unhealthy resin vapours. For cost reasons this method is mainly adopted by rotor blade manufacturers. [18]

Filament winding has decreased in popularity due to increased size of rotor blades, but it's being used again in certain parts of the rotor blades such as wound spars. Major advantage of the method is the high level of mechanization, and it can be done almost fully automatically. In the winding process the fibers go through a resin bath and get impregnated with the matrix material. The process can be controlled numerically by varying the winding patterns and filament tensions with a computer program. Originally the method was developed for production of pressurized vessels that are rotationally symmetric. The method could be used for more complicated shapes, but the downsides become very apparent. In the lamination process the fiber direction cannot be easily adapted to the proper directions, which leads to heavier components and poorer surface quality. [18]

Important part of the composite manufacturing process is quality assurance to determine that the materials and products are suitable for the correct use. Even small things, like deviations from curing conditions or soiled gluing surfaces, affect the strength properties of the finished products. Because of this, the manufacturing processes that are relatively complex and where the production of the material and the component are linked, intensive control measures are required. [18]

2.3 Wind turbine blade structural analysis

Design of wind turbines are regulated by international standards. These standards define various load cases for the wind turbines, both fatigue and ultimate loads, wind conditions, design rules and also requirements for various systems. These standards provide the baseline cases for the turbine design process. The standards

don't generally define individual methods for the analyses, but it is also crucial to understand how the turbines are analyzed and what kind of tools are used in addition to what the standards define. This section goes through the common standards for wind turbines and also how structural and aerodynamic analyses can be done.

2.3.1 International standards

Two international standards are from Germanischer Lloyd (GL) and International Electrotechnical Comission (IEC), both which provide similar standardized load cases for wind turbines. GL published the *Regulation for the Certification of Wind Energy Conversion Systems* in 1993 whereas IEC published the IEC 1400-1 *Wind turbine generator systems – Part 1 Safety Requirements* in 1994. A revised edition of IEC 14001-1 appeared in 1999 with a new number of IEC 61400-1 and GL amended theirs with supplements issued in 1994 and 1998. [2]

Four different classes of wind turbines for different site wind conditions are identified by the IEC 61400-1 *Wind turbine generator systems – Part 1 Safety Requirements* [22]. These classifications and the parameters for wind speed are presented in Table 3. Here the increasing class number corresponds to lower wind speeds. In these classifications the reference wind U_{ref} is defined as the 10 minute mean wind speed at hub-height with a 50 year return period. For the design of wind turbine turbulent intensity (TI) is an important parameter and this is defined as the ratio of the standard deviation of wind speed fluctuations to the mean. Two levels of TI categories A and B are defined by the standard:

$$I_u = I_{15}(a + 15/\bar{U})/(a + 1) \tag{5}$$

In this equation I_{15} is the TI at mean speed of 15 m/s defined as 18% for category A and 16% for category B. Constant a gets values 2 and 3 for categories A and B. These classes are independent of the wind speed classes and in each case the turbulence varies with hub height mean wind speed $\bar{U}$. [2, 22]

Table 3: Parameters of wind speed for different wind turbine classes based on IEC 64100-1 specification [22].

Class	**I**	**II**	**III**	**IV**
Reference wind speed, U_{ref} (m/s)	50	42.5	37.5	30
Annual average wind speed, U_{ave} (m/s)	10	8.5	7.5	6
50 year return gust speed, 1.4 U_{ref} (m/s)	70	59.5	52.5	42
1 year return gust speed, 1.05 U_{ref} (m/s)	52.5	44.6	39.4	31.5

The IEC standard [22] defines external wind and other environmental conditions, but also turbine operational states and fault situations. These have then been combined into specifications of 17 different ultimate load cases and 5 fatigue load cases. These are then used for the wind turbine design. It is to be pointed out, that the standard does not prescribe particular methods of the load analyses. [2]

Same classification of wind turbines is adopted by GL's *Regulation for the Certification of Wind Turbines* [23], which is usually referred as the GL rules, as are used in the IEC 61400-1. Difference between the two is that GL rules only specify one hub-height TI value of 20%. However, GL defines a larger number of load cases, which many are parallel to IEC cases. Based on Burton [2], the GL rules also provide a simplified fatigue spectrum for aerodynamic loading and simplified design loads for turbines with three non-pitching blades. [2] [23]

Setting apart from other standards, the GL rules [23] also describe the design process required for turbine components including design load definition, analysis methods, material strengths and fatigue properties. Also, rigorous treatment of the requirements for control and safety systems, also for the associated protection and monitoring devices, are provided. Finally there are also sections to deal with operation, maintenance, noise and lightning protection. [2]

2.3.2 Extreme loading

As stated by Burton [2], the load cases selected for ultimate load design must cover realistic combinations of a wide range of external wind conditions and machine states. Thus, it is commonly practiced to distinguish between normal and extreme wind conditions, and also between normal and faulty machine states. Hence, the following states are used for defining load cases for design: [2]

- normal wind conditions in combination with normal machine states
- normal wind conditions in combination with machine fault states
- extreme wind conditions in combination with normal machine states

In this case 50 year and 1 year return periods for worst occurring conditions are used for defining the extreme and normal wind conditions. Machine fault states are assumed to occur only rarely and be uncorrelated with the extreme wind conditions. The machine fault state in combination with extreme wind condition does not need to be considered as a load case, because the occurrence of the combination of such even has a high return period. [2]

The extreme load cases are divided into non-operational and operational load cases, where the non-operational machine state is defined as one in which the machine is neither generating power, nor starting up, nor shutting down. The machine may be stationary, so parked or idling. [2]

The non-operational load cases can be again divided into normal machine state and fault state. The design wind speed for normal machine state load case is commonly taken as the gust speed with a return period of 50 years. Here, the magnitude of the gust depends on the gust duration chosen, which should be based on the size of the loaded area. [2] IEC [22] and GL [23] rules specify gust durations of 3 and 5 seconds regardless of the turbine size. For both, the 50 year return gust speed is defined as 1.4 times the 50 year return 10 minute mean. [2]

Examples of the fault state cases are those involving the failure of the yaw or pitch mechanisms. Because of the used assumptions of no correlation between this

kind of an event and extreme wind speeds, the design wind for this case is normally the gust speed with return period of 1 year [2]. GL [23] specifies this to be 80% of the 50 year return gust speed and IEC [22] has this specified lower to 75%.

The operational load cases are divided into normal machine state, loss of load and fault state cases. For the normal machine state cases, several different load cases have to be investigated. This is to evaluate the effects of extremes of gust loading, wind direction change and wind shear. IEC [22] describes the following ultimate-load cases during normal machine state as presented by Burton [2]:

- *Load case 1.1*: Hub-height wind speed equal to U_r or U_0, with turbulence, where U_r is the rated wind speed, defined as the wind speed at which the turbine's rated power is reached and U_0 is the upper cut-out speed.

- *Load case 1.3*: Gust and direction change (ECD). Hub-height wind-speed equal to U_r plus a 15 m/s rising gust, in conjunction with a simultaneous direction change of $720/U_r$ degrees. The gust rise time and period over which the direction change takes place are both specified as 10 seconds. Wind shear is to be included according to the "Normal wind profile model".

- *Load case 1.4*: External electrical fault, with hub height wind speed equal to U_r or U_0. Normal wind shear is included, but turbulence is not.

- *Load case 1.6*: 50 year return rising and falling gust, superimposed on hub-height wind speed of U_r or U_0 with normal wind shear (EOG_{50}). The duration of the gust, T, is specified as 14 seconds.

- *Load case 1.7*: Extreme wind shear (EWS). Additional vertical or horizontal transient wind shear superimposed on the "Normal wind profile model", for hub-height wind speeds of U_r or U_0.

- *Load case 1.8*: 50 year return direction change for steady hub-height wind speed, U_{hub}, of U_r or U_0, with normal wind shear (EDC_{50}. The direction change takes place over a period T/2 of 6 seconds.

- *Load case 1.9*: 15 m/s rising gust superimposed on hub-height wind speed of U_r with normal wind shear (ECG). The gust rise time is specified as 10 seconds.

Loss of load is the second type of operational load cases, and the IEC [22] *Load case 1.5* is considered separately from the extreme load cases. Loss of load happens if the aerodynamic torque will no longer meet with any resistance from the generator, and this occurs if the connection to the grid itself is lost. In this case the rotor begins to accelerate until braking systems activate. The load case may result in critical rotor loading depending on the speed of the braking response. The load case is described as follows: [2]

- *Load case 1.5*: Grid loss, with a rising and falling 1 year return gust, superimposed on hub-height wind speed of U_r or U_0 (EOG_1). The duration of the gust, T is specified as 10.5 seconds.

The grid loss has to be considered in combination with extreme wind conditions, because the loss of load as a machine state is taken to be normal. This is due to the fact stated by Burton [2], that grid loss is likely to be caused by a fault on the utility network and subsequent circuit breaker operation, and may happen at any time. [2]

For the machine fault states, only the normal wind conditions need to be considered, because of the assumption of extreme wind conditions and machine faults to be uncorrelated. Thus, IEC [22] standard specifies two following load cases for machine fault state cases: [2]

- *Load case 2.1*: Control system fault, with steady hub-height wind speed equal to U_r or U_0 and normal wind shear. Partial safety factor: normal.
- *Load case 2.2*: Protection system fault or preceding internal electrical fault, with steady hub-height wind speed equal to U_r or U_0 and normal wind shear. Partial safety factor: abnormal.

As explained by Burton [2], the IEC [22] standard also specifies cases for start-up and shut-down of a wind turbine. These are with a 1 year returning rising and falling gust, and a start up case with 1 year return direction change and an emergency shut-down case. For both hub height wind speeds of U_r and U_0 are to be considered. [2]

The described load cases above provide a set of stresses which acceptability are to be checked, but in addition to these, the tower clearance is to be considered. Insufficient tower clearance results in a collision between the blade and the tower. [2]

2.3.3 Fatigue loading

For fatigue loading Burton [2] states, that the complete load spectrum for any particular wind turbine component has to be rebuilt up from separate load spectra derived for turbine operation at different wind speeds, and from the load cycles experienced at start-up, normal and emergency shut-down and while the machine is parked or idling. This means, that for the hours of machine's lifetime cycle counts for each stress range for 1 hour of operation in a particular wind speed band are calculated and scaled-up. The IEC [22] standard states, that this is to be based on the Rayleigh distribution, with the annual mean wind speed set according to the turbine class specified in Table 3. These different cycle counts for the lifetime of the turbine are combined and added together for the cases for start-ups, shut-downs and periods of non-operation. [2]

2.3.4 Finite Element Analysis

While the methods above lead into transient fluid-structure interaction (FSI) analyses, in the scope of this thesis finite element method (FEM) is briefly discussed, as it is used as a part of the design and modeling process in Chapter 3. It is to be pointed out, that in the scope of this thesis FSI is not considered.

As described by Reddy [24], FEM is a numerical method used for real-world problems that involve complicated physics, geometry and boundary conditions. Here,

the usually geometrically complex domain of the problem is divided into geometrically simple subdomains called finite elements. Each element is independent domain over which equations are derived and solved. Finally the elements are assembled based on the continuity of the solution and balance of internal fluxes. [24]

In the case of wind turbines FEM can be used in multiple ways, from the whole turbine down to a single component. Commonly the full turbine aeroelastic FSI analyses are done with a multibody simulation approach. Here, the fluid dynamics simulation is linked to a structural solver to transfer the loads from the flow into the structure. In this case multiple of elements can be used, and for full wind turbine case beam elements are common.[25]

If more details are required for the structural analyses, the components can be modelled in more detail. If composite blades are to be modeled, a common approach is to use shell elements. [26] This is because blades are commonly thin-walled structures, where the thickness of the structure is relatively small in comparison to the other dimensions. Shell elements are used to discretize the geometries by defining a reference surface. The element doesn't have a physical thickness but it is defined as a section property. [27]

Shell elements are specifically useful for laminates and varying lamination schemes. The material properties of laminates can by layered into the properties of the shell elements without adding computational complexity through more elements for individual layers. But, as stated by Reddy [27], the stiffnesses of the formed laminates depend on the material stiffnesses, layer thicknesses and the lamination scheme of the individual lamina. This then affects the behaviour of the laminate and stresses formed. In the case of FE the key issue represented is the shell element reference plane, which often is taken as the geometrical midplane. [27]

As the behaviour of the shell depends on the created laminate, linear or nonlinear strain-displacement relations can be used to compute the strains associated to the displacement field. All the strain components vary linearly through the laminate thickness, and are thus independent of the material variations, but the stresses do not. As can be seen from the Figure 16 by Reddy [27] the strains, as stated earlier, vary linearly through the laminate, but the stresses are typically stepwise linear through the thickness. [27]

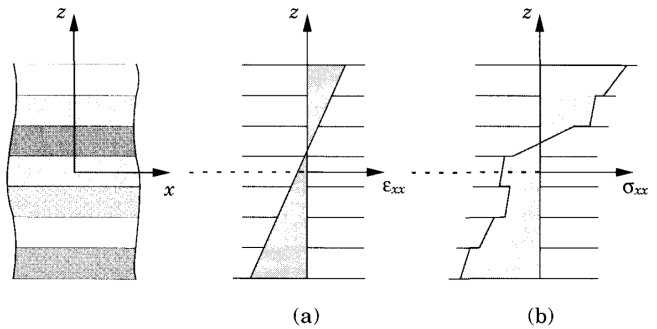

Figure 16: Relation of strains (a) and corresponding stresses (b) through laminate layers and thicknesses. [27]

Alternative shell elements, like solid-shells [28], also exist, which have various uses. For example, solid-shells have a physical element thickness and can be joined with conventional solid elements. This has an advantage when geometries or modeled components would have surface and solid geometries, which otherwise couldn't be easily discretized together. Also, in Chapter 2.5.3 few methods for modeling erosion with FE-approach are presented.

2.4 Wind turbine aerodynamic analysis

While the design standards presented in Chapter 2.3.1 provide the requirements and analysis procedures, they do not take a stand on the aerodynamic analyses of wind turbines. These standards lead into running aeroelastic analyses of the designed turbines in order to fulfil the structural requirements, but the standards do not have sections for aerodynamic performance. Aerodynamic analysis tools thus have a role in both the structural certification and as well in the aerodynamic design parts. As explained in Chapter 2.2, the design of the blades of the turbines need to maximize the annual energy yield and find the optimum aerodynamic design. For this purpose a variety of numerical methods are used in the field and in the scope of this thesis two are presented. Blade element – momentum theory (BEM) is an important tool in the blade design process as a rather fast modeling tool, and computational fluid dynamics (CFD) is commonly used when more details of the flow are required, or when modifications or additional components to existing solutions are researched. For this thesis BEM is presented as a tool recognized as a part of the design process explained in Chapter 2.2 and understanding how existing blade geometries are achieved, and CFD is used in the analysis of the erosion protective solution in Chapter 2.4.

2.4.1 Blade element – momentum theory

The major advantage of BEM is that it is fast to run in comparison to similar CFD setups, and thus it is used in the design process of blades, nowadays often together with numerical optimization. BEM is part of rotor blade theory, and is an extension of blade element theory (BET) combining it with momentum theory. [2]

As stated by Burton [2], the basic assumption in BEM is that the force of a blade element is solely responsible for the change of momentum of the air which passes through the annulus swept by the element as seen in Figure 17. Thus, no radial interaction between flows through contiguous annuli is assumed, which only holds if the axial flow induction factor does not vary radially. So based on Burton [2], in the case of N blade elements resolved in the axial direction the component of the aerodynamic force is the following:

$$\partial L \cos\phi + \partial D \sin\phi = \frac{1}{2}\rho W N c (C_L \cos\phi + C_D \sin\phi)\partial r \tag{6}$$

In this equation L is the lift force, D is the drag force, ϕ is the flow angle of the resultant wind W, c is the local chord, C_L is the lift coefficient, C_D is the drag coefficient and r is the local rotor radius.

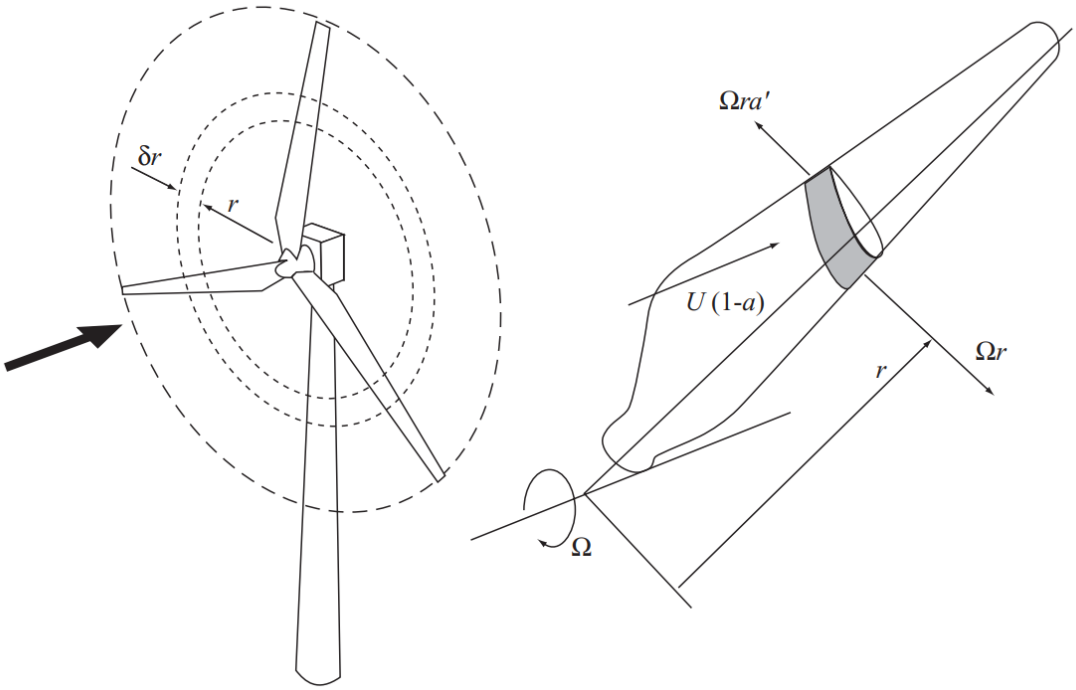

Figure 17: Annular ring swept by a blade element presented by Burton [2].

The following equation presented by Burton [2] presents the axial rotor torque caused by aerodynamic forces on the blade elements:

$$(\partial L \cos\phi + \partial D \sin\phi)r = \frac{1}{2}\rho W^2 N c (C_L \cos\phi + C_D \sin\phi) r \partial r \tag{7}$$

These equations, together with the rate of change of axial momentum of air passing through the swept annulus, increase of dynamic head and the rate of change of angular momentum of the air passing through the annulus, can be solved to obtain values for the flow induction factors with an iterative process using two-dimensional airfoil characteristics. [2]

As a final point of BEM, Burton [2] points out that the theory is strictly only applicable if the blades have uniform circulation. In the case of non-uniform circulation, exchange of momentum between flows through adjacent elemental annular rings happens and there is radial interaction. Thus, it is not possible to state that the only axial force acting on the flow through an annular ring is due to the pressure drop across the disc. But as Burton [2] states, in practice it appears that the error involved in relaxing the above constraint is small for TSRs above 3. [2]

2.4.2 Computational fluid dynamics

In this thesis CFD will be used for an incompressible flow using Reynolds-Averaged Navier-Stokes (RANS) and discretizing the domain with Finite Volume Method (FVM). These methods are briefly explained in this chapter.

In the incompressible case the governing equations are the continuity equation for consevation of mass and Navier-Stokes equation (N-S) for conservation of momentum. The former equation can be expressed the following way for incompressible flow [29, 30]:

$$\nabla \cdot \mathbf{u} = 0 \tag{8}$$

And the latter one takes the following form:

$$\frac{\partial \mathbf{u}}{\partial t} + \nabla \cdot \mathbf{uu} = -\nabla p + v\delta \mathbf{u} \tag{9}$$

As stated by Zikanov [29], most flows in reality are turbulent. Issue with turbulence is that the length and time-scales vary largely, making the direct computation of the N-S unfeasible due to limitations of computational power and memory. So far nobody has found a way to describe and predict turbulent flows mathematically. [29]

This limitation can be formalized by estimating the required computational grid to accurately calculate turbulent flow. Here it becomes obvious, that steps in grid spacing should not be larger than the size of the smallest turbulent eddy η. This, combined with the fact that to reproduce the flow dynamics the computational domain has to be several times larger than the largest turbulent eddies, makes the required size N of computational domain in three dimensions be the following: [29]

$$N^3 \sim Re^{\frac{9}{4}} \tag{10}$$

To overcome the challenge several numerical approaches can be used to either simulate or model the turbulence. Most used and oldest method is currently to model the turbulence with RANS, which is computationally very efficient, but often provides inaccurate results due to the large errors due to the approximations included. [29]

By doing a time-averaging process to the Equations 8 and 10 the RANS equations in the incompressible case can be written as the following:

$$\frac{\partial \overline{u_i}}{\partial x_i} = 0 \tag{11}$$

$$\rho \frac{\partial \overline{u_i}}{\partial t} + \frac{\partial}{\partial x_j}(\overline{u_j u_i}) = \frac{\partial \overline{p}}{\partial x_i} + \mu \left(\frac{\partial^2 \overline{u_i}}{\partial x_i x_j} \right) - \rho \frac{\partial \overline{u_i' u_j'}}{\partial x_j x_i} \tag{12}$$

Here Reynolds stress is presented by the final term of the Equation 12, and according to the eddy viscosity hypothesis presented by Zikanov [29], this represents the influence of turbulent viscosity. Reynolds stress is solved by using a separate turbulence model such as k-ω SST or k-ϵ, which are two commonly used turbulence models used in CFD.

In order to solve the equations presented above numerically, the calculation domain needs to be discretized, and for this the most commonly used method is the

FVM. In this method division to finite volume cells from the continuous calculation domain is done which form the computational mesh. The mesh contains the different flow quantities in a discrete point. In two-dimensional and three-dimensional cases it is possible to choose to create a structured or an unstructured grid. In structured grids the cells used are either quadrilateral in two-dimensional case or hexahedral in the three-dimensional case arranged in a structured pattern along the lines of Cartesian or curvilinear coordinate system. In comparison the unstructured grid may be formed from cells with various shapes like tetrahedras, hexahedras, triangles, or other convex polygons. [29] An example of unstructured grid by Zikanov [29] is presented in Figure 18.

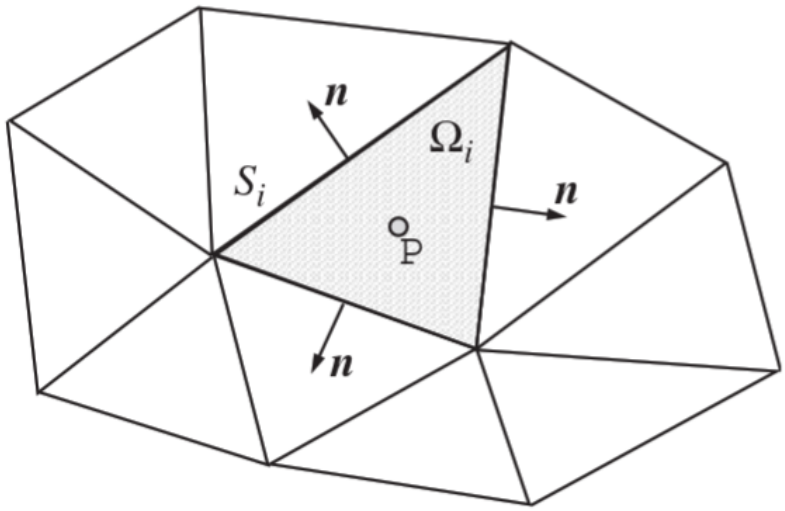

Figure 18: Unstructured two-dimensional finite volume grid [29].

As stated by Zikanov [29], the principle of conservation is reproduced exactly and for the entire computational domain, and it is easy to verify that this global conservation property is valid for two-dimensional and three dimensional volume grids.

As the FVM is used to discretize the spatial computational domain, similarily the temporal discretization needs to be done for the time domain. Thus, the time domain is divided into discrete time steps, and it is possible to use implicit or explicit schemes for the discretization. Often Commercial CFD codes use the implicit schemes, even though they have higher computational demand, but in comparison to explicit schemes they offer more stable solutions. [29]

As can be seen from Equation 12, there is a time derivative present and Taylor series expansion may be used to derive a numerical scheme for the time stepping. First order schemes are commonly used, but higher order schemes offer lower numerical dissipation. This is due to the truncation error $O(\Delta t)$ decreasing by the power of the selected scheme of the Δt it is applied to. [29]

2.5 Wind turbine erosion

The need to design erosion protective solutions for wind turbines comes directly from their operation environment and the existence of erosion. To design effective protective solutions it's crucial to understand the erosion as a phenomena, how it could be modeled and what kind of solutions there already is to protect structures from erosion. This chapter explains the blade erosion phenomena, how it can be modelled and what methods are currently used to protect structures from erosion.

2.5.1 Erosion phenomena

A notable work for understanding the underlying erosion phenomena has been done by Keegan [16]. Blade leading edge erosion comes directly from the environment, and can be divided into rain impact and erosion, hail impact and erosion, sea spray and particulates like sand and dust. Largest of these affecting wind turbines and especially offshore is the rain erosion.

Based on Keegan [16], understanding rain erosion begins by considering the nature of rain droplets and their characteristics as a projectile. Depending on the climate conditions which raindrops are formed typical diameters are commonly cited to be from 0.5 mm to 5 mm. As seen from Figure 19, with moderate rain rates the droplet sizes between 0.5 mm and 3 mm are the most common. The terminal velocity of the droplets is also dependent on the climatic conditions together with the droplet size. [16]

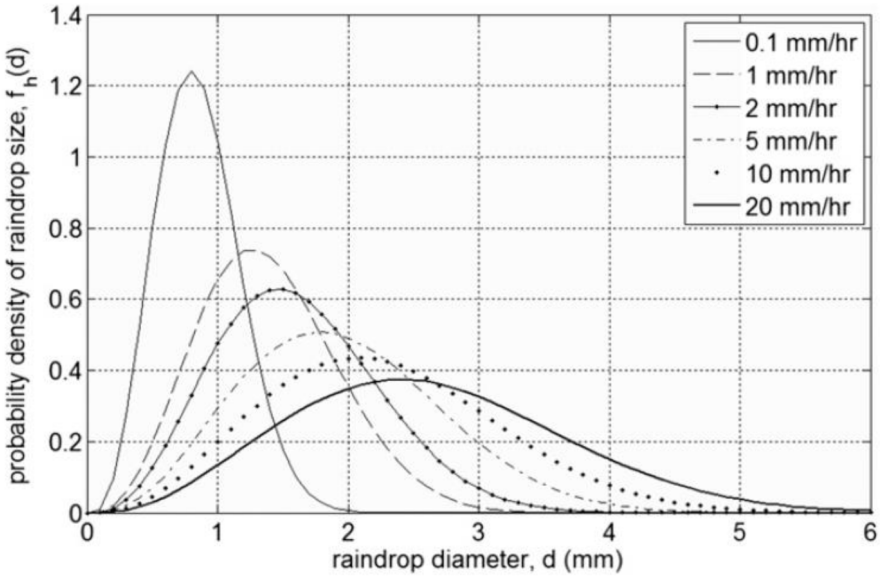

Figure 19: Probability density of rain droplet size with various rain rates [16].

With wind turbines, the terminal velocity of the droplet has only a minor role compared to the blade tip speeds. Simple velocity vector calculations can be used to approximate value of the potential impact velocity through a whole rotor sweep for given rain and turbine operating parameters. Figure 20 shows an example of the raindrop impact velocity throughout the full rotor sweep at the blade tip. Even

though this figure is based on coarse approximations, it shows the potential magnitude of the impact velocity values. It is to be pointed out that even when the blade is rotating in a downwards direction, the impact velocity does not drop below 80 m/s due to the high tip speed. [16]

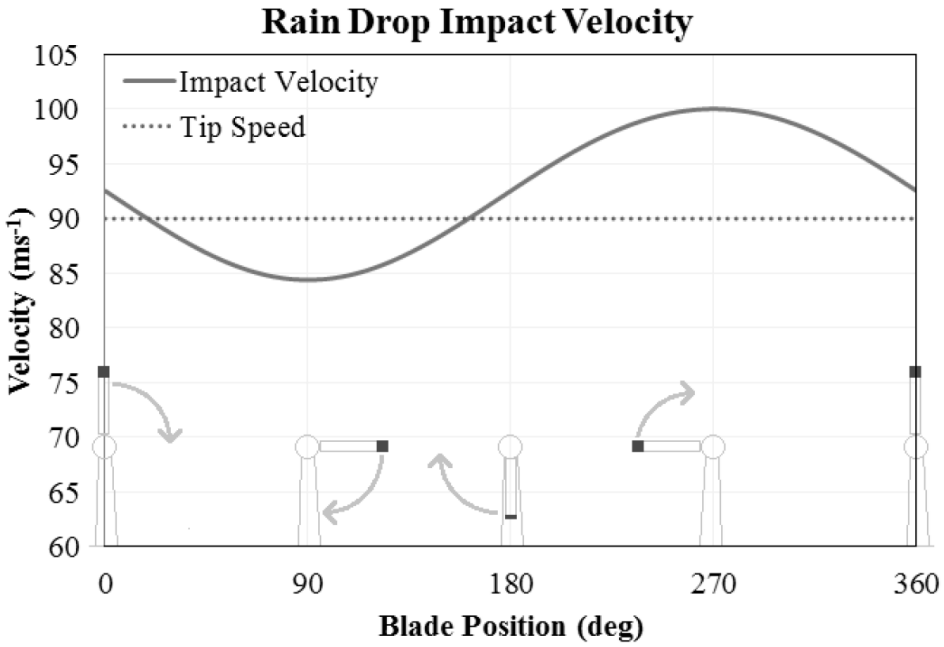

Figure 20: Example of rain droplet impact velocity at the blade tip. Terminal velocity 8 m/s with 20 m/s horizontal wind and hitting the blade tip with 90 m/s tip speed [16].

Figure 21 shows the effects of a round liquid droplet impact on a solid surface. This shows the initial compressional wave followed by a shear wave in the target material. Also, a Rayleigh wave on the target surface is shown. Upon impact, there is a compressed liquid wave front in front of the droplet, and this behaviour is crucial for understanding the impact phenomenon. [16, 31]

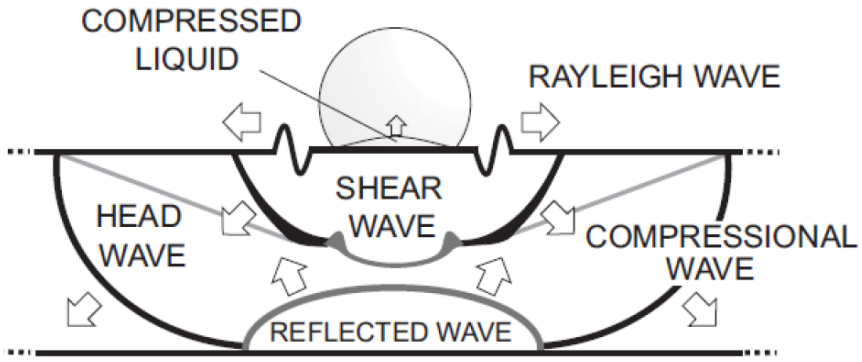

Figure 21: Shockwave propagation upon impact of a spherical drop on a solid surface [31].

These droplets exert a pressure on the surface during the initial phases of contact, and historically the waterhammer equation has been commonly used to predict it:

$$P = \rho_0 c_0 V_0 \tag{13}$$

Here P is the waterhammer pressure during impact, ρ_0 is the undisturbed density of the fluid, c_0 is the speed of sound in the fluid and V_0 is the impact velocity. Originally, this equation was developed to calculate the waterhammer pressures in piping systems and makes some fundamental assumptions. [12]

With these assumptions, the equation gives a good indication of the magnitude of the impact pressure, but does not take into consideration the propagation of pressure through the target body. Following equation shows the modified waterhammer equation, which takes into account both the propagation of pressure through the liquid and the target body during the impact:

$$P = \frac{V \rho_l c_l \rho_s c_s}{\rho_l c_l + \rho_s c_s} \tag{14}$$

In this equation P is the modified waterhammer pressure, V is the impact velocity, ρ is the density, c is the speed of sound and the subscripts l and s refer to the liquid and solid. Although the equation can be good at approximating the impact pressure, it is only capable of predicting the pressures during the initial phases of contact. [12]

For the impact force an instantaneous approximation can be calculated with the following equation:

$$F = \frac{mV^2}{d} \tag{15}$$

In this equation F is the instantaneous impact force, m is the mass of the droplet, d the diameter of the droplet and V the impact velocity. Obviously, the exerted force will vary over the impact event, but this equation provides a good estimate of the magnitude of impact forces. [12]

As stated by Keegan [16], for the leading edge of the blade the forces and pressures exerted by the droplet impact are significant. How the damage is created on the surface depends on the nature of the impact and also the target material. A typical damage formation from a repeated liquid impact on a ductile material is presented on Figure 22. Here it can be noticed, that the initial impact creates a small indented crater, which is then subsequently deepened through further impacts. The change in topology begins to influence the shockwave and consequently the loading pattern on the surface. This results to stress concentrations in the material leading to worsening damage process and removal of material. [16]

Damage threshold velocity (DTV) is usually utilized for evaluating the erosion performance of material under liquid impingement in aviation studies [31]. DTV is the value of lowest impact velocity at which the target material damaging is observed

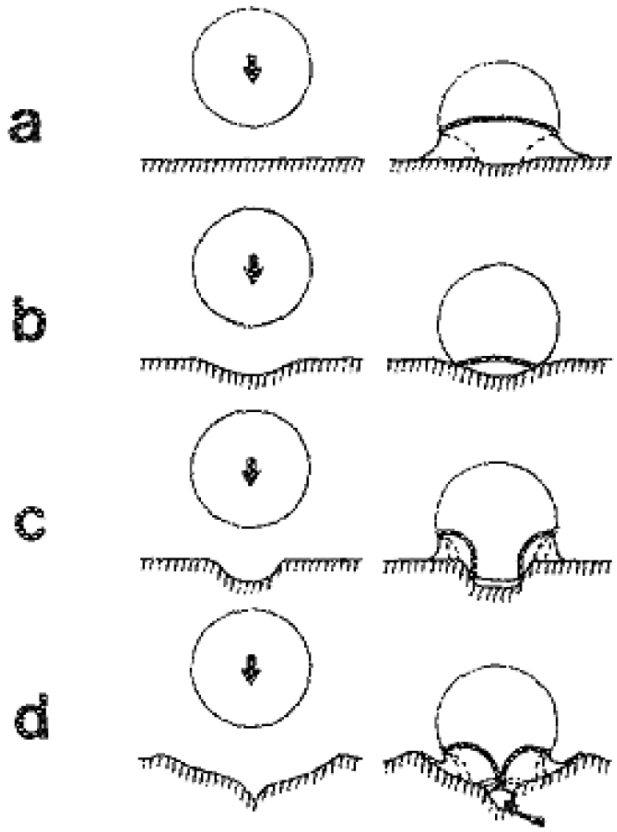

Figure 22: Formation of damage by repetitive droplet impact on a ductile surface [12].

after a certain amount of time. There is no exact classification for this, but one theoretical expression is given by:

$$V_{DT} = c_w 1.41 \left(\frac{K_{IC}^2 c_R}{\rho_w^2 c_w^2 d_w} \right)^{1/3} \tag{16}$$

Here V_{DT} is the DTV, K_{IC} is the material's fracture toughness, c_R is the Rayleigh wave velocity in the target material, ρ_w is the density of water, c_w is the compressional wave speed in water and d_w is the droplet diameter. The Rayleigh wave is created and confined to the target surface, and responsible for approximately 2/3 of the whole impact energy. [12, 31]

For this, the following equation gives the Rayleigh wave velocity c_R:

$$c_R = \left(\frac{0.862 + 1.114\nu}{1 + \nu} \right) \left(\frac{E}{2(1+\nu)\rho} \right)^{1/2} \tag{17}$$

Here ν is the Poisson's ratio, E is the Young's modulus and ρ the density of the target material [12].

Like rain, the wind turbine exposure to hail is very site specific issue and thus less important than rain erosion. By convention, a hailstone has a diameter of at least 5 mm and smaller particles are either ice or snow pellets. The density of hail can vary widely, but for purposes of hail threat standardisation a reasonable worst case density of 917 kg/m^3 has been assumed. Ice is a complex material and has variability to its properties and characteristics and is thus widely considered a class of materials. For this purpose, based on the formation process of hail, only single type of ordinary ice is considered. [16, 12]

As was with rain, the hailstones are also to be considered as projectiles. In this case the large diameter in comparison to rain drops has important effects. With the increased diameter, also the mass of the hailstone increases and thus the impact energy is higher. The increased mass and diameter also increases the terminal velocity, which follows from balancing the gravitational forces to the aerodynamic drag forces. [16, 12] Figure 23 shows the variation of hail terminal velocity increased based on the diameter growth calculated by Keegan [16]. Similarly to Figure 20, Figure 24 from Keegan [16] shows the impact velocity of the hailstones striking to blade tip. As expected the increased terminal velocity of hailstones gives higher impact velocities in the upswing phase and reduces the minimum impact speeds in the downswing phase.

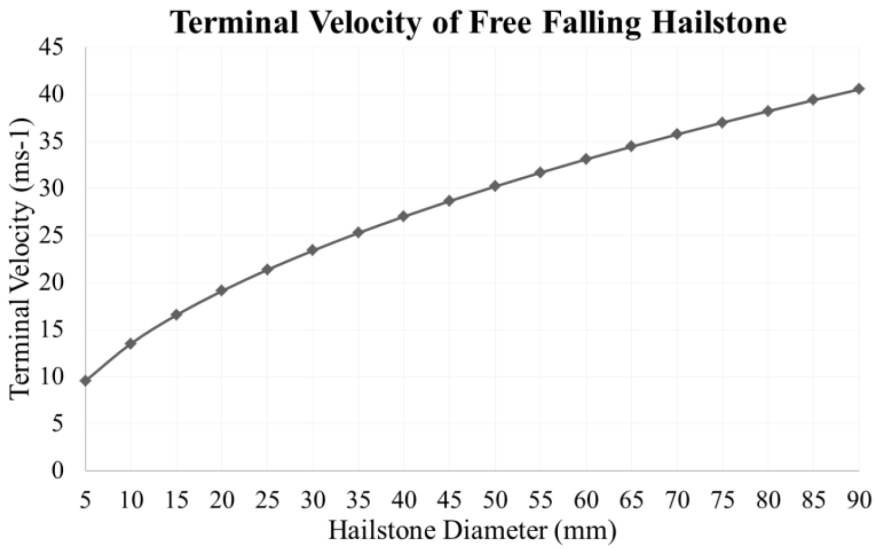

Figure 23: Terminal velocity of hailstones with varying diameter assuming ice density of 900 kg/m^3, air density of 1.29 kg/m^3 and drag coefficient of 0.5 [16].

In offshore environment, the wind turbines come across with the issue of sea spray impacts hitting the blade which may present a threat. As pointed out by Keegan [12], the nature of sea spray impact may be similar to rain, but in some situations larger volumes of water may impact the blade instantaneously in sea spray events. Additional consideration of particulate impacts may arise from the transport of sea salt crystals. Other effects apart from erosion rise from sea salt accumulation on components and leading edge, possibly leading to corrosive damage. [12]

Particulates are a known problem, for rotorcrafts operating in desert and shore

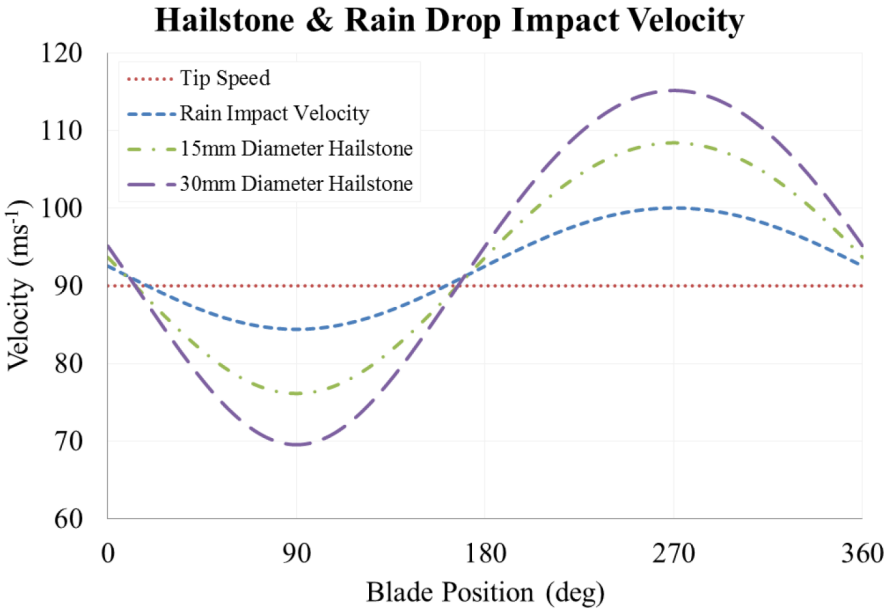

Figure 24: Comparison of hail impact velocities to rain with 20 m/s horizontal wind and blade tip speed of 90 m/s [16].

environments, to cause erosion of the blades. [32] Like other causes for leading edge erosion in wind turbines, exposure to particulates is also cited as an issue. Like with rotorcrafts, also here in warm and arid climates sand and dust are a common type of airborne particulates and pose a threat of leading edge erosion. Like with any other types of environmental effects, also particulates are really site specific issue and with wetter and greener habitats the problem may be non-existent in comparison to dry climates. [12]

2.5.2 Blade erosion

Sareen et al. [33] recognized three phases in the erosion process based on material provided by 3M. The phases in order are pits, gouges and delamination. Erosion process begins with the formation of small pits near the leading edge, and as the density increases they form larger and deeper gouges. In abrasive conditions this process continues until it results in delamination around the leading edge. This erosion and delamination can produce a significant aerodynamic performance degradation. [33]

As stated in Chapter 2.5.1, the liquid water creates a waterhammer effect and the forces and pressures exerted by the rain droplet are significant. The Figure 22 shows the damage formation due to liquid droplet impact into a ductile surface. The impacts begin to create small craters, which can be seen as pits similarly to abrasive damage, and these grow larger creating gouges. These impacts together with the topological changes of the surface results in stress concentrations in the material and eventually removing material. For brittle materials the damage may be manifested through microscopic cracking and other mechanisms. For example, Figure 25 shows a schematic for the damages modes on brittle materials. [16]

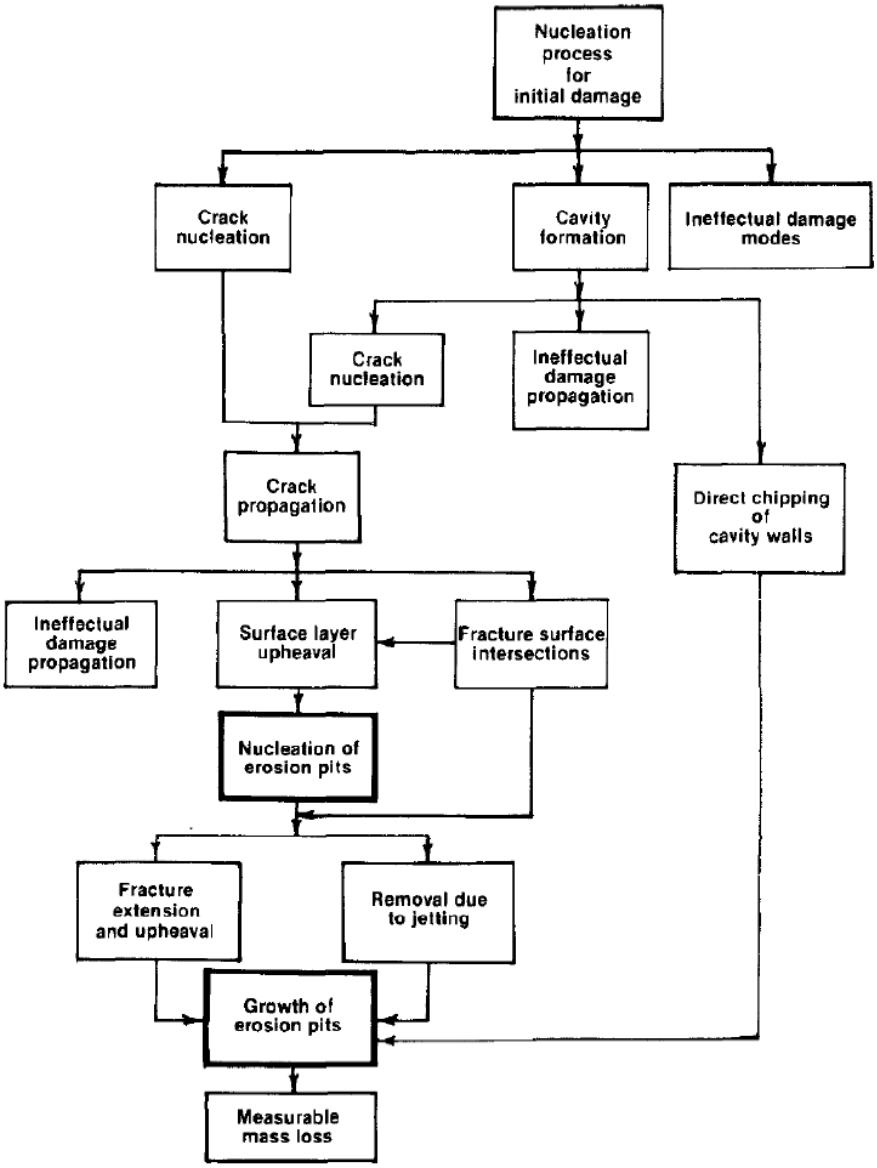

Figure 25: Schematic of damage modes due to rain erosion [34].

Water jet impact testing has been conducted for various polymers and polymer based composites to research the effects of rain droplet induced damage. Results for such test can be seen in Figure 26. These are high speed tests and due to the spreading behaviour and subsequent high pressure creation. a ring-like area of damage seems to form around the impact center. [16]

Surface erosion is not the only material failure mode in the case of hail as is with rain. Hailstone impact can result in propagation of stress throughout the blade skin thickness, and failure in substrate could be an issue for impact effects with enough energy. Delamination between composite plies may occur with combination of shear and normal stresses between plies. This can be detrimental to the static and fatigue properties, and possibly lead to further propagation of delamination. [12]

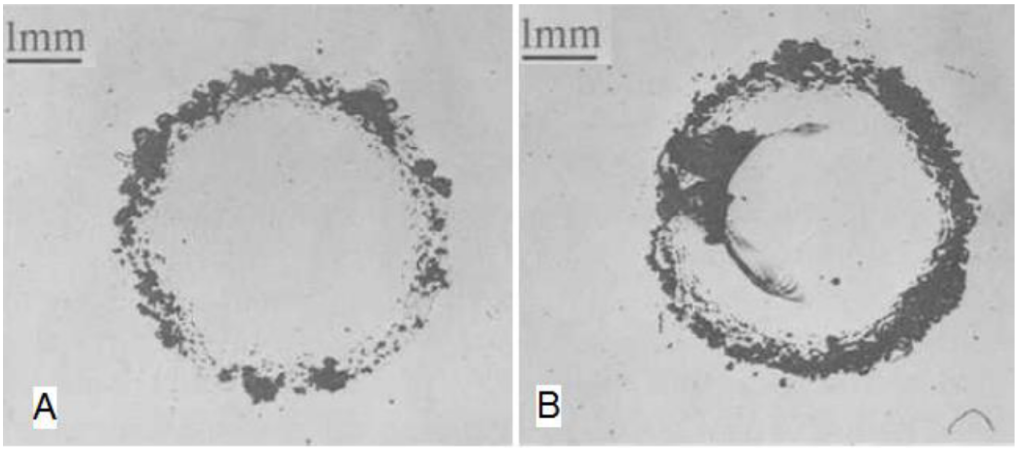

Figure 26: Water jet test surface damage on epoxy material [35].

In reality, the blade leading edge erosion is a combination of the different erosion sources. It can start with aerodynamic degrading pits and gouges, and lead into more serious delamination and composite failure. Figures 7 and 27 shows the effects of leading edge erosion in wind turbine blades with various times of use. As can be seen, only after one year of service the erosion may become an issue, and as time passes the problem grows. The roughness that forms due to the erosion also has an impact to the turbine power curve due to the decreased aerodynamic performance. Figure 28 shows an example of the difference between clean and smooth profile to the original eroded dirty and rough profile. In order to restore the blades' performance, they need to be refurbished, during which the turbine is out of service and is not generating power. This brings direct costs to the operator in the form of salaries of the workers restoring the blades, supplies, and the downtime of the turbine. This is even more serious in the case of offshore turbines where special equipment are required. [16]

Figure 27: Blade erosion progression in field use [16].

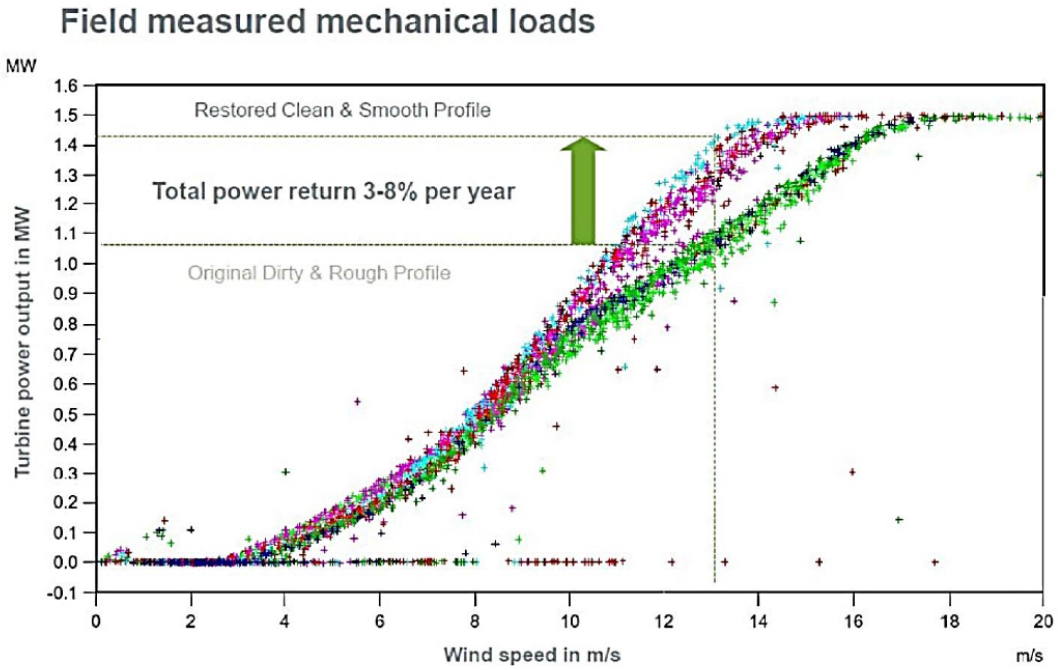

Figure 28: Comparison of eroded and restored blade profiles [16].

2.5.3 Erosion modeling

As stated by Keegan [16], modelling impacts of rain droplets and hailstones numerically presents challenges. Initially they aren't typical engineering components, and do not have easily characterisable material properties. Also, during impact the projectiles experience material failures and rapid and large deformations. Lastly, the target material consists of entirely of polymer resins and composite technologies, which impose challenges in the modelling. Historically modelling liquid impacts on solid surfaces was limited by computing power and sufficient software tools. [16, 12]

Various techniques are used for liquid impact modelling, and some of the earliest FEA studies on impact of water droplets on a solid polymeric targets utilized a wholly Lagrangian meshing method. The relative advantage of this study is being able to model the target material response during impact, and thus evaluate stresses and strains. [12]

Also, Eulerian or combined Eulerian-Lagrangian modeling approaches have been used to model water droplet normal impact on solid surfaces. As explained by Keegan [12], in the validation of this approach the concern was not only the magnitude of forces, pressures and stresses, but also spatial and temporal aspects of droplet-surface impacts. Figure 29 shows an example by Keegan [16] of the results of such analysis representing the characteristic spreading of droplet. This approach was also used to quantify possible stresses created in an approximate representation of a gelcoat applied to blade surfaces. [12]

Similarily to raindrops, multiple approaches for modeling impacts of hailstones have been proposed, but the most developed approach utilizes an Eulerian approach to model the ice projectile. Initially, the model was created to evaluate threat of ice

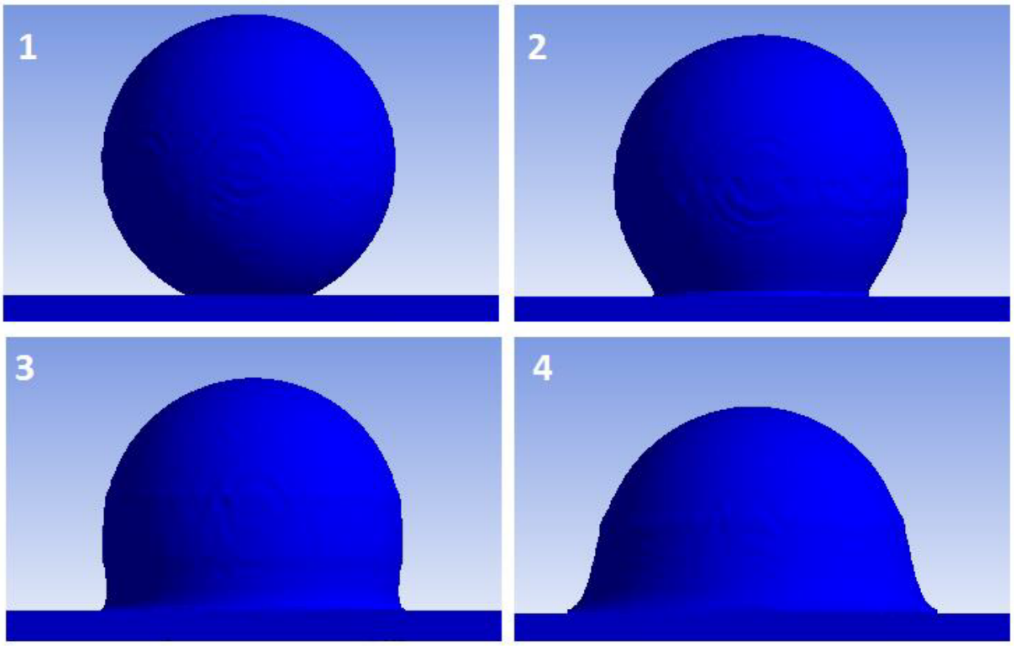

Figure 29: Impact development of a raindrop impacting a solid surface as presented by Keegan [16].

impact on aerospace components, but was further developed to investigate hailstone impact on wind turbine blade's leading edge. [12]

The analysis showed that the formed stresses were greater in magnitude in comparison to the modeled approximation of utility scale blade tip materials. The stresses also far exceeded those generated with liquid impacts in the previous studies. This is due to the increased mass of the projectile and thus increased impact energy. Figure 30 shows the removal of materials due to hailstone impacts, which has lead to the exposure of composite laminate below the epoxy gelcoat. Keegan [12] states, that presented method could provide a powerful design and evaluation tool for blade development, although the results were based on approximate estimates of failure strains of the materials. [12]

These different modeling approaches show, that the impact of rain and hailstones may lead to erosion of the leading edge, and it is important to address the increased impact energies. This is to ensure the performance of the materials selected for the leading edge. Also as stated by Keegan [12], the influence of initial surface defects may again play a role in the development of such erosion. [12]

2.5.4 Current erosion protection in wind turbines

As erosion has been acknowledged phenomena in the field, already means of protection have been developed by blade manufacturers. Various coatings, paints and tapes have been developed to increase the incubation time of erosion and decrease the effects to the performance. Current used materials consist mainly of various polymers and provide different levels of protection, but still not providing a lifetime solution against erosion. [16]

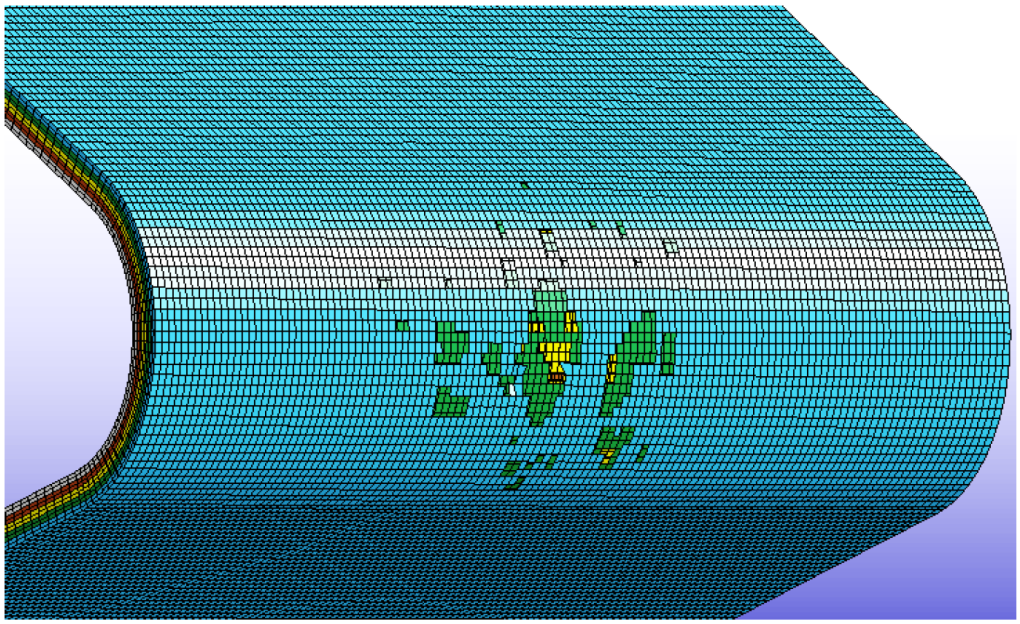

Figure 30: Analysis results of modeled hailstone induced leading edge erosion [12].

As presented by Keegan [16], gelcoat technologies have seen the most use in wind turbines and the ease of incorporation into the blade manufacturing process is the main advantage. The main downside of such coatings is the low durability. In addition to gelcoats, polyurethane based coatings are used. Their benefits mainly are high impact resistance, shape memory from high elasticity and resistance to gouging and abrasion. This is currently utilized by many wind turbine manufacturers and typically applied as an integrated coating in manufacturing. [16]

Currently, where the threat of erosion is considered likely or observations of erosion have been made, additional tapes are commonly utilized. The manufacturers of the tapes claim advantageous impact, abrasion and wear properties. [16]

The polyester gelcoats exhibit significant amount of erosion in tests, even exposing the composite substrate. Figure 31 shows the results of various polyurethane based solutions in a simulated rain field. These show to be much more effective, but at the same time show being susceptible to UV. [16]

In the earlier tests, polyurethane based technologies have proven to increase the lifetime of the leading edges and having high durability against erosion [16]. As stated in Chapter 1, the trend in wind turbines, and especially in offshore, is increasing blade lengths and tip speeds. This leads into increased problem of erosion where the current methods of protection may not be feasible anymore, and do not even currently offer a lifetime solution against erosion.

2.5.5 Erosion protection in other aerospace applications

When exploring metallic solutions against erosion, a good starting point is to look into other aerospace applications. Metallic protection has been long used in aircraft propellers and helicopter rotors. In these use cases, the tip speeds are drastically higher than in wind turbines and they are occasionally used in other extreme conditions

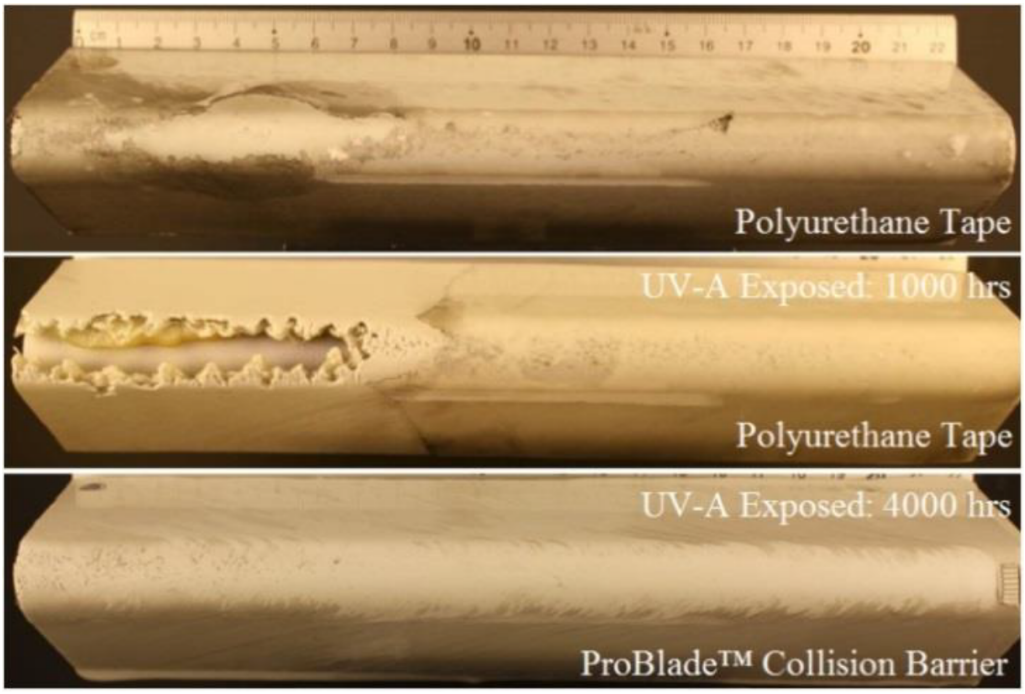

Figure 31: Results of various protective polyurethane-based solutions [16].

experiencing extensive abrasive wear or rain. [32]

As stated by Nissen et al. [32], rotorcraft have been historically designed with a metallic abrasion strip as a sacrificial material. In rotorcraft use, sand erosion is present in takeoffs and landing when the environment is susceptible to it, and rain erosion is present during operations in heavy rainfall. [32] Figure 32 shows the magnitude of erosion present in the results of field survey of V-22 Osprey rotorcraft.

Nissen et al. [32] performed rain erosion testing of various protective materials that could be used for protection of rotorcraft blades varying from polymers to the nickel and titanium used in the V-22. As can be seen from Figure 33, the nickel-, cobalt- and titanium-based materials drastically overperform the tested polymer materials.[32] This is a good indicator that metallic solutions could also be beneficial as a lifetime solution in wind turbines. Also Wölcken [36] raises the point that titanium has an excellent erosion protection performance.

While comparing results between two rather different fields is not trivial. Looking at the results of the V-22 erosion protection tests gives a good idea of the difference in performance between said metals in comparison to polymers. As there is not much progresses in wind power field yet in metallic protection, these results for more demanding use case show a lot of promise for finding better solutions.

Figure 32: Erosion from field observations of V-22 Osprey [32].

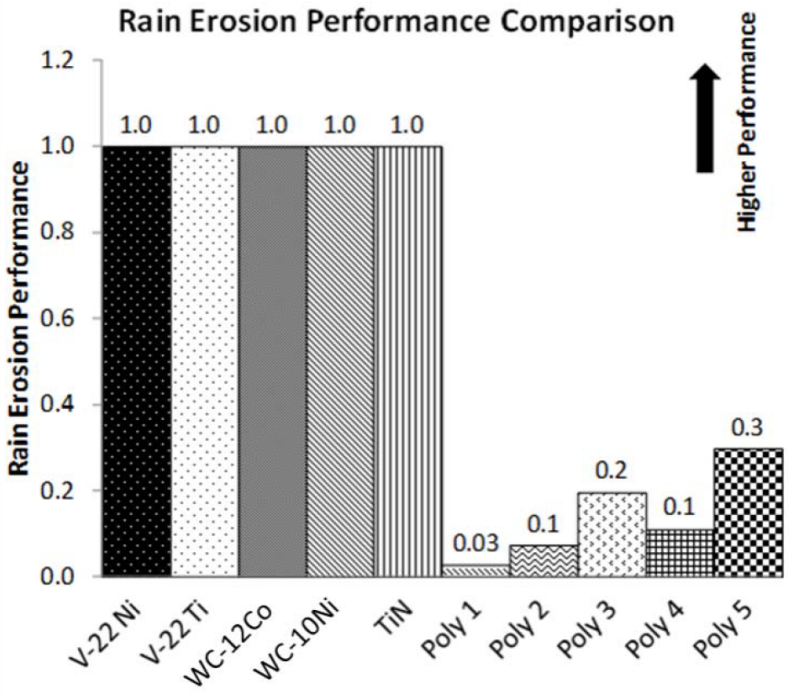

Figure 33: Rain erosion perfomance results by Nissen et al. [32].

3 Design and modeling methods

This chapter presents the methods for designing and analysing the erosion protective solution, and how to model the wind turbine blade it is attached onto. At the beginning of this chapter, the selected reference wind turbine is introduced and how a finite element model for it was recreated. The recreated model is validated against existing data from simple load cases. The later half of the chapter shows the design process and final design of the erosion protective solution. For this final solution structural and aerodynamic analyses are done. For the structural analysis, the recreated blade model is used as the attachment target. The aerodynamic analysis is a simple 2D computational fluid dynamics case. All the simulations were run with HP ZBook 15 G5 with a 6-core Intel i7-8750H 2.20 GHz processor, 64 GB of RAM and Nvidia Quadro P2000 graphics card.

3.1 Reference wind turbine blade

For the analysis of the protective solution, the baseline wind turbine blade was chosen to be from the DTU 10 MW Reference Wind Turbine (RWT) [37]. This turbine is well documented and was done as a part of the Light Rotor project between DTU Wind Energy and Vestas. The turbine has also been used in the EU INNWIND [38, 39] project for testing and benchmarking simulation models and developing new technologies for future 10-20 MW turbines.

Specifications of this wind turbine are found in Chapter 3.1.1, and process to recreate the blade's structural model for FEA is explained in Chapter 3.1.2. Validation results of the recreated model are found in Chapter 3.1.3. The blade structural model was recreated using commercial FEA package ANSYS Mechanical [40] together with ANSYS Composite PrepPost (ACP) [41] composite tool for composite definitions of the turbine.

3.1.1 DTU 10 MW Reference Wind Turbine specifications

Specifications of the wind turbine and the blade can be found in Table 4. The DTU 10 MW RWT is an offshore wind turbine for an IEC class 1A wind climate with a rated power of 10 MW. It is in general a traditional three-bladed upwind turbine with a clockwise rotation. The turbine is a variable speed turbine with collective pitch control operating with rotational speeds between 6.0 and 9.6 rpm. [37]

Based on the DTU [37] blade design report the rotor was designed to be relatively lightweight and this to be possible airfoils with high relative thickness were used. For this the FFA-W3 airfoils were the choice, because they are also publicly available and were frequently used in modern MW wind turbine designs. Geometries of the different relative thickness airfoils of the FFA-W3 family are shown in Figure 34. The minimum relative thickness of the airfoils became 24.1% due to the challenge of aerodynamics and to increase stiffness. Also, an airfoil with relative thickness of 60% was created for interpolation between the cylindrical section and 48.0% airfoil. During the design, an analysis showed that in the inner parts of the blade Gurney flaps increased the performance significantly.

Table 4: Specifications of the DTU 10 MW RWT [37] [38].

Parameter	**Value**
Wind regime	IEC Class 1A
Rotor orientation	Clockwise rotation - Upwind
Control	Variable speed, Collective pitch
Cut in wind speed	4 m/s
Cut out wind speed	25 m/s
Rated wind speed	11.4 m/s
Rated power	10 MW
Number of blades	3
Rotor Diameter	178.3 m
Rotor Mass	227 962 kg
Minimum Rotor Speed	6.0 rpm
Maximum Rotor Speed	9.6 rpm
Maximum Tip Speed	90 m/s
Blade Length	86.366 m
Blade Mass	42894.0 kg
Airfoil series	FFA-W3 & Gurney flap

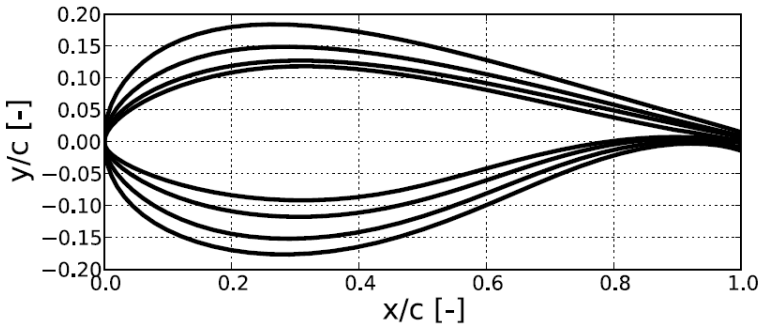

Figure 34: FFA-W3 airfoil shapes with relative thickness of 21.1%, 24.1%, 30.1% and 36% [37].

The blade has a classical approach of load carrying box girder with two shearwebs A and B, with a third shearweb C located close to the trailing edge starting from 21.8 meters of radial position. Representation of the full blade structure can be seen in Figure 35. From this figure the locations of the different blade components can be observed. These different components are used as the basis for the composite layup sequences. [37]

The design is done using glass-fiber reinforced composites and balsa wood as the sandwich core material. Material properties of these are presented in Tables 5 and 6. Layups are defined by stacking-sequence of layers representing multidirectional plies and core. For composite layup definitions the blade is divided to 11 regions circumferentially and 100 sections radially as seen in Figure 35. The layups of the

composites are thus defined in 100 locations across the span of the blade in all the 11 regions. Figure 36 shows three examples of how the composite layups are defined across the span of the blade, for each component with different thicknesses for the materials.

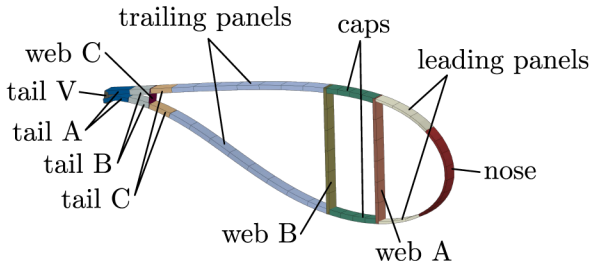

(a) Cross-section of the RWT blade.

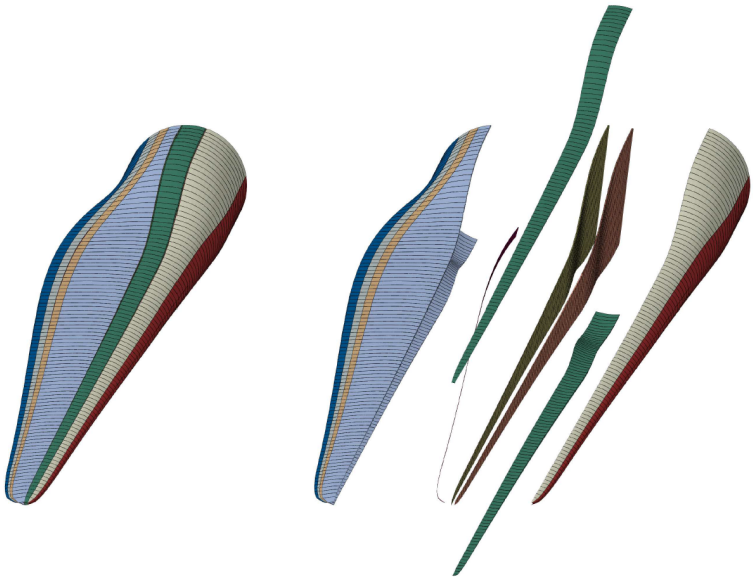

(b) Exploded view of the blade structure.

Figure 35: Blade structure [37].

Table 5: Mechanical properties of the multidirectional plies [37].

Multidirectional Ply	**Uniaxial**	**Biaxial**	**Triaxial**
Young's modulus E_1 (GPa)	41.63	13.92	21.79
Young's modulus E_2 (GPa)	14.93	13.92	14.67
Shear modulus G_{12} (GPa)	5.047	11.50	9.413
Shear modulus $G_{13} = G_{23}$ (GPa)	5.04698	4.53864	4.53864
Poisson's ratio ν_{12} (-)	0.241	0.533	0.478
Density ρ (kg/m^3)	1915.5	1845.0	1845.0

Table 6: Mechanical properties of balsa wood [37].

Property	**Value**
Young's modulus E_1 (GPa)	0.050
Young's modulus E_2 (GPa)	0.050
Young's modulus E_3 (GPa)	2.730
Shear modulus G_{12} (GPa)	0.01667
Shear modulus G_{13} (GPa)	0.150
Shear modulus G_{23} (GPa)	0.150
Poisson's ratio ν_{12} (-)	0.5
Poisson's ratio ν_{13} (-)	0.013
Poisson's ratio ν_{23} (-)	0.013
Density ρ (kg/m^3)	110

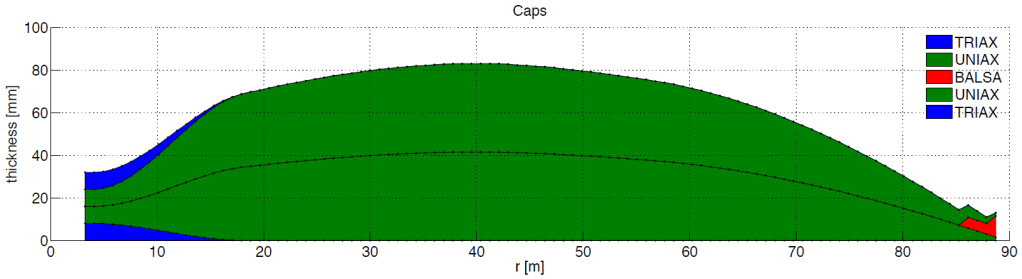

(a) Composite layup sequence of the sparcaps.

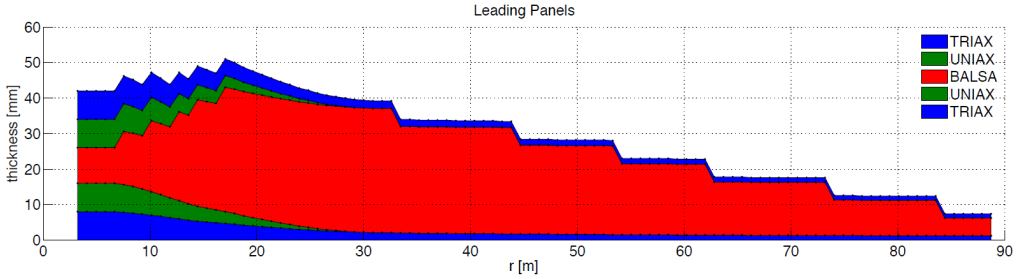

(b) Composite layup sequence of the leading edge panels.

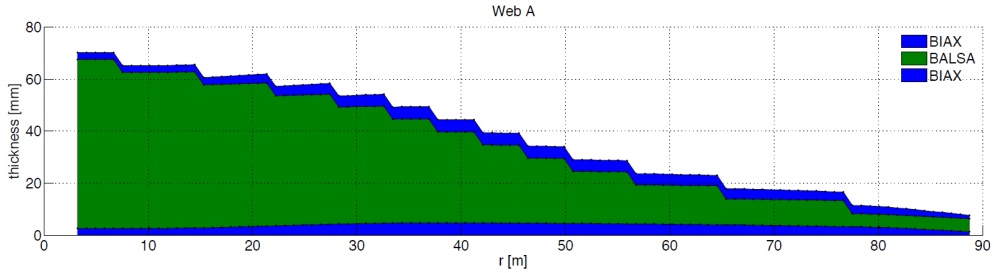

(c) Composite layup sequence of the shearweb A.

Figure 36: Examples of blade composite layup definitions [37].

3.1.2 Recreation of blade structural model

The structural model of the blade was done in ANSYS Mechanical [40] together with the ACP [41] package. Bak et al [42] has a STEP-file available of the turbine blade, which worked as the starting point to recreate a structural model. The 3D CAD file includes all the components as seen in Figure 35.

The model was imported into ANSYS Mechanical, where bonded connections between components were created to unify the blade from the 19 different components. This is to also ensure, that during analysis the blade moves as a whole and no components are separated.

For meshing 3D 4-Node quadrilateral shell elements (SHELL181), without rotational degrees of freedoms and extra shape functions in ANSYS Mechanical, were used [28]. Part of the created mesh of the blade can be seen in Figure 37. It is notable, that the meshing follows the sectioning of the components and conforms the other elements at the edges. Mesh is densest at the tip and gets gradually coarser towards the root of the blade. Some skewed elements can be recognized at the tip areas, but based on the validation in Chapter 3.1.3 their effect is minimal. The final mesh consists of approximately 200 thousand elements.

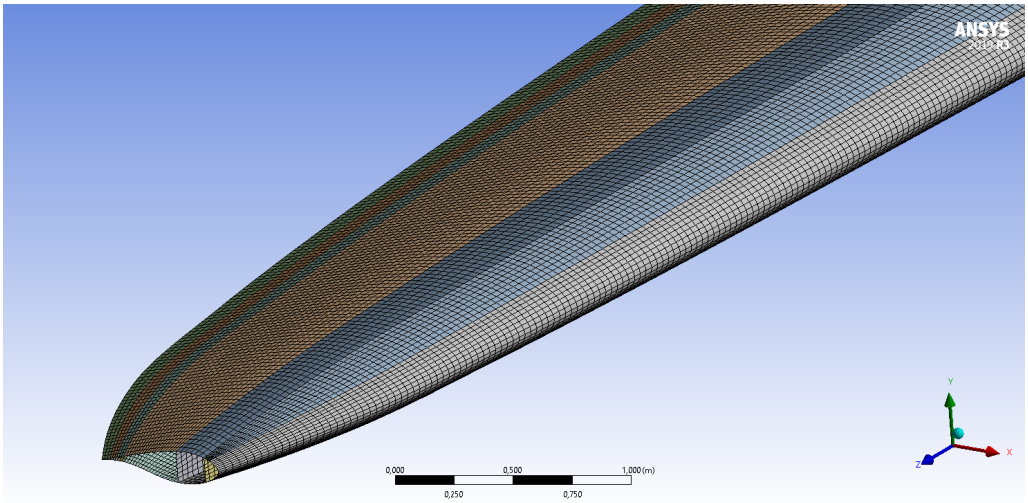

Figure 37: Quadrilateral mesh with shell elements at the blade tip.

ACP was used to define the composite layups along the span of the blade, in all of the components. Layers of 3 or 5 materials were defined based on the layup tables showed in Figure 36 and based on the RWT documentation [37]. The material properties are listed in Tables 5 and 6, these clearly show that the materials are orthotropic.

In ACP [41] by the ACP User's Guide [43] these material properties are given as corresponding engineering constants for individual materials together with a ply type. As can be seen from Figure 36, layering the different materials creates laminates for the different components.

By reviewing Figure 36 in more detail, it can be seen that the stackups vary in the radial direction. As stated in the Chapter 3.1.1, the blade is in 100 sections radially in which the laminates are specified. Thus the laminate definitions in the

recreated model also have a stepwise change, and thus each of the sections have a local z-direction thickness similarly to Figure 16.

3.1.3 Validating blade structural model

To validate the recreated structural model of the DTU 10 MW RWT blade, results from the INNWIND-project were used. Zahle et al. [39] and Lekou et al. [38] represent results to the blade modals and few simple load cases. Part of the project was to benchmark different models and codes, and can thus be used to benchmark the recreated shell model of the blade. For all the validational analyses the blade is clamped from the root section. For the point load case the blade is subjected to point load at the tip of the blade in the elastic center and for the line load the load path goes along the span of the blade through the elastic centers.

Table 7 represents the frequencies of the different blade modes from the recreated model and the results from INNWIND [39]. In the table are presented results from DTU, Politecnico di Milano (POLIMI) and National Renewable Energy Centre (CENER), which all used 3D FE models for the analysis. It is notable how closely the recreated model follows the results by DTU and POLIMI. This indicates that the model behaves similarly to the benchmark models, and maximum difference to the DTU results being 3%.

Table 7: Modal frequency (Hz) results of the recreated blade and comparison to INNWIND [39] results from CENER, POLIMI and DTU.

Mode	**CENER**	**POLIMI**	**DTU**	**Recreated model**
1 (Hz)	0.62	0.61	0.62	0.61
2 (Hz)	1.01	0.91	0.98	0.95
3 (Hz)	1.8	1.74	1.75	1.75
4 (Hz)	3.02	2.77	2.98	2.83
5 (Hz)	3.77	3.55	3.53	3.57
6 (Hz)	6.24	5.67	5.49	5.59

On top of validating the blade model modal shapes, validation was also done on two simple bending cases. Figure 38 shows the results of the blade under the influence of a 9000 N/m line load along the span of the blade, and Figure 39 shows similar results for a 100 kN point load at the tip of the blade. The results are combined with results from Lekou et al. [38] from the INNWIND-project. Here the Cp-lambda, NEREA and hGAST are the various codes used in the model validation as a part of the INNWIND-project.

Looking at the Figures 38 and 39, it is notable that the recreated model follows closely the other models presented by Lekou et al. [38]. In the flapwise direction for both cases the recreated model follows all the other models nicely, but in the tip shows slightly higher values of deflection. This is especially in the point load case, where the difference of the tip deflection is the highest. In the edgewise direction the

recreatd model again follows well the models presented in the INNWIND-project, but again the tip area is slightly different.

For these cases the recreated model slightly underestimates the deflection at the edgewise direction further away from the tip and overestimates closer to the tip regions. In the flapwise direction the recreated model slightly overestimates the results for the length of the blade. Largest variations for both cases in the respective directions were closer to the tip regions. For the line load case the differences at the tip for flapwise and edgewise deflection in comparison to the Cp-Lambda model were 3.0% and -2.5% respectively. Similarly, for the point load case the differences of the tip deflection were 4.5% and -1.5% for the flapwise and edgewise directions in comparison to the HAWC2 model.

For the scope of this thesis, it can be stated that the recreated model represents closely enough the original DTU 10 MW reference blade. For the major parts of the blade, the behaviour is similar to the other models represented in the INNWIND-project by Lekou et al. [38]. Major sources of error most likely comes from the modeling of the recreated blade. There could be slight differences in how the materials are defined in the spanwise direction for the components. This could present a slight difference of stiffness of the blade, especially closer to the tip. This recreated model, with the stated error percentages to the validation cases, were used for the analysis of the designed erosion shield presented in Chapter 3.3.

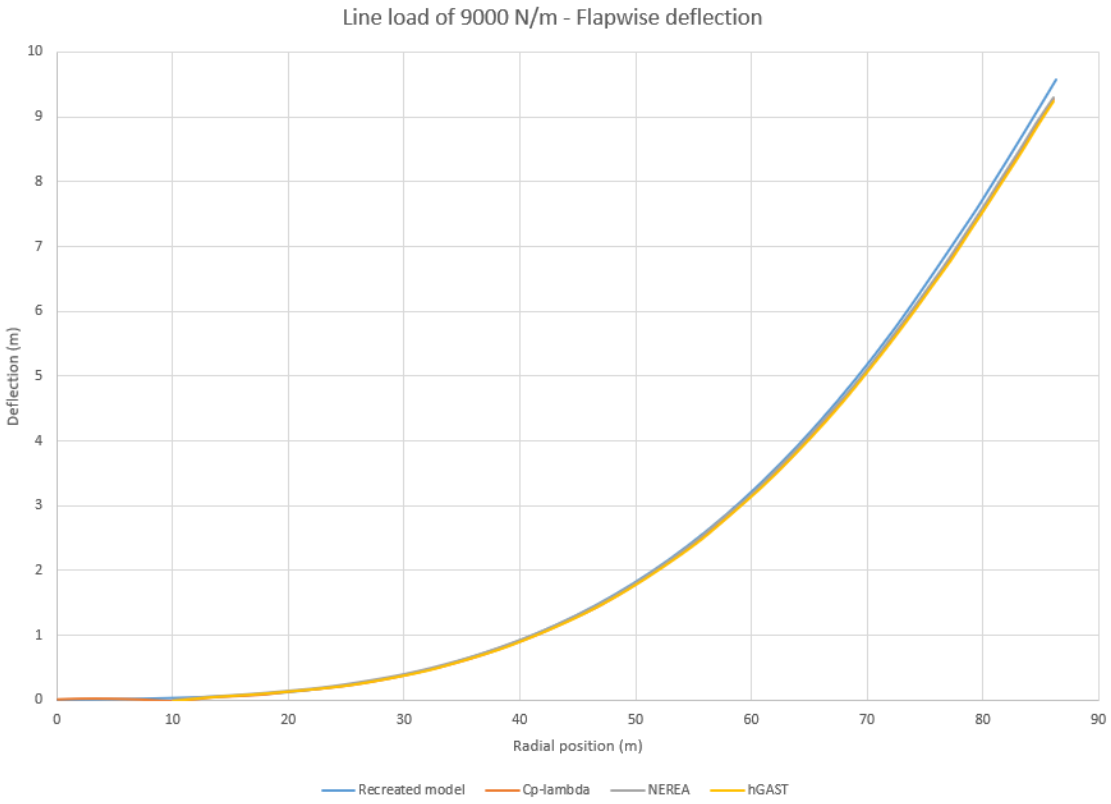

(a) Flapwise displacement.

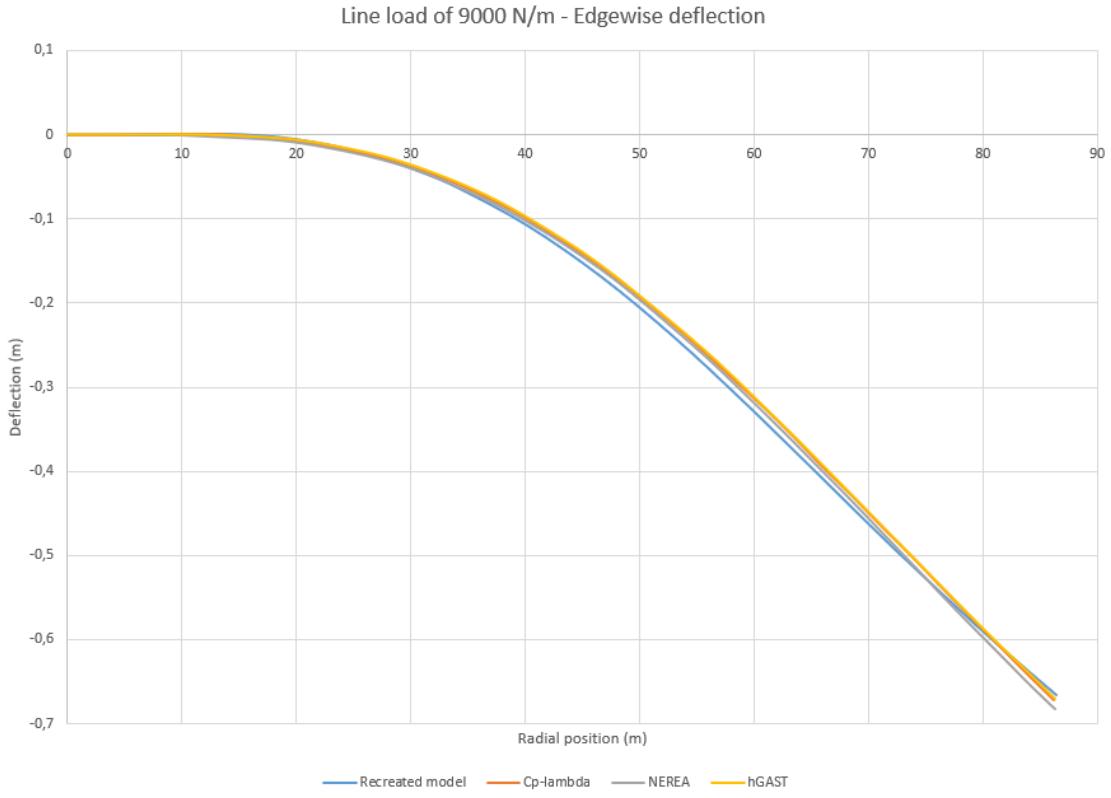

(b) Edgewise displacement.

Figure 38: Line load validation.

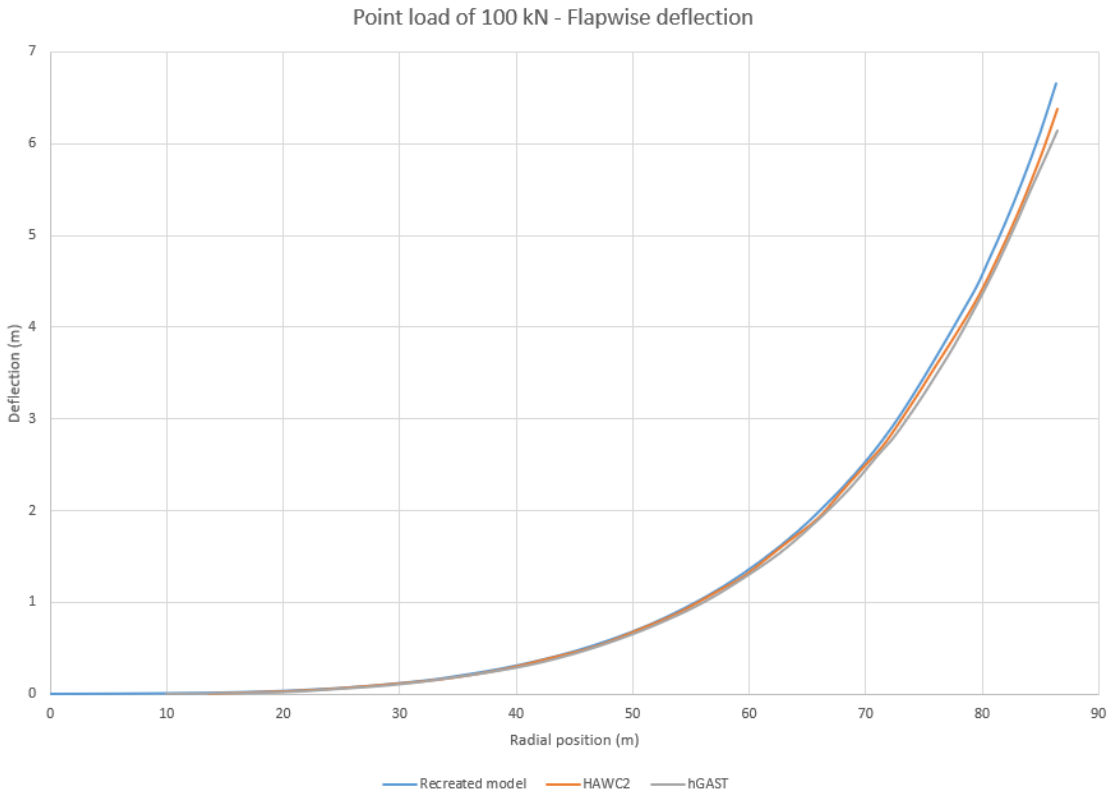

(a) Flapwise displacement.

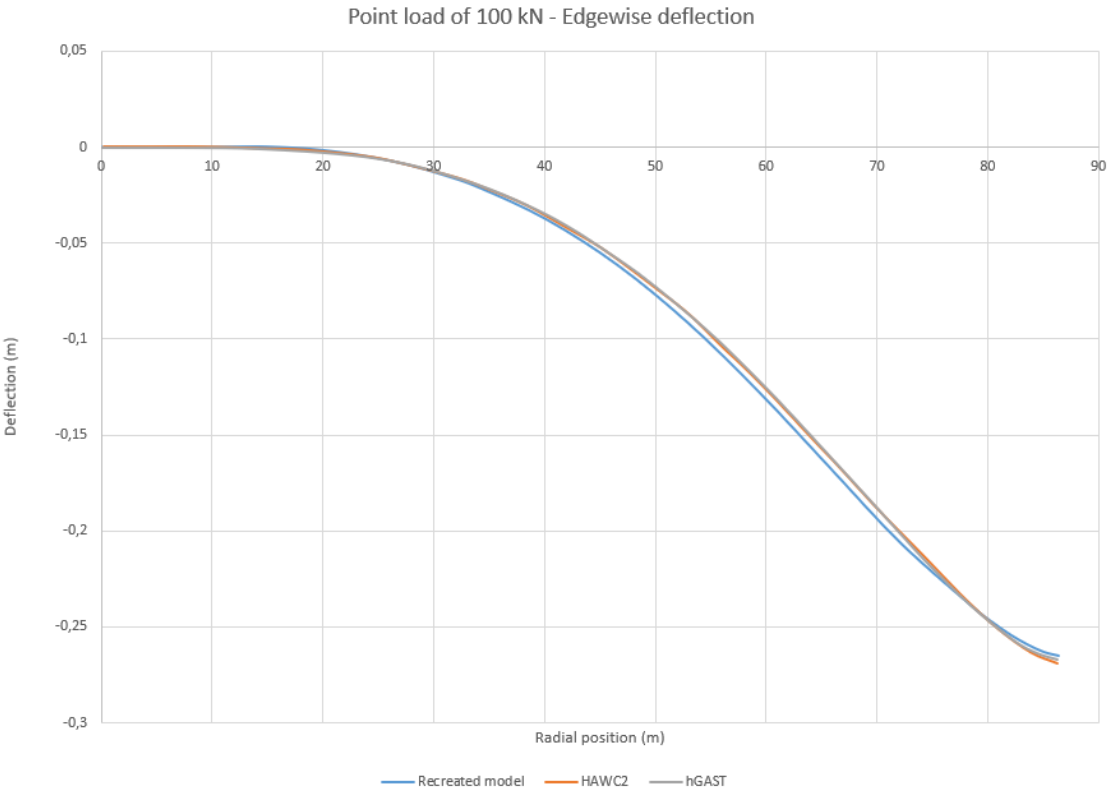

(b) Edgewise displacement.

Figure 39: Point load validation.

3.2 Design of the erosion protective solution

Good starting point to finding new ideas and novel concepts is to use a systematic approach commonly used in product design. One common of these is brainstorming, but in this case to help create creativity, a method called ACCREx developed by Breedveld [44] was used. Initially a list of requirements were created to limit the solution space of the design and have a clear understanding what the solution needs to fulfil. For the created design structural analyses for ultimate load and fatigue life are done to verify that it fulfils the mechanical requirements. Finally a simple 2D CFD analysis is done to study the effect of the backwards facing step forming on top of the airfoil.

3.2.1 Requirements

The initial task was to design a metallic retrofit lifetime solution to protect wind turbine blades from erosion. While design process could be started with just this statement, more requirements are beneficial to figure out. The initial task itself is already quite well abstracted and some of the requirements can be extracted from that.

It is true that the solution must protect the wind turbine blade from erosion, but it is only necessary in a limited section of the blade. Also, a lifetime solution in this case means the lifetime of a wind turbine, which is designed to be between 20 and 25 years. [2]. For the lifetime of the solution it would also have to sustain all structural loads during the operation of the wind turbine. Wind turbine blades' aerodynamics are also precisely optimized and hence the protective solution should have a minimum effects on the aerodynamic properties. The material is to be commercially available Nickel-Cobalt alloy that is already used in variety of aerospace applications. Finally, the solution is to be possible to retrofit into existing wind turbines.

List of the requirements for the erosion shield design:

- Protect the parts of the blade leading edge susceptible to erosion
- Lifetime 20-25 years
- Sustain fatigue loads during operation
- Sustain ultimate loads during operation
- Minimum effect on the blade aerodynamics
- Material: commercial Nickel-Cobalt alloy
- Ability to retrofit to existing wind turbines

These requirements are a good starting point on the design process, and give clear limits for the design space. They also give a clear indication which analyses are crucial, in order to determine the performance of the design and decide what kind

of changes would be required. The material decision raises few additional limits for the design due to the mechanical properties. Doncasters have provided metallurgical data for their Nickel-Cobalt material of which the relevant are represented in Table 8. Values represented in the table are used for the material properties during modeling and design values for the solution.

Table 8: Doncasters Nickel-Cobalt alloy mechanical properties [45].

Property	**Value**	**Tol (±)**
Young's Modulus (GPa)	160	30
Ultimate tensile strength (MPa)	1600	210
Endurance limit SE	430	-
Density (kg/m^3)	8890	-

3.2.2 Design of the solution

ACRREx is a design method to help create creativity presented by Paul Breedveld [44] from TU Delft. The acronym ACRREx stands for Abstracting, Categorizing, Reflecting, Reformulating and Extending. The method is a systematic design method which uses categorization of knowledge in order to find voids in the knowledge and giving chances for innovative solutions to be found in those voids. ACRREx is also possible to combine with other intuitive design methods such as brainstorming or bio-inspired design.

In this thesis, ACRREx was applied to explore the design space for the erosion protective solution. This is done by splitting the full solution into individual functions which it is formed of. For an optimal solution the functions, to find solutions for, are the following: increase lift, decrease drag, sustain ultimate loads, sustain fatigue loads and attach into a blade. The full ACRREx table created is presented in Figure A1 in Appendix A.

It is notable to see from the Figure A1, that in industry solutions, there aren't much voids to be filled. For this solution combining existing solutions for individual functions was used to generate the proposed solution. It is also to be pointed out that biology has a lot of interesting solutions to offer and research more, and in biology there are certain voids present in the solutions matrix. While looking into solutions in biology it's important to remember, as pointed out by Vogel [46], that there are key differences in the philosophy of designs between biology, and what humans have generated. One crucial difference is that biology tends to generate structures that are less stiff and bend in order to minimize effects from high loads, while human create structures tend to be stiff and rigid. [46]

The optimal solution should obviously incorporate all the functions listed for the solution, but for the scope of this thesis, the aerodynamic add-ons were deemed unfeasible and mainly structural solution is explored. The solution created is a thin modular shield structure covering the leading edge of the blade and attached with an adhesive. Shield design can be seen in Figure 40. Each of the segment is 60 cm

in length and follows the profile of the blade's leading edge. Shield is 0.5 mm in thickness, which should be able to protect the blade from erosion effectively, have sufficient structural strength and minimize the aerodynamic effects.

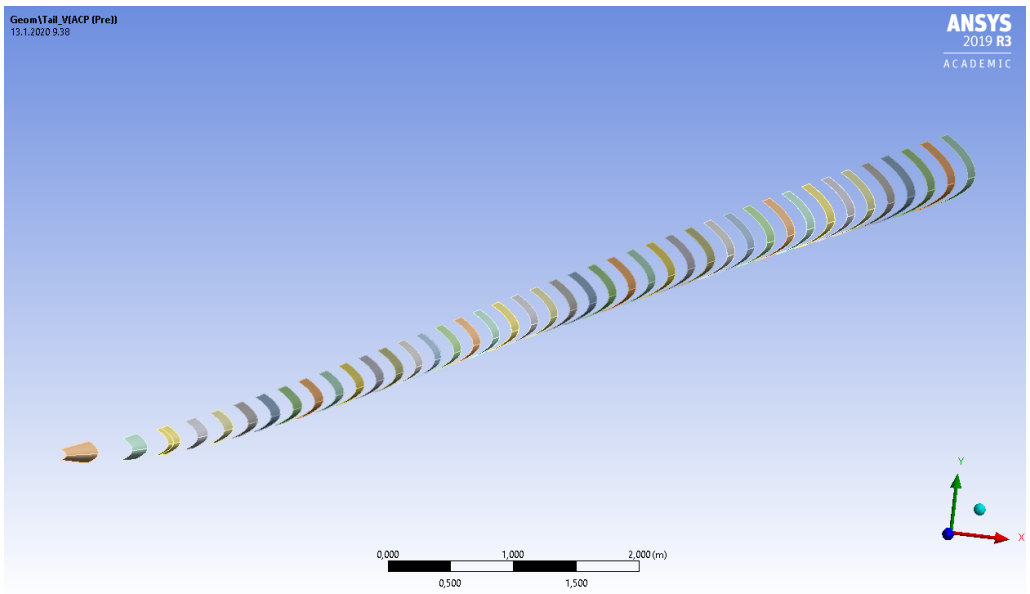

Figure 40: Final design of the created protective shield.

Segmenting of the shield was inspired by looking into the threespine stickelback [47], which has an interlocking armor structure to protect it. This is an interesting solution to allow movement between each of the segments, which then helps to mitigate high loads from large deformations. If the solution was a single piece it would have to be thicker in order to sustain the stresses, meaning increasing weight. This would lead into a contradiction of improving sustained loads by increasing weight. By the principles of TRIZ40 method by Altschuller [48], this is solved by segmenting the object. Now that the solution is already segmented, this contradiction is avoided. This also helps with the installation of the solution in comparison with a single large piece. In the scope of this thesis the interlocking structure between elements is not analyzed, due it leading into high details and complexity of geometry.

3.3 Structural analysis of the protective solution

For structural modeling of the designed solution ANSYS Mechanical [40] was used. The designed shield was attached to the reference blade defined in Chapter 3.1. All the loads were defined onto the blade's structure to represent more closely the behaviour the shield will experience during operation. This chapter defines the structural model of the shield attached onto the blade and the load cases for ultimate loads and fatigue life.

3.3.1 Solution structural model

The shield defined as the result of the design from the earlier Chapter 3.2.2 was created in CAD. A thin structure of 0.5 mm was extruded from the blade leading

edge and trimmed to proper length of 30 meters. This was then split into 60 cm long parts to represent individual modular piece of the shield.

The created 3D model was imported into ANSYS and connected to the recreated reference blade. The durability of the bonding was not in the scope of this thesis, so the shield and the blade are bonded and no separation during analysis is allowed. The reference blade used the mesh created earlier in Chapter 3.1.2 using shell elements. Since the created shield is relatively thin structure, shell elements could be used, but in this case the model is created as a solid and ANSYS offers solid-shell (SOLSH190) elements for these kinds of structures. The final geometry and mesh of the shield is shown in Figure 41. The mesh of the shield is approximately 174 thousand elements making it relatively dense in comparison to the mesh of the blade.

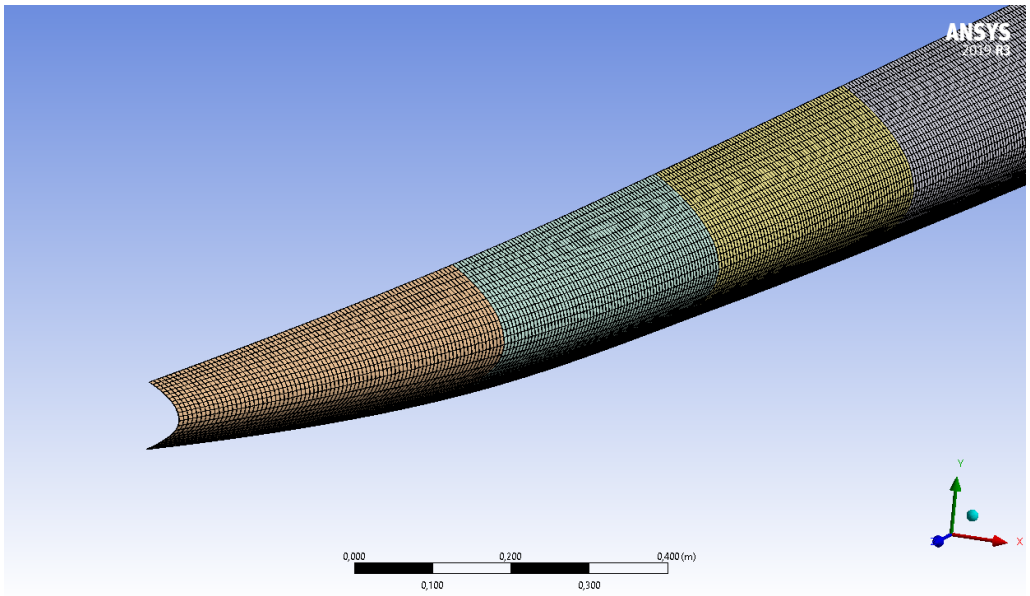

Figure 41: Final solid-shell element hexahedral mesh of the designed protective shield tip region.

As explained in ANSYS Mechanical APDL Theory Reference [28] the solid-shell element is a 3D solid element free of locking in bending dominant situations, and unlike shell elements can be directly connected with other continuum elements. Shape functions for the solid-shell elements are identical to those of an 8-Node brick element without extra shape functions.

Hence, the solid-shell elements have a thickness and has 2-integration points through the thickness. In addition, as by the Theory Reference [28], they utilize special kinematic formulations, which includes assumed strain method to overcome locking when the shell thickness becomes small. Additionally, the element employs enhanced strain formulations to improve the accuracy in in-plane bending situations. Finally, the element allows for parabolic enhanced transverse shear strains and the stresses are then calculated from the enhanced shear strains. [28] An isotropic material was used for the shield material model which material parameters were taken from Table 8.

3.3.2 Ultimate load case

The standards described in Chapter 2.3.1 for evaluating structural integrity of a designed wind turbine defined transient FSI cases. Due to the limitation of computational resources, it was deemed that it is not viable nor required, and it was chosen to define a static load cases resembling the load distributions a blade would experience.

From the DTU design report [37], it can be observed that the maximum tip deflection of 12.4 m happened for the DLC 1.3 which is a power production case. In the appendix of the document, for each of the spanwise sections, a maximum bending moment and corresponding forces are represented for a full turbine analysis case. The data is presented as maximum forces for each direction, maximum resultant force, maximum bending moments for each direction and maximum resultant bending moment. This information was used as the basis to create the force distribution along the span of the blade for a realistic load shape. The forces were defined by components in the x, y and z-directions. Choosing the values from these required some scaling in order to be matched with the corresponding tip displacement value, as they are for the full turbine with a tower from a transient case. For all structural analyses the root of the blade was clamped.

For the ultimate load case the final distribution can be seen from Figure 42, yielding tip deflection of 12.49 meters. It is notable, that for the power production case the rotation plays an effect on the loads in the z-direction. This case is used to analyse stresses forming in the designed shield during ultimate load conditions. The loads are defined on the elastic center for all the 27 different cross-sections.

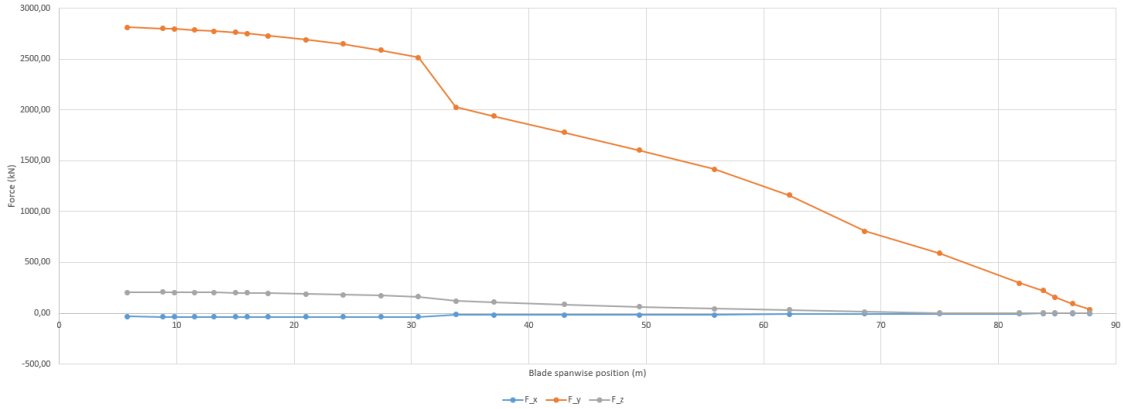

Figure 42: Distribution of forces for each cross-section for the ultimate load case.

3.3.3 Fatigue life case

Similarly to ultimate loads, for the fatigue life case it was observed from the DTU design report [37] that the most severe tip deflections for fatigue cases were from DLC 2.4 yielding 7.86 meters. Defining the case for fatigue life was done similarly as in ultimate load case, by scaling the defined load distribution properly. The load distribution for fatigue life case can be seen in Figure 43, which yields tip deflection of 7.81 meters.

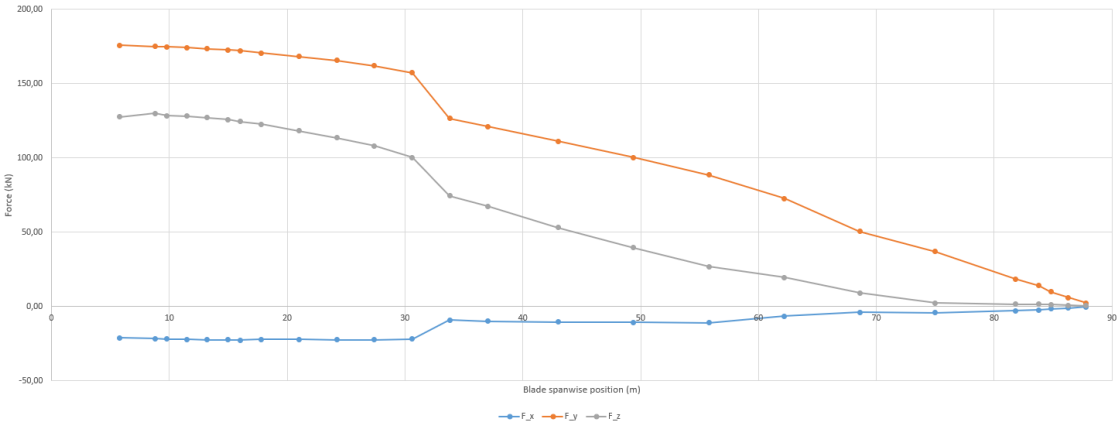

Figure 43: Distribution of forces for each cross-section for the fatigue load case.

For the analysis of fatigue life the lowest value of endurance limit from Table 8 is used to verify does the solution fulfil the requirement of fatigue life. As defined by Ashby [49], the endurance limit is the stress amplitude below which fracture does not occur, or occurs only after a very large number of cycles. This is illustrated in Figure 44. For this purpose, it is assumed later that the loading for fatigue life goes from 0 to the analysed stress value in Chapter 4.1.2.

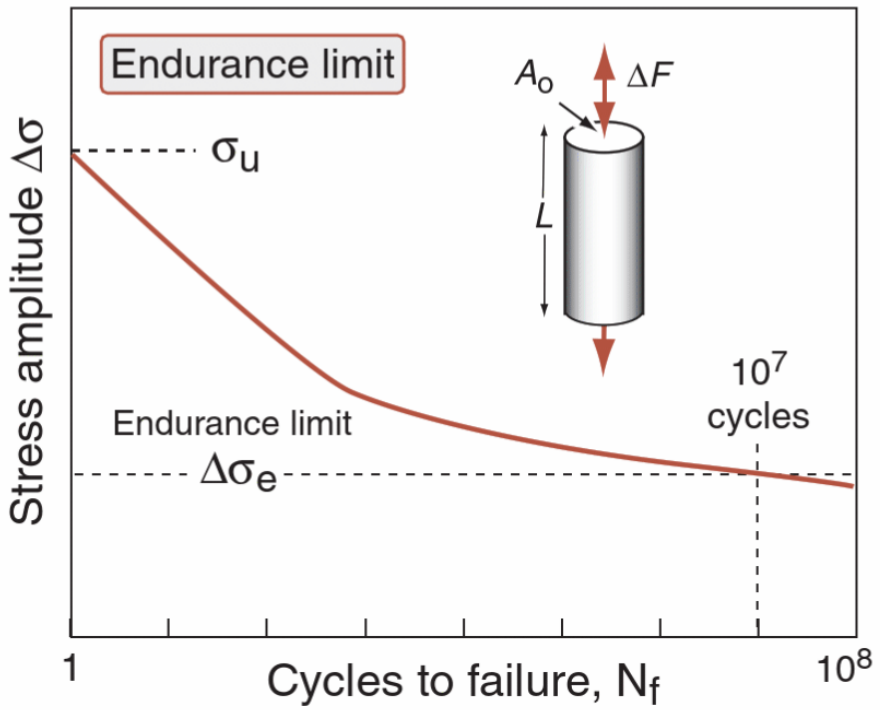

Figure 44: Illustration of endurance limit by Ashby [49].

3.4 Aerodynamic analysis of the protective solution

For the numerical fluid modeling of the blade a commercial CFD package ANSYS Fluent [50] was used to analyse the FFA-W3-241 airfoil with and without the added shield geometry. The reference airfoil data for the FFA-W3-241 is from Björck [51] and the used geometries are showed in Figure 45. In this case the airfoil was modeled to be 2 meters in length to represent a section of the DTU 10 MW blade in which a shield geometry of 1 mm thick was added. The shield covers the leading edge until 8.75% of the chord of the airfoil. The shield forms a backwards facing step which is seen in Figure 45b.

A domain was created around these geometries, which is shown in Figure 46. The height of the domain was 90 meters, length of the straight part 40 meters and the radius of the semi-circle 45 meters. The airfoil was located in the middle with a refinement zone created around it and the area of its wake. The refinement zone begins 1.25 meters ahead of the airfoil and continues until the outlet. It is also 4.2 meters in height. Boundary conditions for the domain were velocity inlets at the semi-circle boundary and also at the farfield walls. Pressure outlet was used at the back wall and airfoil is modeled as a no-slip wall.

An unstructured mesh was created for the domain seen in Figure 47. Coarser mesh was used at the domain edges which refined gradually closer to the refinement zone. A prismatic layer was formed around the airfoil to capture the boundary layer of the flow, and more refined zones were generated at the flat tail and around the shield steps.

For the initial mesh the inlet and farfield edges had element size of 3 meters and the global element size was 1 meter. The airfoil surface was divided into elements of 0.01 meters in size and the flat trailing edge divided into 20 elements. The steps were discretized with 15 elements. For the refinement zone element size of 0.1 meters was used. A surface mesh for the airfoil was created with the first layer being 1E-5 meters in height, maximum layers are 30 and growth rate was defined as 1.2. These values yielded a mesh of approximately 100 thousand elements. For the final analysis grid independence study was done and the results are shown in Chapter 4.2. For this the mesh was gradually refined up to 3 times. Similar value were used for the clean airfoil without the use of the step elements. Figure 48 shows in more detail the mesh around the airfoil with and without the shield.

For this analysis the K-Omega SST was chosen for the turbulence model for it being widely used in the field. The analysis was also run with constant density for the Mach number being under 0.3, where the flow can be assumed to be incompressible [52]. The energy equation was also used. Reynolds number of 12 million was chosen to for the analysis based on the similar CFD results presented in the DTU design document [37], this also represents the conditions during operation. Angle of attack for the case were 6 degrees which is close to how the blade is operated and is also presented in the CFD results by DTU [37].

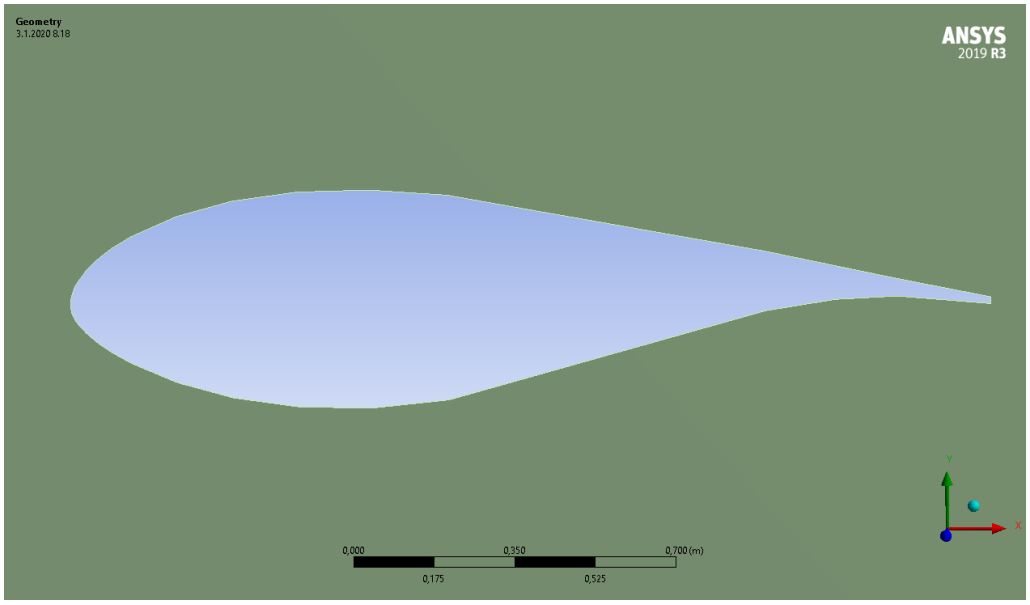

(a) Geometry of the clean FFA-W3-241 airfoil.

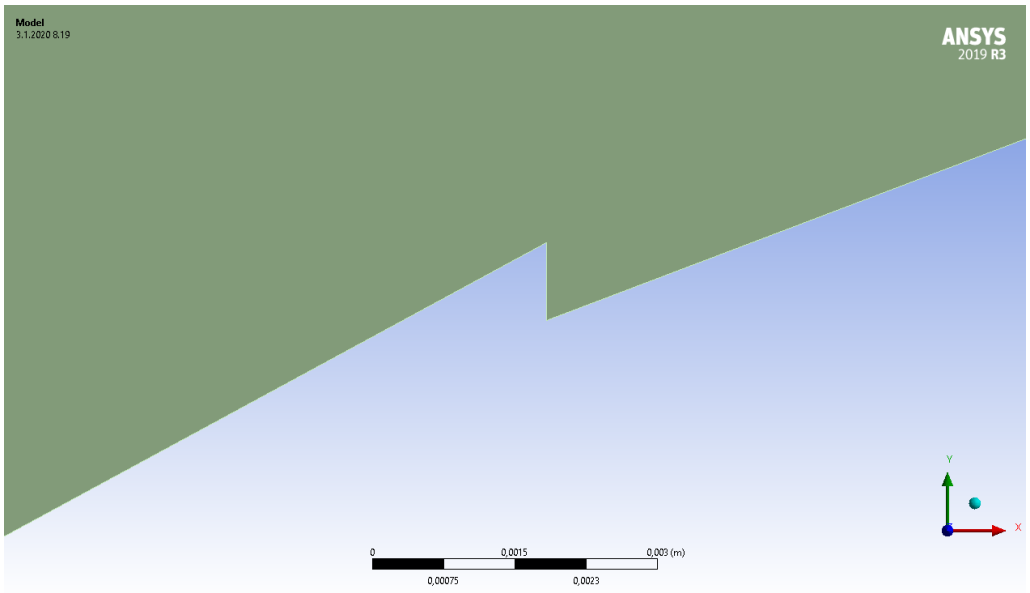

(b) Representation of the step added to the leading edge and creating a backwards facing step.

Figure 45: Geometry for the 2D CFD case.

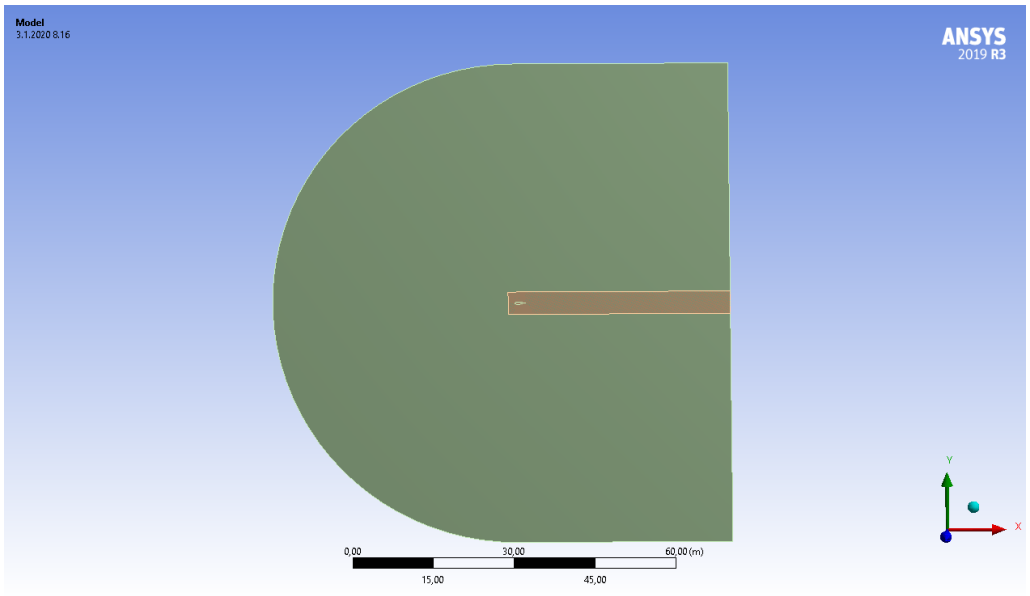

Figure 46: Calculation domain for the 2D CFD case.

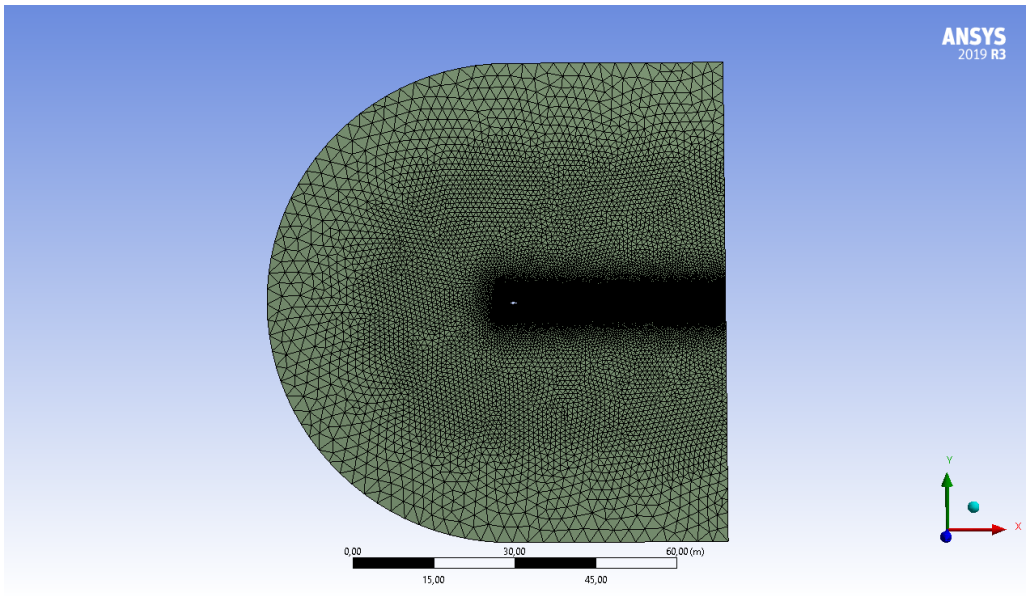

Figure 47: Unstructured mesh for the 2D CFD case.

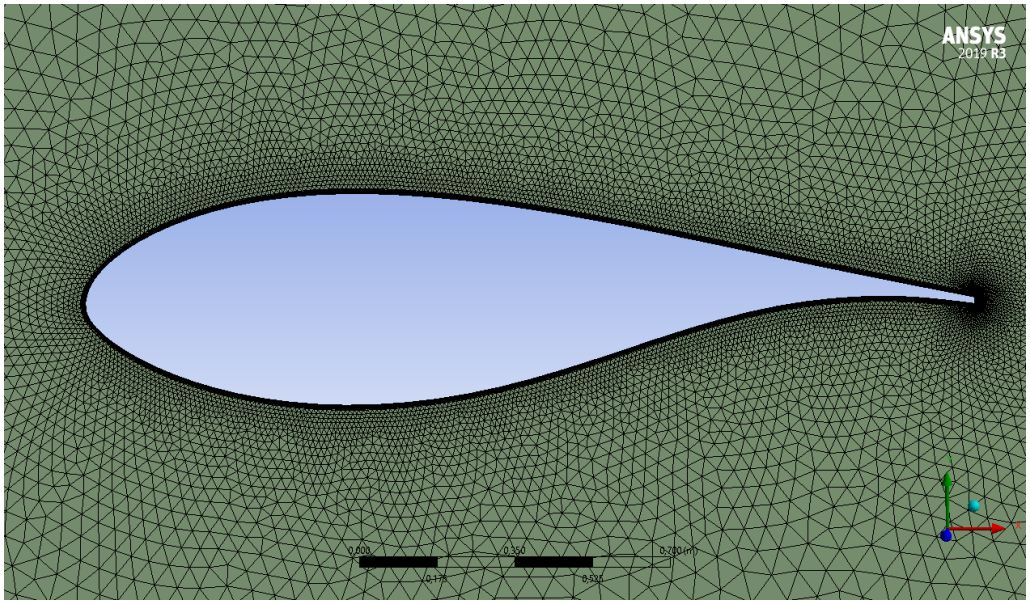

(a) Mesh around the clean FFA-W3-241 airfoil.

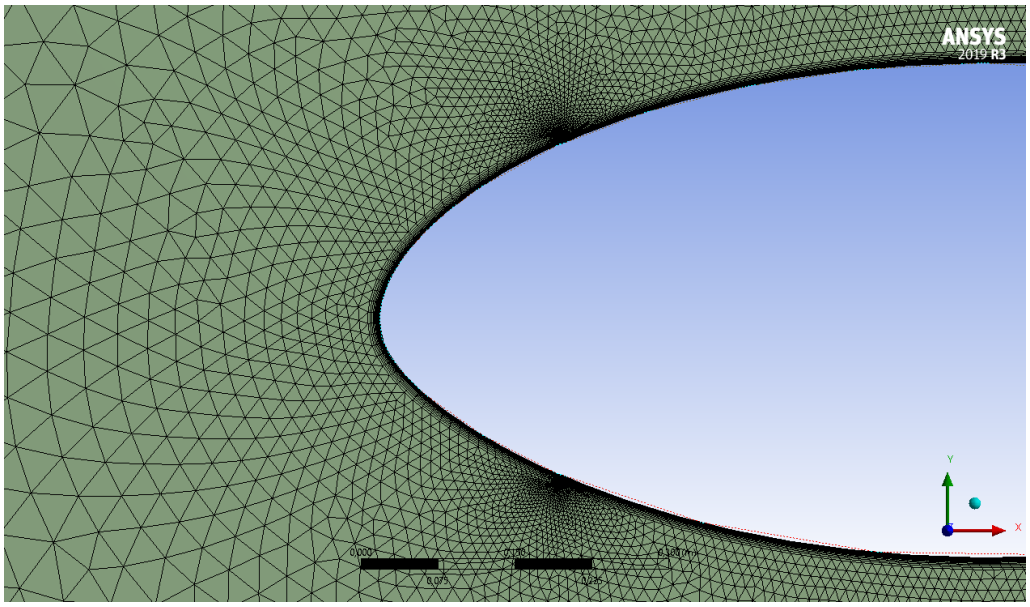

(b) Mesh at the leading edge of the airfoil with the added shield.

Figure 48: Mesh around the airfoils for the 2D CFD case.

4 Results & Discussion

This chapter presents the results of the analyses presented in the previous chapter. Beginning from the structural analyses, both ultimate and fatigue load cases, for the erosion shield. Chapter ends with the results from the CFD analysis and further discussion of the results.

4.1 Structural analysis results

This subsection presents the structural results for the analyses defined in Chapter 2.3. Chapter 4.1.1 represents the results for the ultimate load case and Chapter 4.1.2 the results for the fatigue life case. Both of the analyses were run with the FE-model presented in Chapter 3.3.1.

Doncasters [45] alloy was initially chosen for the solution. The metallurgical data provided clear material properties and unlike others also represented the value for the endurance limit. For the analysis additional information of yield strength is required. For the ultimate load case yield strength of NiCoForm NiColoy® [53] alloy was used. The value for this is 827 MPa. Otherwise the performance of this alloy is inferior of the Doncasters', but provides a value for yield strength which was deemed to be sufficiently close.

4.1.1 Ultimate load analysis

Figure 49 represents the displacement of the whole blade with the shield attached. It is to be pointed out, that with this load case setup the blade experiences mainly flapwise bending, with a significant edgewise contribution, but also some spanwise elongation due to the rotational forces.

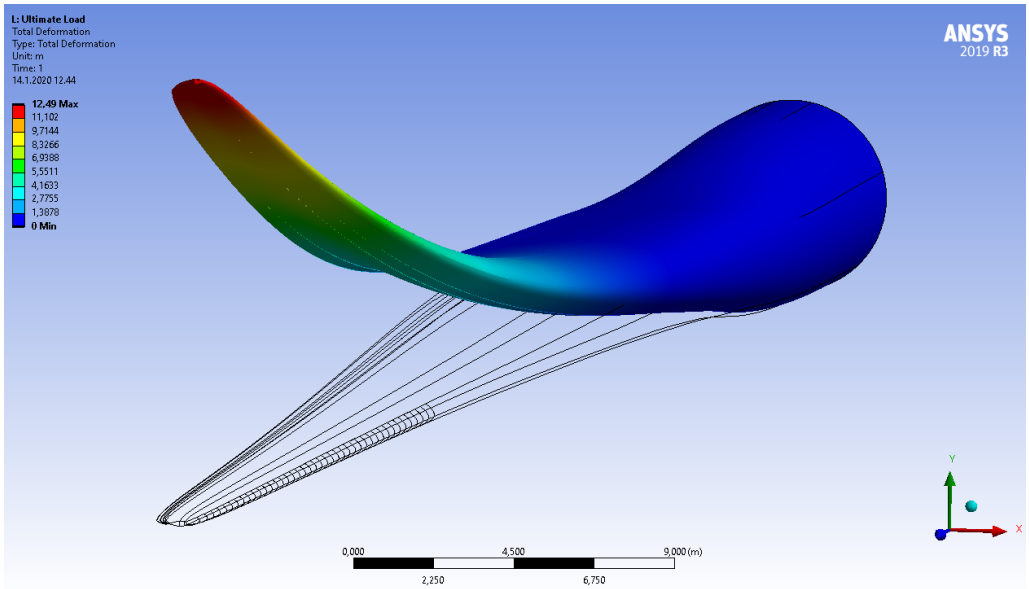

Figure 49: Displacement of the blade during ultimate load case with the shield attached.

Figure 50 shows the stress distribution across the erosion shield elements for the ultimate load case. The stress distribution is represented both with automatic scaling as seen in Figure 50a where the high stress regions can be recognized, and in Figure 50b scaled in accordance to the supplemental yield strength value.

What is notable to recognize from the Figure 50, is that the maximum value of 420.5 MPa is almost half of the defined yield strength of 827 MPa. So, as the basis of this load case it can be stated that during operations and predefined load conditions the designed shield would not yield in operation, assuming that the bonding of the shield pieces hold.

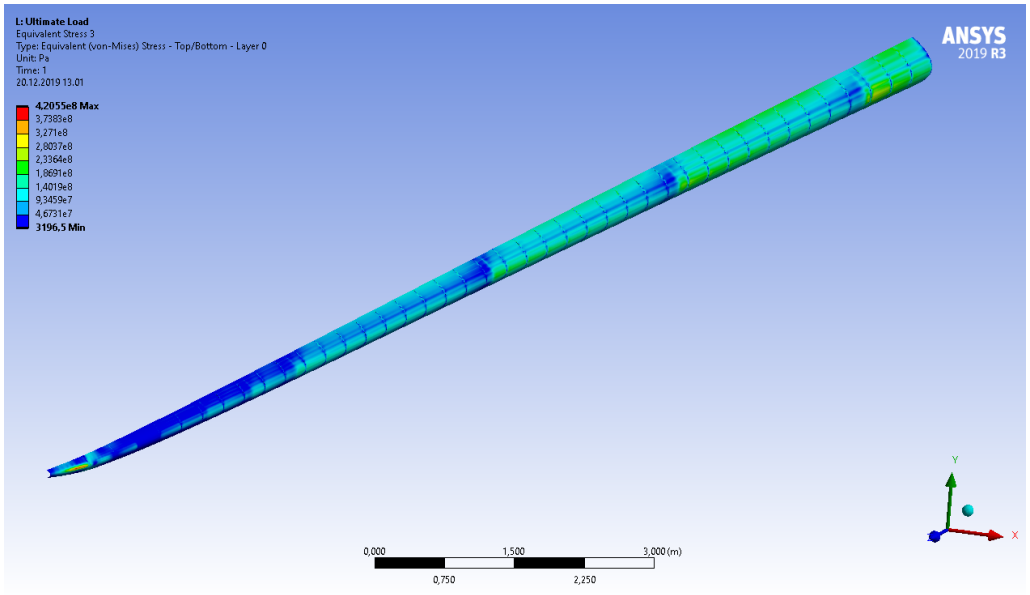

(a) Automatic scale for stresses.

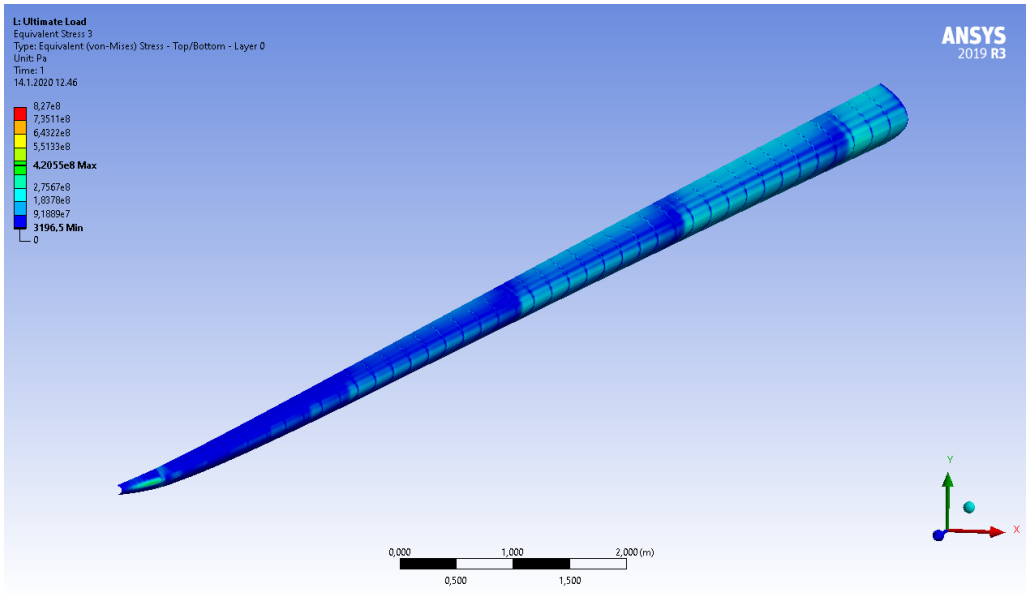

(b) Stresses in comparison to the yield strength.

Figure 50: Shield stresses during blade ultimate load case.

4.1.2 Fatigue life analysis

Again similarly to the ultimate load case, Figure 51 represents the deflection of the blade during the fatigue load case with the shield attached. Since the load distributions are similar in shape but has different magnitude the main difference is the amount of deflection.

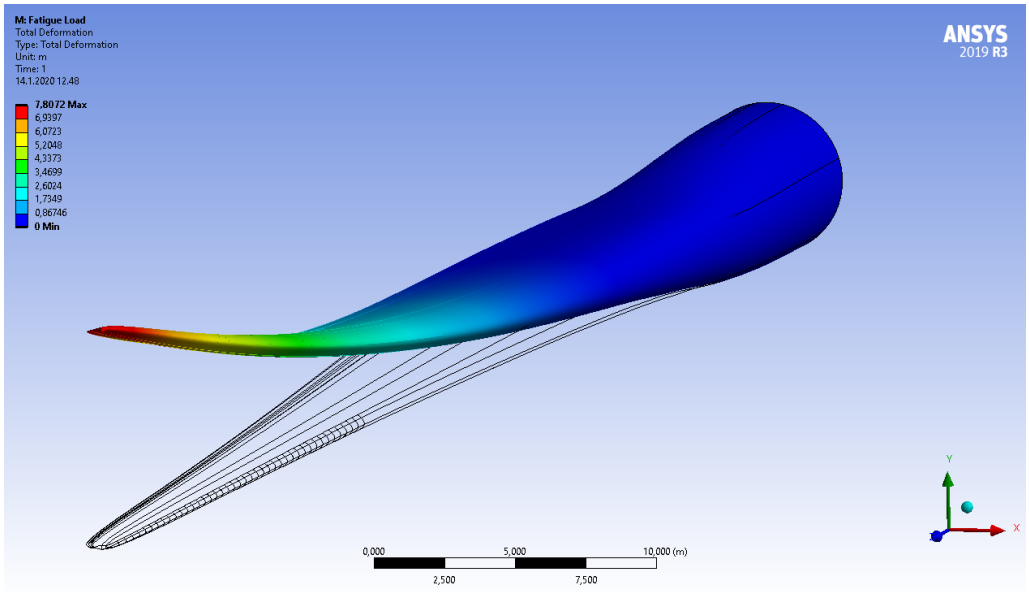

Figure 51: Displacement of the blade during fatigue life case with the shield attached.

Figure 52 shows the stresses in the shield during the fatigue load case. Figure 52a again has the automatic scaling for stresses where the high stress concentration areas and maximum stress value can be recognized. Figure 52b has the stress values scaled against the endurance limit of 430 MPa.

From these figures it can be seen that the highest stress of 221 MPa is under the endurance limit of 430 MPa specified for this material. Referring back to the Figure 44 by Ashby [49], this would mean, by assuming that the stress amplitude goes from 0 to the highest value of 221 MPa, that a fracture and fatigue failure would not occur or would occur after a very long operation. It can also be assumed that all the other fatigue load cases would yield lower stresses and thus also fulfilling the requirement of fatigue life.

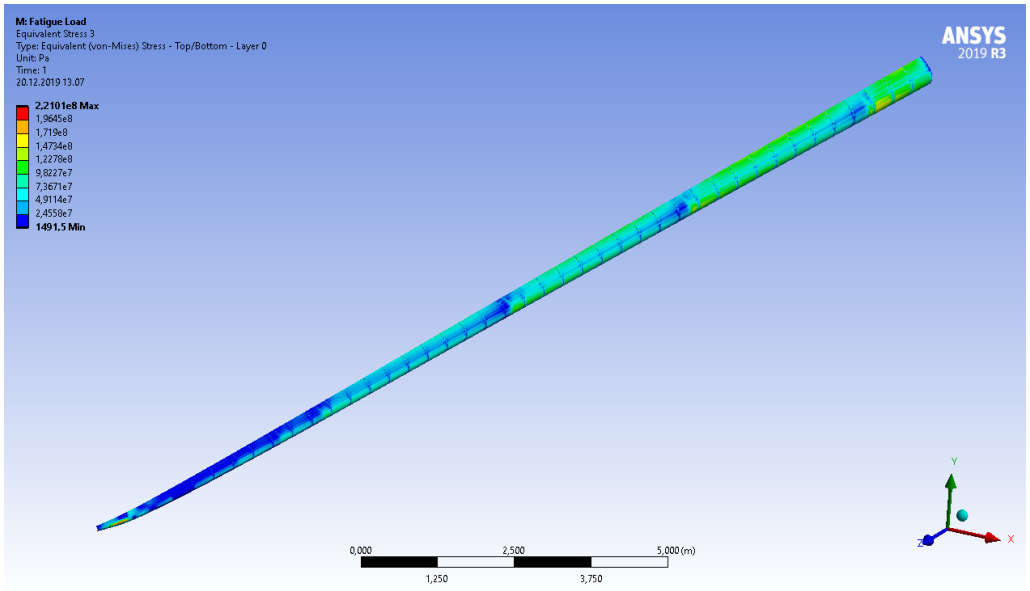

(a) Automatic scale for stresses.

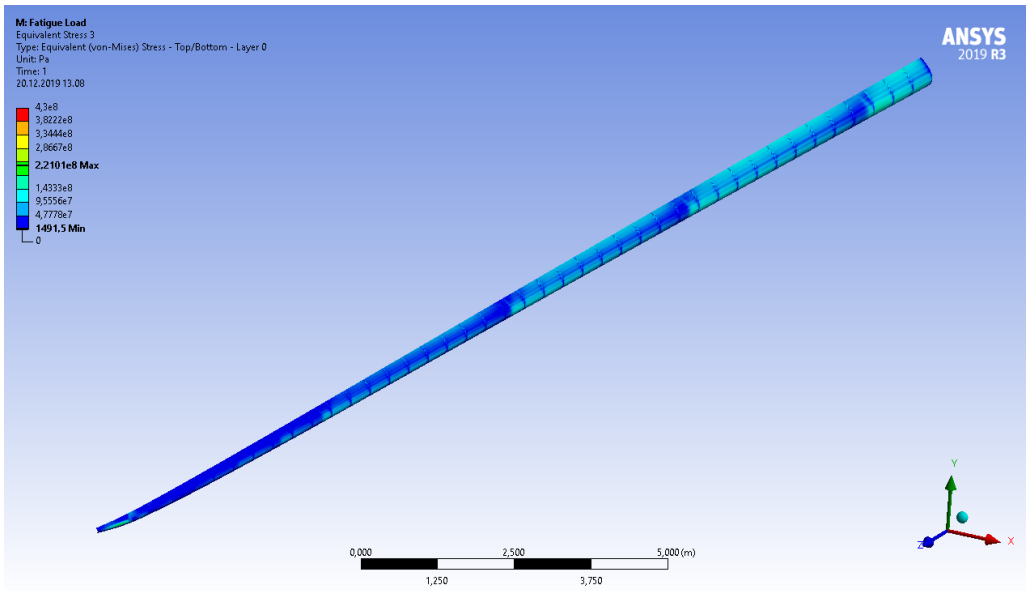

(b) Stresses in comparison to the endurance limit.

Figure 52: Shield stresses during blade fatigue load case.

4.2 Aerodynamic analysis results

The results for the 2D CFD analysis are presented in this chapter. The ran cases were the FFA-W3-241 airfoil as a clean version and then with an added shield geometry. The shield geometry is offsetted from the geometry of the leading edge and forms the backwards facing step as seen in Figure 45b in Chapter 3.4.

A grid independence study was done for the CFD cases, and results of these are presented in Figure 53. For both cases the converge of lift coefficient happens with lower grid densities, as can be seen from Figure 53a. For the drag coefficient the convergence requires the higher grids of 1-4 million elements to have a difference less than 3%, so that grid convergence can be said to be achieved. For the clean airfoil the differences of 1-4 million elements for C_L is -1.16% and for C_D -2.78%. Similarily for the airfoil with shield C_L -0.019% and C_D -1.32%. For final evaluation the values from grid with 4 million elements were used.

The final results for C_L and C_D between the two cases are presented in Table 9. From these results it can be observed, that adding the shield with thickness of 0.2% of the chord decreases the C_L by 1.32%. The C_D on the other hand remains practically the same.

Table 9: Aerodynamic coefficients for clean airfoil and airfoil with the added shield.

	Clean	**Offset**	**Difference (%)**
C_L	1.069	1.055	-1.32
C_D	0.0136	0.0135	-0.13

The Figures 54 and 55 represent the pressure and velocity fields around the FFA-W3-241 airfoil with the shield added. At this scale the effect of the step isn't observable as its thickness is only 0.2% of the chord. The Figure 56 shows what the velocity field with the step looks close to the airfoil on the suction and pressure sides. From this figure, it can be observed that the step is confined in the turbulent boundary layer and that the flow detaches at the step. This creates a small circulation zone right after the step for both suction and pressure sides as can be seen from the streamlines of Figure 56.

This detachment of flow at the step is also what Hoerner [54] describes for geometrical discontinuities like these. For this kind of protuberance, the drag coefficient increases with the Reynolds number, while the skin friction coefficient decreases. The addition of the shield can somewhat be compared to formation of ice on the wing. As Hoerner [54] describes, aircrafts rarely experience any troubles with increased drag, but the main issue is the loss of maximum lift. As can be seen from Table 9, what mainly is happening is loss of lift through the change of lift coefficient. While the drag coefficient can double because of the added ice or in this case added shield with surface imperfection, here it is still relatively small change due to the dimension and operating conditions. But here it can be seen that even a step which dimension is 0.2% of the chord can drop the lift coefficient by 1.3%.

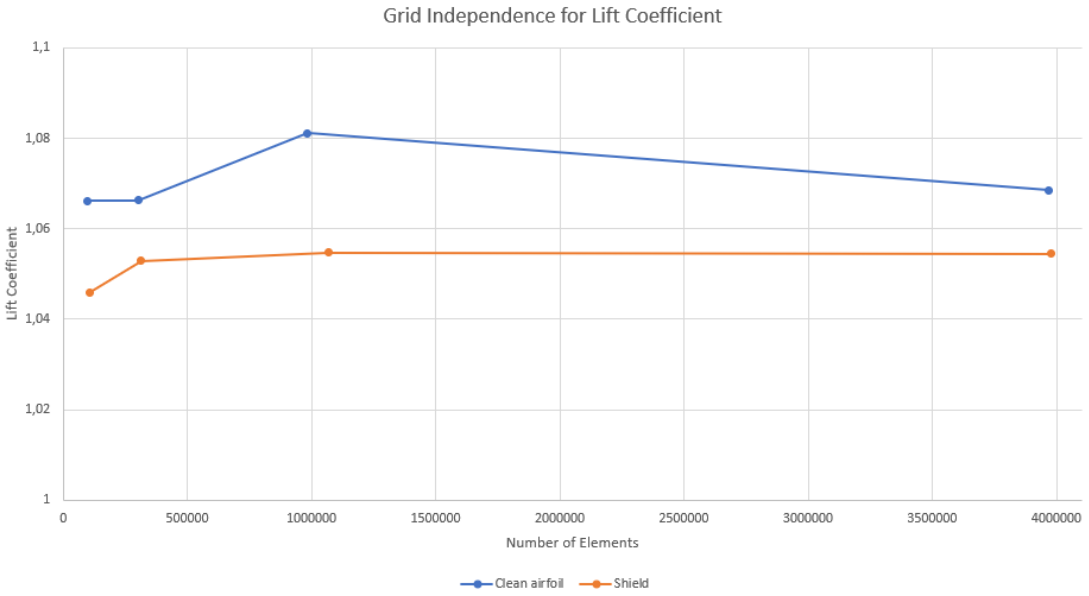

(a) Lift coefficient.

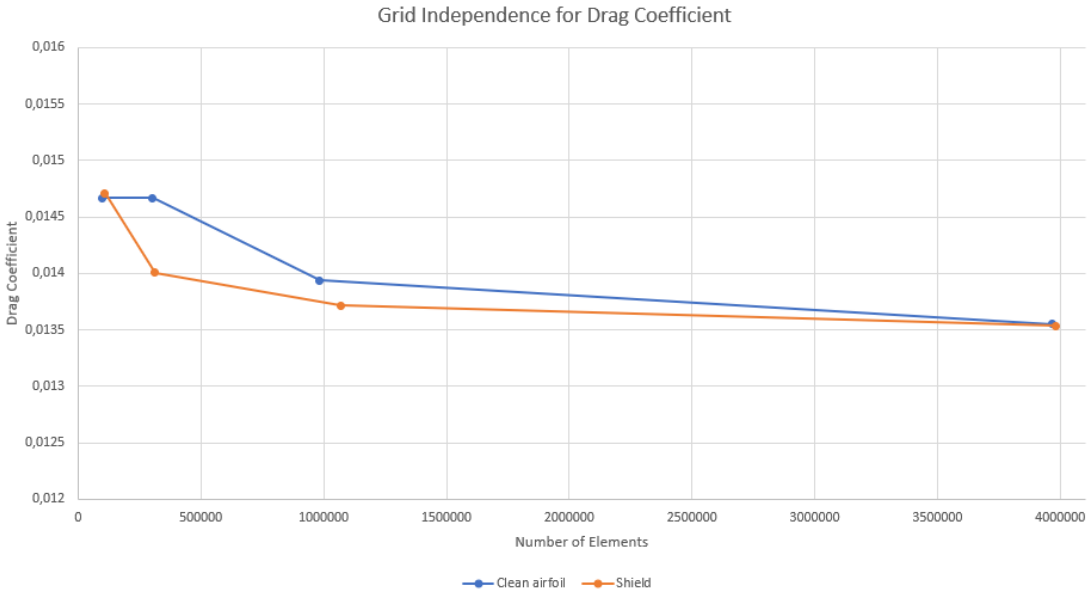

(b) Drag coefficient.

Figure 53: Grid independence study for lift and drag coefficients for clean airfoil and airfoil with the added shield.

4.3 Discussion

The structural results prove, that a modular metallic shield is a viable solution for protecting wind turbine blades against erosion. In the case of the 10 MW RWT, the designed shield could handle the defined ultimate loads without yielding, and in the fatigue load case experience stresses lower than the endurance limit. Also the aerodynamic effects are minimum, although these could still be enhanced.

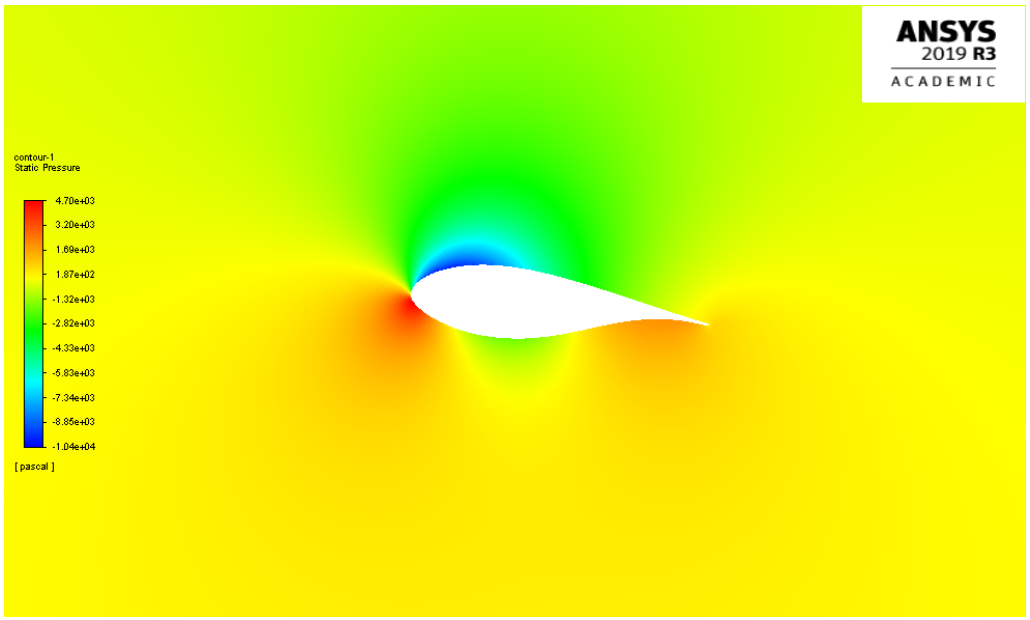

Figure 54: Pressure field around the airfoil.

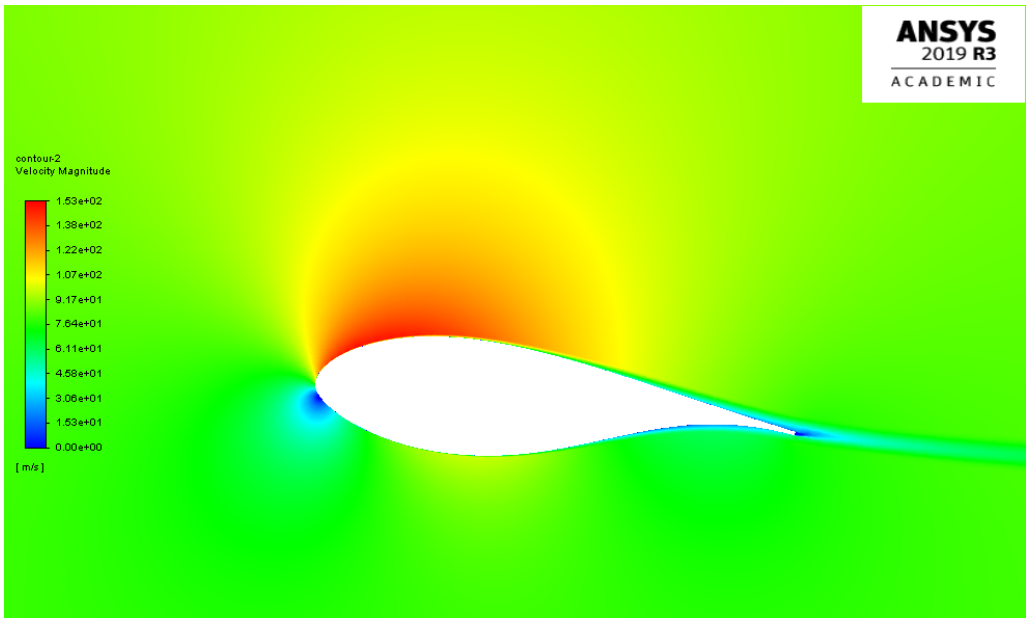

Figure 55: Velocity field around the airfoil.

As can be seen in the Figures 50 and 52, the largest areas of high stresses in the shield segments are observed in the wider parts further away from the blade tip. This is the area of the blade which experiences largest deformations during operations, while the loads go towards zero towards the tip. This is the obvious result of the load distributions in Figures 42 and 43 where highest loads are closer to the root, but because of the higher stiffness of the root section the largest deformations are higher up towards the tip.

For the current design the maximum stress during ultimate load case is 420.5

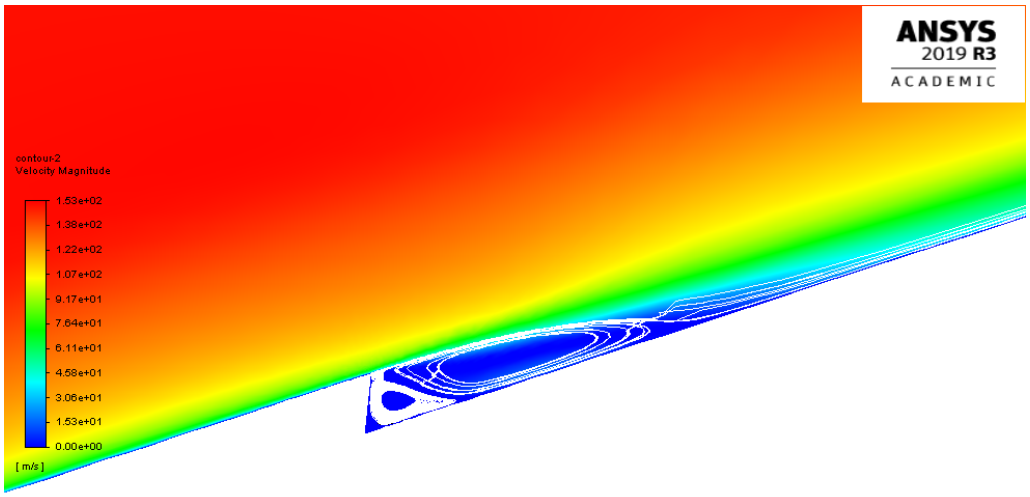

(a) Suction side step.

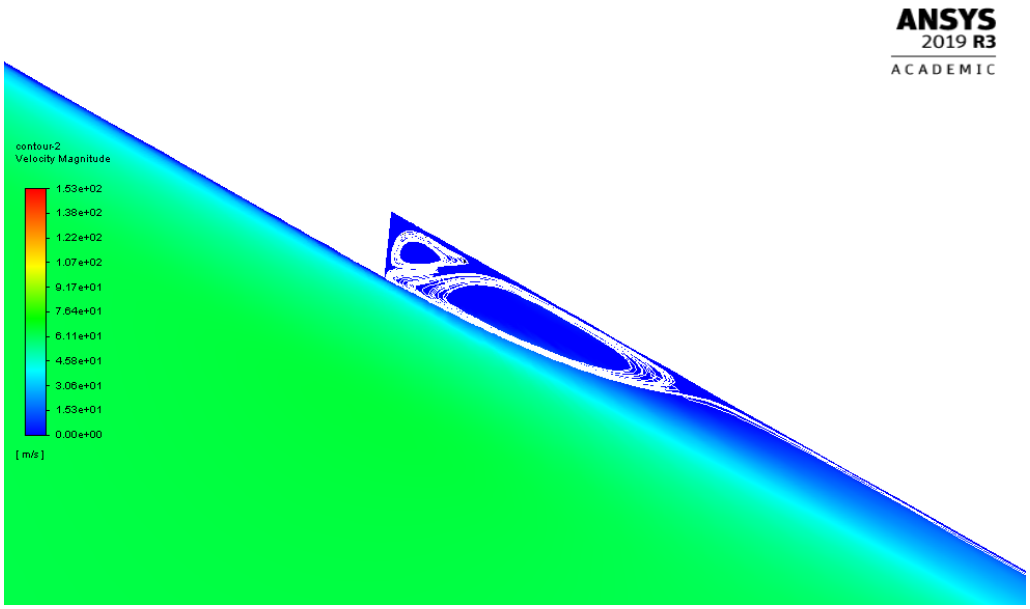

(b) Pressure side step.

Figure 56: Effect of the step to the velocity field close to the airfoil with streamlines.

MPa at the tip segment in Figure 50a. Closer to the root the stresses peaking around 320 MPa are well under the defined yield strength of 827 MPa. The peak forms in the tip segment, which has relatively higher curvature than rest of the modular segments. In this location, the shield part may experience larger elongation than rest of the segments, creating the high stress peak at the middle of the curving part. On the other hand, the value of the stress would still indicate that the main failing point is the adhesive connecting the shield to the blade surface. As the adhesive was

not the scope of this thesis, this requires further research. But for the scope of this thesis, it can be stated that the designed shield solution would endure the ultimate loads during operation.

For fatigue the highest peak stress of 221 MPa is at the tip segment. This is still a value well under the endurance limit of 430 MPa. The stresses in the larger high stress areas closer to the root peak at around 170 MPa, which is under half of the endurance limit. As stated in the Chapter 3.3.3, the load case was defined for the worst case of fatigue. This again would mean, that the shield would provide a lifetime solution when it comes to fatigue.

Additionally, the effect of the shield to the structural response of the blade is minimal based on the analysis. The difference of deflection in the ultimate case, with the shield and without it, is less than 1%. This indicates that the shield does not affect the structural response of the blade, by adding stiffness or mass to it. Also for the blade, the main stresses are still along the sparcaps. The nose section under the shield has only minor differences in stresses and strains due to the shield.

The modular structure itself mitigates the high stresses as the structure does not have to follow the deformation of the blade with the full length. More importantly, the modular structures is a key solution to ease the installation process in retrofit cases. Attaching a single piece to a wind turbine in the field would be a difficult process including cranes and technicians climbing the blades. Also the weight of a single large piece would be hard to handle, where the modular 60 cm pieces are easily handled by a single technician. While the connecting of the shield was not a scope of this thesis, it is still an important aspect to look into more. Modern adhesives are strong and could potentially attach the shield, but long term durability is still unknown. If the adhesive does not hold, the modular pieces create a risk of debris flying off the blade, and even damaging nearby turbines. Possibly other attachment concepts may need to be looked into for attaching shields like this to a wind turbine, but more complex solutions have a risk of creating multiple points of failure.

For the 2D CFD analysis the results are in line with the theory presented by Hoerner [54]. The major effect of attaching the shield is the decrease of lift coefficient, and as the step is small there is practically no effect on the drag coefficient. Since this is a high Reynolds number case, it is similar to aircraft wing icing. The drag changes due to protuberances vary based on the Reynolds number, but the main impact is the loss of lift. [54]

If the pressure and velocity fields in Figures 54 and 55 of the airfoil with shield were compared to the ones for a clean airfoil, major differences could not be observed. In the large scales the fields at these Reynolds numbers stay similar and the crucial difference between the flow fields is the area of locally forming vortexes seen in Figure 56. Thus, it is sufficient to just observe the flow fields of the airfoil with the shield.

The DTU design document [37] also offered results for their CFD analyses of a similar setup, but for a structured mesh. And there was a slight variation in the results. Comparing the clean airfoil setup for the DTU results yields that while the lift coefficients have a difference of 0.35% the drag has difference of 10%. The unstructured mesh yields higher numerical error than structured mesh, but this could be the difference of boundary layer mesh. A more thorough analysis with a higher

quality structured mesh may yield results closer to the DTU [37], but comparing the designed solution to a clean airfoil with similar meshes still yields important results of the performance. At least the difference of lift coefficient is clear, which at least for similar cases in aircraft wings is the main effect with airfoil imperfections as stated by Hoerner [54].

A decrease of 1.32% in the lift coefficient is noticeable but small, it is still lower what erosion can cause. It would still be ideal to smooth out the step of the shield towards the contour of the blade in order to minimize the aerodynamic effects, especially the loss of lift. It would also be beneficial to study the effects of the shield for the whole lift curve to get a better idea of the impact for the full operational envelope. But for the scope of this thesis it is sufficient to state that an shield like this has an impact on the aerodynamic performance, in the most common operational parameters.

While the decrease of 1.3% in lift seems insignificant, it is still in the order of magnitude of erosion even though a bit smaller, it still cannot be said to be negligible. In the large scale with multiple turbines, the effect of lost power generation starts to become a larger issue. Thus altering the original airfoil surface in this way does not provide a sufficiently good solution. The effect of the shield could be mitigated by changing the shield's geometry so that it smooths out closer to the blade's curvature at the location of the current step. There are limits in this approach as the manufacturing tolerances are around 0.1 mm for the electroformed NiCo components. The current thickness of the shield is 0.5 mm so it is really close to the manufacturing tolerances already and possibly only limited effects can be achieved. Other solution would be during installation to smooth out the step with a filler material, but this filler may have limits on the erosion resistance. So improving the design in the current form would need balancing between the induced losses, losses due erosion, manufacturing capabilities and any additional materials used. Other options that may improve the performance would be to include vortex generators into the design or additionally attach them during the installation process. They would improve the blade aerodynamics by creating a vortex delaying local flow separation and stalling, which may be increased by the shield and the formed step.

5 Conclusions & Future Work

As is clear erosion of wind turbine blades is an increasing issue with more installed capacity and larger turbines. The current polymer-based protective solutions only lengthen the time between blade refurbishments, which is troublesome especially in offshore environment. Thus metallic solutions have became more interesting in the field.

Designing an effective metallic erosion shield for wind turbines is a tedious process when trying to accommodate the structural requirements and minimize aerodynamic effects while also providing a solution that' is easy to install. Objective of this thesis was to design and analyze said erosion shield. A single design was proposed and proven to work in the limitations of the current scope. Analysis of the combined metal and composite structure proves that the behaviour of said materials can be accommodated but this can only finally be verified with physical testing and choosing proper solution for the connection. For the blade aerodynamics the best solution would be looking for an integrated solution of the shield, but this would require a complete redesign of the blade structure.

Erosion is still an increasing problem when more and more wind farms are built and largest free capacity is in offshore. Especially when the trend of wind turbines is larger in size and constantly higher tip speeds, which increase the speed of erosion caused problems. The solution presented in this thesis is only an initial step for further research of erosion protective solutions in VTT trying to tackle this problem.

Work is continued by creating solutions for connecting the metallic shield to wind turbine blades and looking also into adhesives. Once the solutions are developed further a test campaign is planned to validate the computational results of the structural analyses. Integrated solutions may also be researched as retrofit solutions of metallic shield provide to have a large amount of challenges to overcome and the effects on aerodynamics can more easily be minimized. But all in all more development and research for new solutions is required to minimize effects of erosion to decrease downtime and maximize the energy yield of wind turbines.

6 References

[1] David A. Spera. *Wind turbine technology: fundamental concepts of wind turbine engineering*. Vol. 3. ASME press New York, 1994.

[2] Tony Burton, David Sharpe, and Nick Jenkins. *Handbook of wind energy*. John Wiley & Sons, 2001.

[3] GE Renewable Energy. *Haliade-X Offshore Wind Turbine Platform*. Available: `https://www.ge.com/renewableenergy/wind-energy/offshore-wind/haliade-x-offshore-turbine`. Accessed: 22.08.2019.

[4] Rob Faulkner. *Scroby Sands Wind Farm, off Great Yarmouth*. Available: `https://commons.wikimedia.org/wiki/File:Wind_Turbines_(5132099985).jpg`. Accessed: 22.08.2019. Leeds, UK.

[5] UN. *Paris Agreement (Dec. 12, 2015)*. UNFCCC, COP ReportNo. 21, Addenum, at 21. U.N. Doc. FCCC/CP/2015/10/Add,1. Paris, France, 4 November 2016.

[6] European Comission. *COMMUNICATION FROM THE COMMISSION TO THE EUROPEAN PARLIAMENT AND THE COUNCIL The Road from Paris: assessing the implications of the Paris Agreement and accompanying the proposal for a Council decision on the signing, on behalf of the European Union, of the Paris agreement adopted under the United Nations Framework Convention on Climate Change*. Available: `https://ec.europa.eu/clima/policies/international/negotiations/paris_en`. COM/2016/0110 final.

[7] Eurostat. *Share of energy from renewable sources in the EU member states, 2017*. Available: `https://ec.europa.eu/eurostat/statistics-explained/index.php/Renewable_energy_statistics`. Accessed 20.01.2020.

[8] Directorate-General for Energy (European Comission) and Joint Research Center (European Comission). *SET Plan delivering results: The Implementation Plans*. ISBN: 978-92-79-96478-7. European Union, 2018.

[9] Technical University of Denmark (DTU), World Bank Group, and Vortex. *Global Wind Atlas*. Online: `https://globalwindatlas.info/`. Accessed: 27.08.2019.

[10] WindEurope. *Wind energy in Europe in 2018: Trends and statistics*. February 2019.

[11] Global Wind Energy Council. *Global Wind Report 2018*. April 2019.

[12] Mark Hugh Keegan, DH Nash, and MM Stack. "On erosion issues associated with the leading edge of wind turbine blades". In: *Journal of Physics D: Applied Physics* 46.38 (2013), p. 383001.

[13] Luis Bartolomé and Julie Teuwen. "Prospective challenges in the experimentation of the rain erosion on the leading edge of wind turbine blades". In: *Wind Energy* 22.1 (2019), pp. 140–151.

[14] Javier Serrano-González and Roberto Lacal-Arántegui. "Technological evolution of onshore wind turbines—a market-based analysis". In: *Wind Energy* 19.12 (2016), pp. 2171–2187.

[15] HM Slot, ERM Gelinck, C Rentrop, and Emile Van Der Heide. "Leading edge erosion of coated wind turbine blades: Review of coating life models". In: *Renewable Energy* 80 (2015), pp. 837–848.

[16] Mark Hugh Keegan. "Wind Turbine Blade Leading Edge Erosion: An investigation of rain droplet and hailstone impact induced damage mechanisms". PhD thesis. University of Strathclyde, 2014.

[17] Arvid Naess and Torgeir Moan. *Stochastic dynamics of marine structures*. Cambridge University Press, 2013.

[18] Erich Hau. *Wind turbines: fundamentals, technologies, application, economics*. Springer Science & Business Media, 2013.

[19] Fabian Vorpahl, Holger Schwarze, Tim Fischer, Marc Seidel, and Jason Jonkman. "Offshore wind turbine environment, loads, simulation, and design". In: *Wiley Interdisciplinary Reviews: Energy and Environment* 2.5 (2013), pp. 548–570.

[20] P. Suurnäkki. "Kärkipyörteiden vaikutusten hallinta erilaisilla wingleteillä". Aalto University, 2017.

[21] G Bir and P Migliore. *Preliminary structural design of composite blades for two-and three-blade rotors*. Tech. rep. National Renewable Energy Lab., Golden, CO (US), 2004.

[22] International Electrotechnical Commission. "IEC 61400-1: Wind turbines part 1: Design requirements". In: *International Electrotechnical Commission* (2005).

[23] GW Guideline and Germanischer Lloyd. "Guideline for the certification of Wind Turbines". In: *Hamburg: Germanischer Lloyd Wind Energie GmbH* (2010).

[24] JN Reddy. *An introduction to the finite element method*. McGraw-Hill New York, USA, 2006.

[25] B Dose, H Rahimi, I Herráez, B Stoevesandt, and J Peinke. "Fluid-structure coupled computations of the NREL 5MW wind turbine blade during standstill". In: *Journal of Physics: Conference Series*. Vol. 753. 2. IOP Publishing. 2016, p. 022034.

[26] Kevin Cox and Andreas Echtermeyer. "Structural design and analysis of a 10MW wind turbine blade". In: *Energy Procedia* 24 (2012), pp. 194–201.

[27] J.N. Reddy. *Mechanics of laminated composite plates and shells: theory and analysis*. CRC press, 2003.

[28] ANSYS Inc. *ANSYS® Mechanical APDL Theory Reference*. 2019.

[29] Oleg Zikanov. *Essential computational fluid dynamics*. John Wiley & Sons, 2019.

[30] Charles Hirsch. *Numerical computation of internal and external flows: The fundamentals of computational fluid dynamics*. Elsevier, 2007.

[31] Omid Gohardani. "Impact of erosion testing aspects on current and future flight conditions". In: *Progress in Aerospace Sciences* 47.4 (2011), pp. 280–303.

[32] Jeffrey Nissen, Peter Holemans, and Jonathan Venezia. "RotorShield Advanced Rotor Blade Erosion Protection, Application to V-22". In: *American Helicopter Society International Annual Forum* 71 (2015), pp. 2478–2489.

[33] Agrim Sareen, Chinmay A Sapre, and Michael S Selig. "Effects of leading edge erosion on wind turbine blade performance". In: *Wind Energy* 17.10 (2014), pp. 1531–1542.

[34] William F Adler and Stephen V Hooker. "Rain erosion mechanisms in brittle materials". In: *Wear* 50.1 (1978), pp. 11–38.

[35] DA Gorham, MJ Matthewson, and JE Field. "Damage mechanisms in polymers and composites under high-velocity liquid impact". In: *Erosion: prevention and useful applications*. ASTM International, 1979.

[36] Piet Christof Wölcken and Michael Papadopoulos. *Smart intelligent aircraft structures (SARISTU): proceedings of the final project conference*. Springer, 2015.

[37] C. Bak, F. Zahle, R. Bitsche, T. Kim, A. Yde, L. C. Henriksen, A. Natarajan., and M. Hansen. "Description of the DTU 10 MW Reference Wind Turbine". In: *DTU Wind Energy Report-I-0092* (June 2013).

[38] DJ Lekou et al. "Results of the benchmark for blade structural models, part A". In: *Deliverable D* 2 (2013).

[39] F Zahle, V Riziotis, L Bergami, and HA Madsen. "Benchmarked Aerodynamic-Structural Design Methods: Part B "Benchmarking of Aerodynamic and Aeroelastic Models". In: *Deliverable D* 2 (2013).

[40] *ANSYS® Mechanical 2019R3*.

[41] *ANSYS® Composite PrepPost 2019R3*.

[42] Christian Bak et al. "The DTU 10-MW reference wind turbine". In: *Danish Wind Power Research 2013*. 2013.

[43] ANSYS Inc. *ANSYS® ACP User's Guide*. 2019.

[44] P Breedveld, JL Herder, and T Tomiyama. "Teaching creativity in mechanical design". English. In: *Diversity and Unity. Proceedings of IASDR2011*. 2011, pp. 1–10.

[45] Doncasters Bramah. *Doncasters Electroform Brochure*. Holbrook Works, Station Road, Halfway, Sheffield S20 3GB.

[46] S. Vogel. *Cats' Paws and Catapults: Mechanical Worlds of Nature and People*. New York, NY, USA: Norton, 1998. ISBN: 9780393046410.

[47] Juha Song, Steffen Reichert, Ilan Kallai, Dan Gazit, Matthew Wund, Mary C Boyce, and Christine Ortiz. "Quantitative microstructural studies of the armor of the marine threespine stickleback (Gasterosteus aculeatus)". In: *Journal of structural biology* 171.3 (2010), pp. 318–331.

[48] G Altschuller. *40 Principles: TR1Z Keys to Technical Innovation*. Technical InnovationCenter Inc. Worcester MA, 1998.

[49] Michael F. Ashby. *Materials Selection in Mechanical Design (Fourth Edition)*. Fourth Edition. Oxford: Butterworth-Heinemann, 2011. ISBN: 978-1-85617-663-7. DOI: https://doi.org/10.1016/B978-1-85617-663-7.00024-2.

[50] *ANSYS® Fluent 2019R3*.

[51] Anders Björck. *Coordinates and calculations for the FFA-Wl-xxx, FFA-W2-xxx, FFA-W2-xxx and FFA-W3-xxx series of airfoils for horizontal axis wind turbines*. Tech. rep. Technical Report, 1990.

[52] Ann S Almgren, John B Bell, Charles A Rendleman, and Michael Zingale. "Low Mach number modeling of type Ia supernovae. I. Hydrodynamics". In: *The Astrophysical Journal* 637.2 (2006), p. 922.

[53] Ltd. Songan Plastic Technology Co. *NiCoForm NiColoy® E Electroformed Nickel-Cobalt*. Available: http://www.lookpolymers.com/pdf/NiCoForm-NiColoy-E-Electroformed-Nickel-Cobalt.pdf. Accessed 14.01.2020.

[54] Sighard F Hoerner. *Fluid-Dynamic Drag, published by the author*. 1965.

A ACRREx table

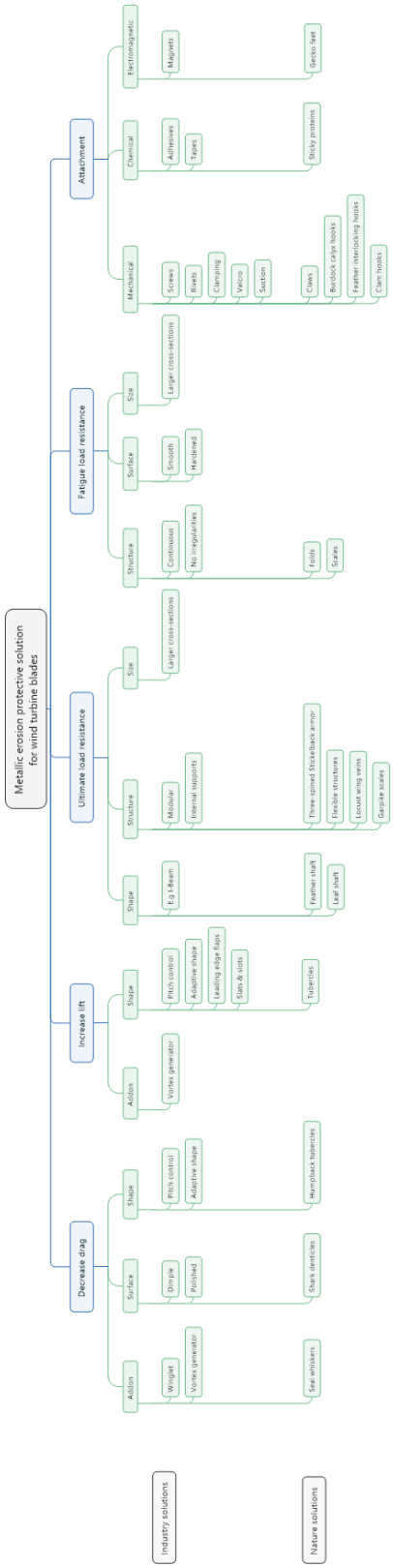

Figure A1: ACRREx table